

CRACK INITIATION AND
PROPAGATION IN ROCK

by

PARVIZ FOROQTAN-RAD

Civil Eng., Tehran University
(1964)

M.Sc.C.E., Ohio State University
(1966)

Submitted in partial fulfillment
of the requirements for the degree of

CIVIL ENGINEER

at the

Massachusetts Institute of Technology

June 1968

Signature of Author
Department of Civil Engineering, May 17, 1968

Certified by
Thesis Supervisor

Accepted by
Chairman, Departmental Committee on Graduate Students

ABSTRACT

CRACK INITIATION AND
PROPAGATION IN ROCK

by

PARVIZ FOROOTAN-RAD

Submitted to the Department of Civil Engineering on May 17, 1968, in partial fulfillment of the requirements for the degree of Civil Engineer.

Theories of crack initiation, propagation and bifurcation in perfect solids based on energy equilibrium criteria, elasticity theory considerations and particulate body mechanics are reviewed. Modifications of these and their applicability to rock are discussed. Different testing methods used to study the fracture characteristics of rock are reviewed; a bending method was chosen as most suitable for the purpose. A literature review on the effect of heat treatments on rock weakening are discussed. The principles of a continuous duty, high powered gas laser as a heat source are described.

The values of the fracture surface energy were determined for four different geometries of a granite specimen; the results show that if a stable fracture is obtained, the value is independent of geometry. Results of the heat treatment and laser treatment studies on marble and granite show the thermal exposure causes a decrease in the value of ultimate flexural strength because of intergranular and transgranular cracks induced in the specimen.

Thesis Supervisor:

Fred Moavenzadeh

Title:

Associate Professor of Civil Engineering

ACKNOWLEDGEMENTS

The author wishes to thank Professor Fred Moavenzadeh for his excellent guidance, constructive criticism and constant supervision throughout the preparation of this thesis. The author further thanks Professor F.J. McGarry and Professor R.B. Williamson for their valuable and helpful suggestions.

Sincere appreciation is also extended to Professor R.C. Hirschfeld, for many enlightening discussions and the United States Department of Commerce for providing financial support.

CONTENTS

	<u>Page</u>
Title page	1
Abstract	2
Acknowledgments	3
Table of Contents	4
I. Introduction	7
II. Fracture of Perfect Solids	9
1. Crack Growth to Critical Size	9
a. Energy Equilibrium	9
b. Elasticity Theory Criterion	13
c. Particulate Body Mechanics	15
2. Propagation Velocity and Branching of Cracks	16
a. Energy Equilibrium	17
b. Elasticity Theory	18
c. Particulate Body Mechanics	19
d. Experimental Observations	20
III. The Fracture of Rock	22
1. Theories for Fracture of Rock	23
a. Modified Griffith Theory	23
b. Coulomb-Navier Theory	24
c. Mohr Theory of Failure	25
d. Modification of Coulomb-Navier-Mohr Theory	27

	<u>Page</u>
2. Experimental Methods in Rock Fracture	27
a. Unconfined Compression	28
b. Compression with Lateral Pressure	28
c. Torsion	29
d. Punching	30
e. Hollow Cylinders Subjected to Axial and Hydrostatic Loads	30
f. Disks Subjected to Transverse Load	31
g. Brazilian Test	32
h. Indentation	32
i. Tension	33
j. Bending	33
IV. Heat Treatment of Rocks	35
1. Weakening of Rocks	35
a. Macroscopic Scale Analysis	35
b. Microscopic Scale Analysis	36
2. Laser Treatment	39
a. Laser	39
b. Laser Radiation	40
V. Experimental Procedure and Materials	43
1. Testing Method	43
2. Testing Details	44
3. Materials, Equipment and Specimen Preparation	44
VI. Results and Discussion of Results	46
1. Fracture Surface Energy of Untreated Specimens	46
2. Fracture Surface Energy of Treated Specimens	48

	<u>Page</u>
3. Crack Propagation Observations	52
VII. Conclusions and Suggestions for Future Work	54
Tables	56
Figures	61
References	
1. References on Fracture	106
2. References on Heat Treatment	110
3. References on Laser	113
Appendices	
Appendix I List of Figures	116
Appendix II List of Tables	121
Appendix III List of Additional References	122

I. INTRODUCTION

The study of rock mechanics is a relatively new area, the importance of which has increased greatly in the past two decades. Several factors have been responsible:

1. The fast growth of the mining industry.
2. The increase in the number of projects such as dams, water tunnels, subsurface power houses, subways, automobile and railroad tunnels being built.
3. The increasing interest and demand for underground storage chambers for petroleum products, chemicals, food, and supplies.
4. The need for underground military installations.

The primary purpose of rock mechanics studies is to develop methods to predict the performance of various rocks under different loading systems. This involves an analysis of applied loads, as related to rock failure, and the prediction of internal effects such as strain, flow, and microcracking. The internal effects may arise from residual stresses or from the application of external loads.

Knowledge of rock behavior is used for two purposes: safe design of structures in rock, and for more economical methods of excavation. In the design area, more accurate knowledge of the behavioral properties of rock will decrease the number of failures of structures on or beneath the earth surface. In excavation, knowledge particularly of the fracture characteristics aids the design of new machines and techniques for the construction of tunnels and underground chambers.

Since the properties of rock are highly dependent on composition and internal structure it is usually necessary to test representative samples to determine the pertinent characteristics. Conventional methods of testing require large specimens and, if the rock is stratified, it is inconvenient

to measure the strength for different strata. A testing method that would utilize thin or small specimens would overcome these disadvantages. Further, it would be feasible to cut such specimens from any desired strata.

Fracture in brittle materials is a consequence of crack initiation and propagation from regions where there are stress concentrations, hence it is desirable to investigate patterns of crack propagation and their major governing factors in rock. Thin specimens are useful for this purpose, too.

One goal of this study was to develop a technique to observe the fracture characteristics and crack propagation patterns in granite and marble. To achieve this;

- a) A suitable geometry for thin section specimens was determined.
- b) A special three point bending apparatus was designed and developed.
- c) The value of fracture surface energy obtained from these sections was correlated with that obtained from larger specimens.
- d) The effect of notch depth on the propagation and branching of cracks was determined.
- e) The influence of material type on propagation and branching of cracks was investigated.
- f) Heat treated and laser treated specimens were studied to determine the effect of such treatments on the parameters governing the propagation and branching processes.

The following three chapters present surveys of literature on the fracture of perfect solids, the fracture of rock, and heat treatment of rock. The balance of the report describes experimental work and its significance.

II. FRACTURE OF PERFECT SOLIDS

This chapter reviews the theories of fracture of perfect solids and consists of two sections: 1) crack initiation phenomena, where different approaches used to define crack growth to critical size in perfect solids are presented, and, 2) velocity and bifurcation phenomena, where analyses of the velocity and branching of moving cracks in perfect solids are discussed and also pertinent experimental data are presented.

1) CRACK GROWTH TO CRITICAL SIZE

The tensile strength of a perfect, homogeneous, elastic, isotropic, solid is of the same order of magnitude as its molecular cohesion. This is larger than the experimentally observed strength by a factor of 100 - 1000 (30,31). According to Griffith (16), the difference results from the presence of small cracks or flaws around which severe stress concentrations develop when the solid is stressed. The theoretical strength is attained in these small, highly stressed volumes of the material, even though the average stress which is usually measured remains low. In order to assess the effect of such cracks on the strength of the material, and to determine the mechanism responsible for the growth of the crack, one of the three following criteria can be used: a) energy equilibrium, b) elasticity theory, or c) particulate body mechanics.

a. Energy Equilibrium

When a material is stretched, the distance between two neighboring planes of atoms is increased by an amount proportional to the elastic energy stored in the specimen. This potential energy can provide the surface energy required for newly formed surfaces if the material fractures. However,

the presence of a crack changes the stress distribution from uniform to non-uniform and lowers the fracture strength of the material. The variation of fracture strength with crack depth in glass is a declining straight line on the log-log scale, as shown in Figure 1 (2). For simplicity, the Griffith analysis refers to the two dimensional problem of a plane plate with a stationary central crack of elliptical shape. By making the ellipse very sharp at its ends and assuming that Hooke's law holds, Griffith calculated the critical nominal stress under which the material fails using the Inglis analysis (16). According to Inglis, the local stress at the tip of such a crack is:

$$\sigma_{\max} = 2\sigma \sqrt{\frac{c}{\rho}}$$

where:

- σ_{\max} = stress at crack tip,
- σ = applied nominal stress,
- c = crack half length,
- ρ = radius of curvature at the crack tip.

Calculating the stored elastic energy by using this equation, and equating it to the energy required by the newly created surfaces, Griffith obtained for the critical stress:

$$\sigma_c = \sqrt{\frac{2E\gamma}{\pi c(1-\nu^2)}}$$

where:

- σ_c = critical applied nominal stress that causes fracture,
- E = Young's modulus of elasticity,
- c = crack half length,
- γ = fracture surface energy,
- ν = Poisson's ratio.

According to this theory, the strain energy of the system increases with increasing applied stress prior to initiation of crack growth. After initiation, however, the change in

strain energy of the system depends upon the magnitudes of the kinetic energy and the surface energy. The kinetic energy of the system is initially zero but at the critical stress when the crack begins to propagate, the kinetic energy starts to build up and increases as the crack length increases. Figure 2 shows the general relation between kinetic energy and crack half length.

The locus of the stress and strain at the onset of crack instability is shown in Figure 3 (3). Fracture occurs when the stress-strain curve of the sample intersects this locus. For a typical sample the point of intersection is in the region where the slope of the locus is positive. The possible discrepancy between the observed stress and that predicted by the Griffith equation is related to the angle between the stress-strain curve of the sample and the locus at the point of intersection. As the length of the crack increases, the value of this angle approaches 90° , where the sample satisfies the Griffith criterion. This implies that, due to the difference in the strain-energy stored in the specimen prior to fracture, an initially small crack in a sample would have a high starting velocity while an initially large crack would have a low starting velocity.

An interesting feature of this locus is that it can be used for the determination of fracture surface energy and kinetic energy (3). Consider a sample containing a crack of length $2c$ extended to fracture, and the ultimate stress maintained constant as the crack increases in length; the path followed is OAB as shown in Figure 4. The part of the work expended as surface energy, the part expended as kinetic energy, and the strain energy of the system can be determined, at any time after the initiation of the crack, by measuring the corresponding areas identified in Figure 4.

To obtain the solution for a moving crack, the Griffith criterion can be incorporated into the equations of motion (3). To do this it is assumed that the system possesses only potential energy up to the critical crack length point, and then has both potential and kinetic energy beyond this point. The kinetic energy at any stage is the difference between the work done on the system and the increase in potential energy of the system. The relation between the length of the crack and the elapsed time is established from an expression for the kinetic energy of the system. The result is:

$$\frac{V_m}{c_o} t = (\alpha-1)^{1/2} [\alpha-(n-1)]^{1/2} + n \ln \left\{ (\alpha-1)^{1/2} + [\alpha-(n-1)]^{1/2} \right\} - \frac{n}{2} \ln(2-n)$$

where the incorporation of the fracture criterion determines the value of n ;

$$n = \frac{\sigma_g^2}{\sigma_c^2}, \quad \text{and}$$

- c_o = initial crack half length,
- c = extended crack half length,
- t = time,
- ρ = density of the material,
- E = Young's modulus of elasticity,
- k = a numerical constant,
- σ_g = fracture stress predicted by Griffith Theory,
- σ_c = observed fracture stress,
- V_m = terminal velocity of the crack propagation,

$$\alpha = \frac{c}{c_0},$$

$$V_m = \left(\frac{2\pi}{k}\right)^{1/2} \left(\frac{E}{\rho}\right)^{1/2}.$$

The Griffith criterion was extended to the solution of a two-dimensional crack in a three-dimensional medium by Sack (39) and Sneddon (44). Conditions of rupture were calculated for a brittle solid containing a number of plane circular cracks when one of the principle stresses acted normally to the plane of these cracks. This loading pattern was chosen based on the simplifying assumption that the tensile strength of the brittle material in one direction is not affected by the stresses at right angles to it. The highest stress that can thus be applied in a direction normal to the plane of the disk shape crack is:

$$\sigma_c = \sqrt{\frac{\pi E \gamma}{2c(1-\nu^2)}}$$

where

- σ_c = nominal stress applied perpendicular to the plane of the crack,
- E = Young's modulus of elasticity,
- γ = fracture surface energy,
- ν = Poisson's ratio,
- c = radius of the disk.

This solution differs from Griffith's solution by a factor between 1.57 and 1.8 depending upon Poisson's ratio of the material (39,44).

b. Elasticity Theory Criterion

Another method to find solutions for an unstable crack is to use elasticity theory. The crack is assumed to be a narrow

slit which may be regarded as the limit of an ellipse with its minor axis approaching zero. The stresses in the neighborhood of the tip of the crack are then calculated. The stress distribution near one end of the crack is not influenced by its distance from the other end so the solution is obtained by considering the case in which a crack of constant length is moving through a plate. The problem of finding the stresses in the neighborhood of the crack tip then reduces to finding the stresses in a plate which is subjected both to a uniform tension and a disturbance caused by the crack passing across the plate. This disturbance is represented by a system of elastic waves of constant speed and form. The stress at the tip of the crack is given by:

$$\sigma = \frac{T}{H\sqrt{2k}} \left\{ [(\lambda+\mu)\left(\frac{1}{\gamma} - \gamma\right) - \mu\left(\frac{1}{\gamma} + \gamma \cos 2\theta\right) \cos \frac{\theta_1}{2} - 2\mu \sin 2\theta \sin \frac{\theta_1}{2}] / (\cos^2 \theta + \gamma^2 \sin^2 \theta)^{1/4} + \frac{2\beta}{1+\beta^2} [2\mu \cos 2\theta \cos \frac{\theta_2}{2} + \mu\left(\frac{1}{\beta} + \beta\right) \sin 2\theta \sin \frac{\theta_2}{2}] / (\cos^2 \theta + \beta^2 \sin^2 \theta)^{1/4} \right\}$$

where σ = stress in the vicinity of the crack tip,

T = nominal applied stress,

k = a small constant,

λ, μ = Lamé constants,

$$\beta = \sqrt{1 - c_0^2 / c_1^2},$$

$$\gamma = \sqrt{1 - c_0^2 / c_2^2},$$

$$\begin{aligned}
r, \theta &= \text{polar coordinates,} \\
\tan \theta_1 &= \gamma \tan \theta, \\
\tan \theta_2 &= \beta \tan \theta, \\
c_1 &= \text{propagation velocity of longitudinal waves,} \\
c_2 &= \text{propagation velocity of shear waves,} \\
c_0 &= \text{propagation velocity of the crack,} \\
H &= \frac{\lambda}{\gamma} - (\lambda + 2\mu) + \frac{4\mu v}{1 + \beta^2}.
\end{aligned}$$

If the crack velocity is set equal to zero in this expression, it properly reduces to the Inglis solution for stresses around a stationary crack (45).

A very similar approach to the problem of a moving crack, using the theory of elasticity, assumes a semi-infinite crack propagating in an elastic medium (14). This method gives an estimate of the force required to drive the crack. The two solutions agree quite well (14, 46).

c. Particulate Body Mechanics

Three different treatments of crack propagation have been made by particulate body analysis. Cottrel (11), using dislocation theory, obtained a solution identical to Griffith's. Crowan (29,30), assumed that the smallest possible radius for the crack tip was the interatomic spacing and obtained a solution identical to Griffith's except for a numerical factor well within the approximations necessary in such analyses.

The third approach (34,35,36) resulted in a different solution. According to this theory, if a particle pair in a particulate body is broken due to excess energy, the particles form new surfaces and the potential energy released is converted to surface energy. The vibrations induced in these particles due to breakage of the bond between them generate elastic waves which also dissipate the elastic strain energy stored in the body prior to fracture. This energy dissipation

causes a momentary cooling in the newly formed fracture surfaces. However, both of the two vibrating particles remain part of the body and cannot move very far so they cause disturbances in it instead. Perpendicular to the new surface this propagates as a longitudinal wave which has a displacement of the separated particles. Along the new surface, the disturbance propagates as a transverse wave, which has a displacement also in the same direction as that of the separated particles. The longitudinal waves impose a compression on the bonds of the body which were previously extended by the applied tensile stress; they thus relieve these stresses. The transverse waves, however, cause an additional tension on the unbroken bonds at the edge of the crack, increasing the probability that they will break. If the particles of the broken bond reform before the bonds at the new crack edge break, the whole process is merely an exchange interaction between bonds. If, however, the edge bonds do become broken before the previously broken bonds reform, the new transverse waves emanating from the latter prevent the broken bond from reforming. The fracturing process, therefore, continues by straining new bonds at the edge of the extended crack, and the new free boundaries develop as an irreversibly propagating crack.

2) PROPAGATION VELOCITY AND BRANCHING OF CRACKS

The velocity with which a crack propagates is dependent upon the material, the stress pattern imposed on it, and the amount of energy stored in the system at the time of fracture initiation. There exists a limit known as the terminal velocity. This is a property of the material. If the energy available to the crack exceeds that sufficient to drive it at the terminal velocity, the crack will either oscillate or bifurcate, or it will propagate at the terminal velocity and the excess energy will appear in other forms. Again, the problem can be approached on any of the following bases: a) energy

equilibrium, b) elasticity theory, c) particulate body mechanics, or d) experimental observations.

a. Energy Equilibrium

Agreement between theoretically calculated and experimentally measured values (38) for brittle cracks has suggested that the terminal velocity is governed by the supply of kinetic energy to the crack field. Figure 5 shows the kinetic energy distribution for a crack of instantaneous length $2c$.

If, upon the initiation of crack propagation, the displacements are immediately communicated to the outermost parts of the specimen, then the crack may move with a very small terminal velocity. Stress waves, however, limit the volume of material to which kinetic energy must be supplied because the communication of the displacements is limited by the velocity of elastic waves. Figure 6 shows the effect of stress wave propagation on crack velocity (38). The terminal crack velocity is given by:

$$V = 0.38 \sqrt{\frac{E}{\rho(1-\nu^2)}} \sqrt{1 - \frac{c_0}{c}}$$

where

- V = terminal crack velocity,
- E = modulus of elasticity,
- ρ = density of the material,
- c_0 = original length of the crack,
- c = extended length of the crack,
- ν = Poisson's ratio.

It has been shown that the terminal velocity of a crack is independent of the surface energy and also that the stress state in the material surrounding the moving crack is approximately equal to the corresponding stress state in the static case (26,38,46). Using these assumptions, the terminal crack velocity in a brittle material is found to be about 38% of sound velocity,

$$\sqrt{\frac{E}{\rho}}$$

b. Elasticity Theory

It has been predicted (46) that a crack of constant length propagating in a direction normal to an applied tensile stress may reach a critical velocity (about 60% of the velocity of a shear wave) at which point its path tends to curve. The change in direction is caused by a redistribution of stress ahead of the crack tip. Figure 7 shows the maximum stress orientation ahead of the crack for different propagation velocities. Analysis of the semi-infinite crack case yields a terminal velocity which is 57% - 81% of the shear wave velocity, depending on the value of Poisson's ratio for the material (14).

Figure 8 shows the relation between crack speed and the force required to maintain it: as the speed increases, the force decreases (14). Thus, if a stress causes a crack to initiate the crack may continue to propagate even though the stress decreases. Catastrophic propagation may occur under a load which decreases fairly rapidly after reaching a maximum.

This suggests that bifurcation must occur well before the velocity reaches that of Rayleigh surface waves, since at the higher velocities the cracking process tends to be self-maintaining.

The solution for a two dimensional crack propagating in a three dimensional medium can be obtained by studying the displacements and stresses in a semi-infinite solid (8). In this, the solid is assumed to sustain:

1. A constant pressure, acting on an infinite strip, the width of which is symmetrically increasing from zero with constant velocity.
2. A pressure outside the strip such that the normal displacements of the surface outside the strip are zero.

The terminal velocity of the crack is independent of the value of surface energy (26) and in the analysis the surface energy term is assumed to be zero. This makes it possible to assume that the crack nucleates from an infinitesimally small origin, and that it propagates with maximum velocity from its start. From the analysis it is concluded that a two dimensional crack moves in one plane, without bifurcation, at a constant velocity equal to the velocity of surface Rayleigh waves (8).

c. Particulate Body Mechanics

Using the particulate theory of fracture (34,35,36), the equation for the mean value of crack velocity based on the stress condition at the crack tip is as follows :

$$V = \frac{c_2}{2} \exp\left(-u \frac{E_0}{kT}\right)$$

where

V = mean crack velocity,

c_2 = transverse wave velocity,

E_σ = contribution of strain energy to fracture surface energy,

E_0 = contribution of thermal energy of the body to fracture surface energy,

$u = E_\sigma/E_0$,

k = Boltzmann constant,

T = absolute temperature in degrees Kelvin.

This equation states that the terminal velocity of propagation is one-half the transverse wave velocity.

The major causes of bifurcation in terms of particulate mechanics can be summarized as:

1. Broken bonds on both sides of the crack edge relieve the stresses in their neighborhood and prevent the propagation of the crack in the same direction.
2. The orientation of the major principal stress usually changes from place to place in the stressed body.
3. The configuration of the body produced by the propagating crack induces a change in the stress pattern so rapid that it is not in static equilibrium and elasticity considerations cannot be applied.

d. Experimental Observations

When the stress condition in a sample exactly satisfies the Griffith criterion, the sample is in an unstable state and a crack begins to propagate if the stress increases infinitesimally. Practically, the stress in such a sample continuously increases until it breaks. The value of

the fracture stress depends on the rate of load application and on the geometry of the specimen. Figure 9 shows the relation between crack length and time elapsed after crack initiation. The time required to obtain a certain crack length decreases as the applied stress is increased. This difference is caused by the difference in initial velocities of crack propagation for different stress levels. The terminal velocity, however, is the same for all levels; Figure 10 shows this and also it shows that for lower stress levels, a longer crack has to be developed before the terminal velocity is attained.

The results of experiments on glass (42,43) confirm that the terminal velocity of all the cracks is the same, Figure 11, unless a crack slows down or stops because of bifurcation. The velocity of the crack propagation, however, is not uniform across the width of the specimen (40). Further, the velocity characteristics of each individual fracture are influenced by such factors as the degree of load relaxation occurring during the dynamic phase of the process.

The velocity history in a specimen subjected to bending stress is of different form. The crack initiates from and propagates through the tension zone but if the crack then approaches the terminal velocity, the neutral axis cannot shift fast enough as the crack approaches it. To shift the neutral surface out of the way of the propagating crack requires that the condensation waves emitted from the propagating crack reach one end of the specimen and reflect back to the crack as dilatational waves. This takes considerably more time than is required for the transverse crack to reach the neutral surface. Figure 12 shows the result: the velocity decreases with depth in measurements on glass bars under flexural stress. The decrease is due to the fact that the crack has passed beyond the original neutral axis location.

III. THE FRACTURE OF ROCK

The solutions obtained for the fracture of perfect materials predict local failures in a perfectly homogeneous, elastic, and isotropic material. However, all rocks are inhomogeneous, inelastic, and anisotropic. Thus the theories cannot be directly applied to rock although modifications of certain solutions do give satisfactory results. These modifications include the incorporation of the behavior of cracks in rocks under pressure (23), and the assumption that local failures in rock can occur simultaneously in different locations.

If the analysis is done on a large or macroscopic scale, the rock may be assumed homogeneous and the flaws randomly oriented. It also can be assumed that the density and the size of existent flaws are uniform throughout the rock specimen. With these assumptions, Coulomb type failure theories can also be successfully applied to predict the fracture of rock if necessary modifications are made, taking into account the effect of flaws and imperfections. This is accomplished by assuming a low tensile strength for rock without any reference to its cause: the presence of prior flaws and imperfections. Further, most rock fracture theories have been developed and improved to explain certain phenomena previously observed in tests; thus the testing methods play an important role in the study of rock fracture.

This chapter has been divided into two sections: 1) theories for fracture of rock, where theories which have been used in the literature to predict failure of rock are discussed, and 2) experimental methods in rock fracture, where the different testing methods used to determine the

fracture characteristics of rock are reviewed, to identify the application of theories and to clarify the testing method used in the present study.

1) THEORIES FOR FRACTURE OF ROCK

The following theories have been used to predict the fracture characteristics of rock:

- a. Modified Griffith Theory,
- b. Coulomb-Navier Theory,
- c. Mohr Theory,
- d. Modified Coulomb-Navier-Mohr Theory.

A brief description of each follows:

a. Modified Griffith Theory

The crack propagation theories discussed in the previous chapter assumed that no forces are carried across the faces of the crack. For rock, however, it is possible for cracks to close, and carry normal and shear stresses, through friction (23,29). These secondary stresses will tend to increase the strength of the rock by reducing the stress concentration at the tips of the crack from the value it would have if the friction stress did not exist. The failure condition for such a specimen is:

$$\mu(\sigma_3 + \sigma_1 - 2\sigma_c) + (\sigma_1 - \sigma_3)(1 + \mu^2)^{1/2} = 4T_0 \left(1 - \frac{\sigma_c}{T_0}\right)^{1/2}$$

where σ_1, σ_3 = external normal stresses,

μ = coefficient of friction for the crack surface,

σ_c = stress normal to the crack required to close it,

T_0 = tensile strength of the rock.

If the applied stress is simple compression in one direction, and if $\sigma_c = 0$, the above equation reduces to:

$$\frac{C_o}{T_o} = \frac{4}{\mu - (1+\mu^2)^{1/2}}$$

where C_o = compressive strength of the rock.

Combining this equation with the preceding one results in a straight line relationship between two external normal stresses (29).

b. Coulomb-Navier Theory

The Coulomb-Navier Theory postulates that failure will occur in a material when the maximum shear stress on a plane in the material reaches the shear strength, and that the normal stress acting across the plane increases its failure resistance in proportion to the magnitude of the normal stress. The shear strength is given by (29):

$$S_o = \mu \frac{\sigma_1 + \sigma_3}{2} + \frac{\sigma_1 - \sigma_3}{2} (\sin 2\theta + \mu \cos 2\theta)$$

where S_o = shear strength of the material,
 μ = coefficient of internal friction,
 σ_1, σ_3 = applied normal stresses,
 θ = inclination of the shear plane.

The maximum shear acts on a plane whose orientation is defined by $\tan 2\theta = \frac{1}{\mu}$ and its value is:

$$S_{\max} = \frac{\sigma_1}{2} [\mu + (\mu^2+1)^{1/2}] + \frac{\sigma_3}{2} [\mu - (\mu^2+1)^{1/2}]$$

The criterion for failure in tension is obtained by substituting $\sigma_1 = T_o$ and $\sigma_3 = 0$ into the above equation:

$$\frac{T_o}{2} [\mu + (\mu^2+1)^{1/2}] = S_{\max}$$

The criterion for failure in compression is obtained by substituting $\sigma_1 = 0$ and $\sigma_3 = -C_o$ into the equation:

$$\frac{-C_0}{2} [\mu - (\mu^2 + 1)^{1/2}] = S_{\max}$$

Combining the above three equations results in a straight line, DE, in Figure 13, described by:

$$\frac{\sigma_1}{T_0} - \frac{\sigma_3}{C_0} = 1$$

According to the Coulomb-Navier Theory, if the material experiences stress conditions outside the area DEB, it fails.

c. Mohr Theory of Failure

This is based on the earlier Coulomb concept of failure as a sliding action along planes inclined to the direction of principal stresses. The resistance to sliding consists of two parts: a constant shearing strength, or internal cohesion, and a frictional resistance which is proportional to the normal stress acting across the plane of sliding. Analytically, the Coulomb Theory states:

$$(|\tau| + \mu\sigma)_{\max} = S_s$$

where S_s = ultimate strength in shear,
 μ = internal friction coefficient,
 σ = normal compressive stress,
 τ = shear stress.

The Mohr Theory is a generalization of the Coulomb theory; it states that the material acts as a homogeneous body and that there is a relation between the normal stress and the shear stress in any plane which governs the resistance of failure along that plane.

According to the Mohr Theory a material will fail when (15):

$$\left\{ \sigma_n - \frac{(\sigma_3 + \sigma_1)}{2} \right\}^2 + \tau^2 = m^2 (\sigma_1 - \sigma_2)(\sigma_3 - \sigma_2) + \left\{ \frac{(\sigma_3 - \sigma_1)}{2} \right\}^2$$

where: $\sigma_1, \sigma_2, \sigma_3$ = externally applied stresses,
 σ_n = strength of material in axial loading,
 τ = shear strength of the material,
 m = direction cosine of the plane being studied.

Graphically, any material whose stress state falls outside the outermost circle, in Figure 14, will fail; the plane of the failure can be determined by this method, both graphically and analytically. Failures under tension are represented by circles on the positive side of the normal stress axis. Failures under compression are represented by circles on the negative side (Figure 15). Similarly, the graphical representations of shear and combined loading are circles of different diameters with their centers at different points on the normal stress axis. The failure is represented by the points lying on the envelope of these circles (45). Using the Coulomb Theory of internal friction, this envelope is represented by two straight lines tangent to the circles; Mohr's generalized theory results in a curved envelope. The failure condition in terms of two normal stresses can be represented graphically as shown in Figure 16. If the applied stress state is defined by a point outside the shaded area, the material fails.

d. Modification of Coulomb-Navier-Mohr Theory

Based on experimental evidence a modification of the failure envelope (13, 32, 33) can be made. Although the analytical requirements for this modification are not always clear, it is widely used because of the simple graphical representation. To construct the envelope, two lines tangent to the uniaxial compression circle are drawn with the slope equal to the angle, ϕ , of internal friction of the material. The envelope consists of these two tangents and a tension cut-off line drawn tangent to the uniaxial tension circle; see Figure 17. Available data show that the Coulomb-Navier-Mohr Theory of fracture can describe the results of the compression tests adequately but cannot provide a realistic description of tension or torsion tests. The modified theory, however, represents fully the results of three simple tests: shear, tension, and compression. In essence it states that a brittle material fractures on either the plane where the shear stress reaches a critical value or on the plane where the maximum tensile stress reaches a critical value, whichever occurs first.

Another graphical representation of this theory is shown in Figure 18. The shear stress condition is represented by the inclined line BC and the tension condition is represented by the tension cut-off AB. The results obtained using this theory generally agree very well with experimental data for brittle materials, including rock (32,22).

2) EXPERIMENTAL METHODS IN ROCK FRACTURE

Rocks are relatively hard to machine so the method used in any experimental study should employ simple specimens. Depending upon what characteristic is sought, usually a particular method and specimen are used. Thus, several methods have been developed, each suitable for a certain type of measurement.

The following methods are discussed in this section:

a. unconfined compression, b. compression with lateral pressure, c. torsion, d. punching, e. hollow cylinders subjected to transverse load, g. Brazilian splitting test, h. indentation, i. tension, and j. bending.

a. Unconfined Compression

This is the oldest method for measuring the strength of rock (19,20,21,32,33). The common practice is to use cylinders with a length-diameter ratio of 2:1 although the actual dimensions of the cylinders have shown an effect on the failure pattern; the strength and the inclination of the fracture plane are higher in short samples (25). One difficulty in this method of test concerns the degree of lubrication of the end plates which has a pronounced effect on the mode of specimen failure. With lubricated end plates the macroscopic failure cracks occur parallel to the axis of compression (Figure 19). If the Coulomb-Mohr Theory is used to analyze the condition, the angle of internal friction of the rock sample is found to be 90 degrees. This value is much larger than ordinary. With unlubricated plates, however, the cracks form at oblique angles to the axis of compression. Therefore, it appears that although the Coulomb-Mohr Theory is excellent for predicting fracture loads, it is not useful for predicting the direction of the failure planes.

b. Compression with Lateral Pressure

This method simulates a more complex stress condition. The general effect is shown in Figure 20. The assumption that cracks close under a confining pressure and thus contribute to the strength of a rock specimen has been verified by experimental data (23). Further, despite the unconfined compression test results, the fracture angles for specimens failed by compression and lateral pressure agree very well with the Mohr Theory (25).

c. Torsion

A cylindrical bar of a brittle material subjected to torsion usually fractures in a single plane. This plane intersects the surface of the cylinder in a helix inclined at an angle of 45 degrees to the cylinder axis. The helix is perpendicular to the direction of maximum tension.

If a cylindrical specimen is subjected both to a torque and a confining pressure, the principal stresses are (20):

$$\sigma_1 = \frac{1}{2}(P_a + P_o) + \frac{1}{2}[(P_a - P_o)^2 + 4T^2]^{1/2}$$

$$\sigma_2 = P_o$$

$$\sigma_3 = \frac{1}{2}(P_a + P_o) - \frac{1}{2}[(P_a - P_o)^2 + 4T^2]^{1/2}$$

where

$$T = 2M/\pi a^3,$$

a = radius of the cylinder,
M = applied torque,
P_o = confining pressure,
P_a = axial pressure.

As a result of the confining pressure, the tensile principal stress is reduced and the compressive principal stress is increased. Under these conditions, the torque can be increased to a higher value and the angle of the helical cleavage plane also increases.

d. Punching

In this method a small disk is punched out of a plate which usually is also a disk of larger diameter (19). The stress system approximates simple shear so a well defined disk is punched out. The periphery of the specimen can also be under a confining pressure to obtain a state of combined stresses, if desired. This method is useful when measurements on anisotropic materials are to be made: specimens can be cut in the principal directions where the shear strength is to be determined.

e. Hollow Cylinders Subjected to Axial and Hydrostatic Loads

If a hollow cylinder is subjected to an axial load, an internal pressure and an external confining pressure (20), the radial and tangential stresses are given by:

$$\sigma_r = \frac{[P_c - \rho^2 P_i + (P_i - P_c) \left(\frac{a^2}{r^2}\right)]}{(1 - \rho^2)}$$

$$\sigma_\theta = \frac{[P_c - \rho^2 P_i - (P_i - P_c) \left(\frac{a^2}{r^2}\right)]}{(1 - \rho^2)}$$

where

- σ_r = radial stress,
- σ_θ = tangential stress,
- ρ = ratio of internal to external radius,
- P_i = internal pressure,
- P_c = confining pressure,
- P_a = axial loading,
- r, θ = polar coordinates,
- a = inside diameter.

Several different fracture modes can be obtained by varying the three applied loads.

f. Disks Subjected to Transverse Load

In this method disks are prepared with a central hole and then tested in diametral compression. From the results the tensile strength of the rock can be calculated (37) as follows:

$$P = \frac{W}{\pi ta} (6 + 38\rho^2)$$

where

P = tensile strength,

W = load at failure,

t = thickness of disk,

a = radius of disk,

ρ = ratio of the internal to external radii.

Most specimens fail by a crack running vertically through the central hole. Sometimes this is accompanied by secondary cracks. Basically four different types of crack pattern can be distinguished. Figure 21 shows these:

1. single fracture
2. S shaped fracture
3. branched fracture
4. cross shaped fracture.

The load at failure is a function of the orientation of pre-existing flaws and defects with respect to the direction of the applied load. To confirm the existence of such a preferred orientation, point load tensile testing can be performed on solid disks of the same material. In this, a compressive load is applied to the center of a disk specimen by means of two opposing hemispherical indentors, Figure 22. Failure generally occurs as a single fracture bisecting the disk parallel to the axis of loading. The applied stresses are symmetrical about the loading axis, and if the rock is isotropic, failure will be random. The failure for most rocks, however, has a preferred orientation (24).

g. Brazilian Test

In this method, a solid disk is transversely loaded to fracture. The principal stresses induced to such a specimen (1) are:

$$\sigma_1 = \frac{-P}{\pi R t} \left(\frac{MN + 2R^2 N}{MN + 2R^2 L} \right)$$

$$\sigma_3 = \frac{-P}{\pi R t} \left(\frac{MN - 2R^2 N}{MN + 2R^2 L} \right)$$

where

$$M = x^2 + y^2 + R^2,$$

$$N = x^2 + y^2 - R^2,$$

$$L = x^2 - y^2 + R^2,$$

R = radius of disk,

P = applied load,

t = thickness of disk.

Fracture usually initiates at the exact center of the disk but after the initiation of the main crack some secondary cracks start forming. These are shown in Figure 23. In this method, the load at failure is also a function of orientation of the direction of pre-existing flaws.

h. Indentation

Classically hard brittle materials such as rocks become ductile during indentation or under confined compression. Further, the deformation caused by indentation of several fine-grained crystalline rocks has been found microscopically to be the same as the deformation of these rocks in the conventional compression test carried out under moderate confining pressure (4). From the analysis of various microscopic and macroscopic observations, however, it has been concluded

that the apparent ductility of rock is more likely due to systematic microfracturing on a scale too small to be observed, rather than due to slip (4).

The indenter is a diamond pyramid which is forced against the surface of the rock. The force acting on the indenter divided by the area of indentation is called the hardness. Hardness is thus the average normal stress applied to the surface of the specimen by the indenter. The strength of rocks estimated from hardness testing is approximately that measured in conventional tests.

i. Tension

Due to the difficulty of fabricating and testing tensile specimens, less attention has been paid to the direct application of tensile stresses. Most testing of rock, in tension and/or in shear, is done indirectly, as some of the previous techniques illustrate.

j. Bending

This method has not been used very widely for the study of fracture of rock despite its ease of operation. If a rock beam is loaded at midspan, it is very unlikely that the specimen will fail exactly at its center. Instead, failure occurs where a combination of the prior crack length and the applied stress imposes the most severe condition (18). Due to geometry and the energy storage characteristics of the specimen, the fracture is always a catastrophic one, even if testing is performed with a hard machine. The total elastic energy stored in the system at the time of fracture initiation is the sum of the energy stored in the specimen and the energy stored in the apparatus, Figure 24. The stored elastic energy is dissipated in the fracture process. If it is greater than that required to form two new surfaces, the fracture is catastrophic (Figure 25) and the excess energy

is released in other forms: kinetic energy of fragments for example. However, if the elastic energy is smaller than the energy required for the formation of new surfaces, additional work is required to propagate the crack and the fracture is stable.

The energy required to fracture the original test piece and create two new surfaces (28) is given by:

$$U = 2A\gamma$$

where γ = fracture surface energy,
A = nominal cross section,
U = required energy.

Measurement of the fracture surface energy from the force-deflection curve is accurate only for stable fractures. To avoid the usual catastrophic fracture in bending, an artificial crack is introduced on the tension side of the specimen, at midspan, and a stable or semi-stable fracture (Figure 25) is obtained. In this case, the calculation of fracture surface energy from the force-deflection diagram becomes valid. The method has proven to be a most convenient one to use for determining the fracture surface energy of rock materials.

IV. HEAT TREATMENT OF ROCKS

The use of heat in breaking rock has been known from antiquity. Generally the results of quenching after heating have seemed to obscure the fact that heating alone is effective so the study of just heating effects became secondary to the development of combined heating and quenching methods. Heating of rock can use conventional methods such as torch and flame jets or more unusual devices such as a laser which provides radiation of uniform wavelength. Both methods are discussed in this chapter.

1) WEAKENING OF ROCKS

Most rocks are weakened by heating and do not regain their strength after cooling. The weakening is achieved at temperatures much lower than the melting point. Numerous attempts have been made to assess the effectiveness of heat treatment in various heating and quenching cycles. Basically, two different approaches are used:

- a) On a macroscale where the material is assumed to be completely homogeneous and the damage is due to thermally induced shock and the resulting stress distribution.
- b) On a microscopic scale where the material is recognized to be granular and its response depends upon the characteristics of the constituent grains and their interactions.

a. Macroscopic Scale Analysis

The fracture of rock on this scale is caused by thermally induced stresses which exceed the ultimate strength of the rock. The parameters affecting the thermal shock resistance of rock are strength, modulus of elasticity, Poisson's ratio, coefficient of thermal expansion, thermal conductivity, specific heat, porosity, and density. For laboratory tests,

the size and shape of the specimens also affect the results as do the heat application procedure and any quenching experience.

Since on this scale the rock is assumed to be homogeneous, the only weakening process which may operate is the development of stresses due to the temperature gradient present in the rock. A crack initiates at a point where the stress exceeds the ultimate strength of the rock. If the elastic energy stored in the specimen is sufficient to drive the crack through the specimen, it will fracture catastrophically; otherwise, the crack will stop after the stored energy is exhausted.

b. Microscopic Scale Analysis

On the microscopic scale several mechanisms have been suggested (52) as responsible for weakening of rock due to heating. In almost all cases, a combination of two or more of these mechanisms can be identified in the heat treatment. These include gross chemical changes, gas or water pocket expansion, spalling and anisotropic thermal expansion.

Gross Chemical Changes: Good evidence exists that gross chemical changes do not occur in certain rocks such as marble (52) but such changes have been observed in heat treated quartz (61). The latter are believed to be molecular in nature. For example the ease of crushing heat treated specimens of quartz with one's fingers is cited as an indication of an internal debonding caused by heating (61).

Gas or Water Pocket Expansion: These are usually accompanied by fragmentation of the specimen and by the noise of small explosions. When such behaviors are observed during heating, this mechanism is considered responsible for weakening of the rock.

Spalling: Spalling is caused when various rocks have low thermal conductivity and appreciable thermal expansion.

It depends on the temperature gradients established, which are determined by the heating rate. Spalling could also be caused by a high anisotropy and/or low thermal conductivity. It has been observed (59) that rocks containing abundant quantities of quartz are highly spallable.

Anisotropic Thermal Expansion: Differential thermal expansions of adjacent grains in rock can cause separations along the grain boundaries. However it has different consequences for isotropic and anisotropic materials. If the rate of heating of an isotropic material is slow enough to avoid a large temperature gradient, each grain expands equally in all directions and there is no differential movement among them. Further, on cooling, the rock returns to its normal size and shape. If the rate of heating is rapid enough to produce a large temperature gradient, some grains expand more rapidly than others resulting in differential movement which may cause the formation of intergranular spaces.

When an aggregate of anisotropic grains is heated, the grains expand differently in different directions pushing each other apart, creating open voids. Upon cooling, the openings do not quite retrace their previous movements, leaving some spaces unfilled and causing a permanent change in dimensions (47). If the aggregate is heated again, an additional permanent expansion is developed although the latter is not so large as the first one.

The separation caused by expanding grains is dependent upon the orientation of one grain relative to its neighbor, and the grain pairs having the greatest difference in stress orientation are subjected to the greatest shear at any given temperature. Therefore, they are the first to fail when the temperature is raised. As the temperature increases and more bonds are broken, only the bonds with less misorientation remain. This requires successively higher temperatures

to achieve successive shear failures at grain boundaries and eventually a point will be reached where no further effect can be observed.

In most of the possibilities listed, rupture at the grain boundaries seems to be a major factor, thus knowledge of the nature and behavior of grain boundaries seems desirable. Most of the work which has been done on intergranular bonding, however, has been directed towards metals, with little or no attention to rock. Various models have been suggested. Mott (70) proposed that the boundaries consist of islands of good fit and areas of bad fit between the lattices of adjacent grains. Ke (62) mentioned that boundaries consist of a concentration of lattice vacancies or disordered groups. Brown (52) described the boundary as a series of dislocations of one type or another. Grain boundaries are frequently very strong and thus cracks developed during heating or mechanical testing do not always follow intergranular paths. With metals this is much more common than with rocks since rarely in metals does one find the extreme difference between adjacent grains that are possible and normal in rocks. For example, two metals rarely differ from each other as radically as quartz differs from a feldspar, yet these two minerals are associated in granite in which very little intergranular fracture is observed in fractured specimens unless heat treatment has been applied.

Other mechanisms such as metallic type brittle fracture, phase transformation, intergranular corrosion, anisotropic heat transfer, strengthening of grains by annealing, and diffusion of impurities into grain boundaries are also suggested in the literature as possible mechanisms responsible for rock weakening. It appears, however, that most such, although responsible for weakening in other materials especially metals, can be dismissed or their effects can be considered secondary for rock (52).

2) LASER TREATMENT

The invention of the laser and its subsequent developments have provided science and industry with a new and powerful tool. The term "laser" is an acronym for "Light Amplification by Stimulated Emission of Radiation". Basically, a laser is a device which converts energy into a highly intense and narrow beam of light or electromagnetic radiation. Prior to discussion of use of laser radiation in the fracture of rock the principle of laser operation will be reviewed.

a. Laser

Atoms of a material may occupy any one of many discrete or quantum levels of energy, depending upon the temperature of the material. If the system is in thermal equilibrium, most of the atoms will occupy the lowest possible energy levels, where they are referred to as being in the ground state. They can be excited to higher energy levels, excited states, by absorbing energy from some external source. This may be in the form of heat, light, or other types of radiation. Atoms that are in an excited state will relax to a lower energy state by releasing some of the absorbed energy. Such energy release is the basis for the operation of lasers. Materials research and research in other fields related to laser have led to a variety of materials which will produce laser action; these include hard crystals, gases and gaseous mixtures, plastics, glasses, semiconductors and liquids. Many of these materials may be operated in either a pulsed or a continuous mode.

In pulsed lasers, electric energy is stored in capacitors and then it is discharged in a gas filled flashlamp, resulting in an intense flash of white light. The laser material is placed where this light can be absorbed most efficiently. When sufficient energy is absorbed by the material, its characteristics change and it becomes an amplifying medium (80).

The optical cavity is developed by placing two highly reflective surfaces at the ends of the laser material. One of these surfaces is slightly transparent and the other is totally reflective. In relaxing to the lower energy level, the atoms emit photons which are principally directed along the axis of the laser material. The photons produce a wave of light which grows in amplitude until it reaches the semitransparent reflecting surface. Some of the light passes through the surface while the remainder is reflected to undergo further amplification. When the light reaches the totally reflecting surface, it reverses its direction and the process is thus repeated. The light which has been amplified but is not directed along the axis of the material, leaves the laser material through the sides of the cavity. In gas lasers where the output can be either pulsed or continuous, the excitation is accomplished by running a cold cathode discharge in a flowing gas mixture. In general, the gas laser tubes are constructed with pyrex tubing which is cooled by means of a water jacket. Further, the dissociation of the molecular gases, which is due to emission of photons from the gases, requires a flowing system of gases in the tube.

The output of the laser is in the form of a narrow beam of light or electromagnetic radiation. In addition, the output is essentially coherent in both space and time: all wave fronts of the light are perpendicular to the direction of propagation and there is a definite phase relationship between the wave fronts, or they follow each other at regular intervals (6).

b. Laser Radiation

There has been a wide interest in the laser from an application point of view because it has a unique set of capabilities: a) output is coherent, b) high frequency,

c) monochromatic or narrow spectral line width, d) well collimated beam, e) high power density, and, f) continuous or pulsed operation. Many practical applications of the laser also depend upon the fact that the beam may be focused to a small spot with simple inexpensive equipment.

The radiant energy delivered to a surface is consumed in one or more of the following processes: a. reflection, b. heating, c. boundary interaction, d. phonon generation, e. acoustic phonon generation and f. reradiation.

The relative magnitudes of the different energy consumptions depend strongly upon the thermal and optical properties of the material exposed to the radiation, as well as on the characteristics of the laser. The development of boundary interaction, such as radiation pressure, or other effects that may develop shock waves, has not been observed in the experiments performed. Further, phonon generation and acoustic phonon generation have been observed only in materials that are transparent to the laser wave length. Thus the mechanisms by which the laser energy is consumed in rock are heating, reradiation and, to a much smaller extent, reflection.

When a rock specimen is exposed to the laser beam the temperature of the exposed surface suddenly increases and a temperature gradient is developed. The rise in temperature and the development of the thermal gradient across the specimen causes two types of stresses. Neighboring grains, due to differences in orientation, will expand unequally and the thermal gradient will cause a stress field which assists in fracturing the specimen. Either or both of these stresses may be responsible for the weakening and eventual rupture of the specimen. Since the laser energy is almost totally absorbed by the rock specimen, a large temperature gradient will be developed in a short time, causing failure. The misorientation of two neighboring grains located at the surface

of the specimen will also cause spalling. If the temperature of the exposed area is increased by increasing the exposure time, the mechanisms already mentioned will be accompanied by partial melting of the exposed zone. The energy lost will increase because of heat reradiation from the incandescent molten zone. If the temperature further increases, some of the material which has melted will evaporate. It is postulated (81) that with very high power intensities and poor thermal conductivities, an internal explosion may develop, shattering the material.

If lasers are to be used as an aid to excavation, it is desirable to keep the temperature below melting so the rock is only weakened. Melting is economically unattractive and technically unnecessary, since extreme weakening occurs before melting takes place.

V. EXPERIMENTAL PROCEDURE AND MATERIALS

A review of the literature shows the most suitable testing method to be used both for measurement of fracture surface energy and for crack propagation observations is the bending technique. With it the value of fracture surface energy for beams of size 1 x 1 x 12 inches and .1 x 1 x 4 inches and two intermediate sizes were measured for different notch depths. The crack propagation patterns were observed for different notch depths in marble and granite specimens. They were also observed for heat treated and laser treated specimens of marble and granite. In this section the experimental procedures and the materials used are presented.

1) TESTING METHOD

Due to the presence of flaws and imperfections, rock exhibits its lowest strength in tension and fails when the maximum tensile stress reaches the ultimate strength. Testing methods which produce complex stresses in the specimen obscure this fact and make the analysis of crack propagation more difficult. Most methods also require fairly large specimens, which are inconvenient to prepare. In the bending method, the stresses acting on the specimen are tensile and shear below the neutral axis and compression and shear above it. By making a notch at the midspan, the value of the tensile stress is greatly increased, locally. Thus the crack initiates under essentially pure tension. In a properly chosen specimen containing a notch of the right size, the tensile stress at midspan reaches the ultimate strength of the rock before the strain energy stored in the specimen is sufficient to drive the crack to the top of the specimen. This ensures the production of a stable crack which is required for accurate calculation of the fracture surface energy. Thus the bending method was selected for this study.

2) TESTING DETAILS

The specimens were tested in flexure with a concentrated load applied at the midspan in the Instron Universal Testing Machine using specially designed adaptors. The 1 x 1 x 12" beams were tested on a 10" span (Figure 27) and the 0.1 x 1 x 4" beams were tested on a 3" span. The beams that were 0.1" thick were tested in a special apparatus to prevent side motion of the beam during testing (Figure 28). The testing machine is a "hard" one which applies a constant rate of deflection. The loads due to the imposed deflection are recorded automatically. The area under the load-deflection curve is the work done by the machine to break the beam and to create the new surfaces. The fracture surface energy is then obtained by dividing the energy by twice the remaining cross-section of the beam at the point where it was notched.

To find the effect of notch depth and material type on the crack propagation patterns created, specimens were notched to 0.25", 0.5", and 0.75" and then tested at the cross-head rate of .02"/min. Using time lapse photography with a camera having a maximum speed of 64 frames per second, pictures of the crack propagation patterns were taken for subsequent examination.

3) MATERIALS, EQUIPMENT AND SPECIMEN PREPARATION

The tests were conducted on specimens of Chelmsford (Mass.) granite and Danby (Vt.) marble. The properties of these rocks are given in Table 1. The rocks were received in the laboratory in the form of 1 x 1 x 12" beams.

Four different geometries of beams were used in this study and for each geometry, tests were conducted on different notch depths. The beam geometries were as follows:

Type A	1" x 1" x 12"
Type B	1" x 1" x 4"
Type C	0.5" x 1" x 4"
Type D	0.1" x 1" x 4"

The notching and/or cutting of the specimens were done by a modified horizontal shaper (Figure 26).

To heat-treat the beams, they were placed in an electric oven set for 1000°F., and kept there for 50 minutes. The specimens were cooled to room conditions after removal from the oven and tested within 24 hours.

Other specimens were exposed to laser radiation for five seconds (Figure 29) producing a total exposure of 600 watts. The specimens were then cooled to room conditions and testing was done within 24 hours after exposure.

VI. RESULTS AND DISCUSSION OF RESULTS

In this section the experimental results are presented and discussed in three sections:

1. Fracture surface energy of untreated specimens.
2. Fracture surface energy of treated specimens.
3. Crack propagation observations.

1. FRACTURE SURFACE ENERGY OF UNTREATED SPECIMENS

The variation of fracture surface energy with notch depth for type A, 1" x 1" x 12", granite beams tested at a mid-span deflection rate of .002 inches per minute is shown in Figure 30. The curve has a sharp descent between 0 - 0.3" notch depth. The high values at low notch depths are caused by semi-stable or unstable fractures. The variations of fracture surface energy with notch depth for the three other geometries used in this study (B,C,D) are shown in Figures 31, 32, and 33. The shape of all these curves is similar.

The input work, from which the value of fracture surface energy is calculated, is the area under the load deflection curve. The weight of the beam, however, contributes to the input energy through the displacement of the beam during testing. At large notch depths the value of the energy contributed by the specimen weight becomes significant. A correction can be made for this discrepancy by adding the contribution of beam weight to the value of fracture surface energy which is computed from the load deflection curve. The corrected values corresponding to all sizes are plotted in Figure 34 and a very good agreement is evident. This indicates that the value of the fracture surface energy is independent of the dimensions of the specimen, providing a stable fracture is achieved. The value of fracture surface energy for a particular geometry and notch depth is, however, dependent

upon the rate of deflection as well as on the nature and the duration of any treatment which the specimen may have undergone prior to testing.

As mentioned earlier, all rocks have a preferred orientation for their pre-existing flaws which may change their apparent strength if the direction of the applied stress is changed. The reason for this variation is that in conventional testing methods, fracture is always catastrophic because of the excess energy stored in the specimen prior to crack initiation. However, the critical crack propagates when the applied stress and its orientation causes a tensile stress at the tip of the crack equal to the ultimate tensile strength of the rock. Since the fracture is always catastrophic and the load to rupture is dependent upon crack orientation, a large variation in the apparent strength is obtained.

For the granite used in this study, the mica particles which comprise the principal weak-points seem to be oriented in parallel planes. To find the effect of orientation on the fracture surface energy two series of specimens were prepared; one parallel to the mica plane and the other perpendicular to the mica plane. The difference in the values of fracture surface energy obtained for these two was well within the experimental scatter. This indicates that the value of fracture surface energy, being a property of the material, is less affected by the orientation of pre-existing flaws.

The corrected variation of fracture surface energy with notch depth for granite, at the mid-span deflection rate of .02 inches per minute, is shown in Figure 35. The value of stable fracture surface energy is higher than that obtained for the rate of .002 inches per minute. This increase is probably due to the fact that the fracture crack follows a

path other than one of minimum energy when tested at higher deflection rates.

The corrected variation of fracture surface energy with notch depth for marble beams, at the mid-span deflection rate of .002 inches per minute, is shown in Figure 36; and the corrected variation of fracture surface energy with notch depth at the mid-span deflection rate of .02 inches per minute is shown in Figure 37. Comparing these two figures reveals that the values are not significantly affected by the increase in loading rate.

The difference in the rate sensitivity of marble and granite possibly is due to the fact that granite is a multi-phase system whereas marble is more homogeneous. A micro-hardness study of the surfaces of these specimens showed that there is a large variation, up to a factor of 3, between the hardness of the constituents of granite while the variation in the hardness of marble grains is only 20%. Further, the average size of grains is smaller in marble than granite. This indicates that imperfections in a marble specimen are much more closely spaced than in granite although they may not be equally serious in both rocks. Therefore the length of micro-cracks created as a result of a higher deflection rate is greater in granite than in marble, leading to the consumption of higher energies when tested at higher deflection rates.

2. FRACTURE SURFACE ENERGY OF TREATED SPECIMENS

The corrected variation of the fracture surface energy of heat-treated granite specimens with notch depth at mid-span deflection rate of .02 inches per minute is shown in Figure 38. The application of heat reduces the value of the fracture energy of granite specimens, as is evident from a comparison of Figures 35 and 38. This reduction is due to the

partial rupture of grain boundaries and the creation of transgranular cracks.

The effect of heat-treatment on the ultimate flexural load carried by the specimens is shown in Figure 39. This figure was obtained by dividing the ultimate flexural load by the average of such values for untreated specimens. The reduction in the ultimate load is more significant than the reduction in the value of fracture surface energy.

For specimens having a notch depth of 0.25" the fracture mode changes from unstable to semi-stable as a result of heat-treatment, making the change in fracture surface energy less significant than the change in ultimate load.

For specimens having a notch depth of 0.5" the fracture mode does not change significantly after heat treatment, although it tends to approach the stable mode. The deformation to failure, however, increases considerably resulting in a value for fracture surface energy equal to that of untreated specimens.

For specimens having a notch depth of .75" the fracture mode does not change at all after heat treatment but the deformation to failure is increased and the ultimate load is reduced. The value of fracture surface energy for specimens with a .75" notch is lower than that for identical untreated specimens.

The corrected variation of fracture surface energy of heat-treated marble specimens at mid-span deflection rate of .02 inches per minute is shown in Figure 40. Comparison of this figure with the one obtained for unheated marble at the same mid-span deflection rate (Figure 37), shows that the value of fracture surface energy of unnotched marble is not greatly reduced by heating. There is, however, a decrease

in the value of fracture surface energy of specimens with notch depths 0.25" and 0.5". Further, the decrease in the value of ultimate flexural load is quite drastic for marble specimens as shown in Figure 41.

Since marble is a uniform system, the magnitude and orientation of the thermal expansions of neighboring grains are roughly the same, whereas in granite, which is a multi-phase system, they are usually different. Thus the extent of intergranular and transgranular cracking in granite specimens is much greater than in marble. The decrease in strength is not as drastic in granite because even the untreated specimens of granite have a substantial amount of micro-cracks and imperfections which reduce the ultimate strength by stress concentrations. The granite fracture surface energy decreases from heat-treatment because after the treatment there remains a smaller number of grain boundaries to be separated to completely break the specimen. In marble, however, the fracture surface energy does not decrease much because the imperfections causing the decrease in ultimate load constitute a very small portion of the cross section and they do not change the value of stable fracture surface energy.

Microscopic observations of the heat-treated specimens of both marble and granite showed that in heat-treated specimens, transgranular cracks are present as well as intergranular cracks as seen in Figures 42 through 50. In the untreated specimens, however, most of the inherent flaws are intergranular. It is believed the anisotropic expansion of grains was the major factor in producing the intergranular cracks and the transgranular cracks are also created due to the anisotropic expansion of the grains. If heating merely developed intergranular fracture, through anisotropic expansions, then the extent to which a rock can be affected would depend on the

number of boundaries available for fracture, and once these are broken, no further effect should be possible. However, since the grains of a rock are not arranged in any particular order, expansion of one of the crystals may create shear and/or bending stresses in the neighboring grains. Thus, by heating the rock after most of the intergranular cracks have been formed, grains will be subjected to stresses that are indirectly dependent upon temperature. Again, after numerous transgranular cracks have been created, there comes a point when the grains or their fractions do not exert any force on each other and no further cracks will be formed. It is possible that part of the apparent strength of heat-treated specimens is due to mechanical interlocking of these grain pieces.

The corrected variation of fracture surface energy with notch depth for granite specimens exposed to laser and tested at mid-span deflection rate of .02 inches per minute is shown in Figure 51. Comparison of this Figure to Figure 35, which is for untreated granite, shows a pronounced decrease in the fracture surface energy. The changes in fracture modes observed in the specimens exposed to the laser were also observed in heat-treated specimens of granite. The decrease in the value of ultimate flexural load is shown in Figure 52.

Microscopic examination of the lased specimens showed (Figures 53 through 56) the reason for the weakening: the development of cracks due to the temperature gradient, as well as some granular weakening. The corrected variation of fracture surface energy of marble specimens with notch depth for specimens exposed to laser radiation is shown in Figure 57. The decrease in the value of fracture surface energy of marble is not as significant as in granite, although the reduction in ultimate flexural strength is much greater (Figure 58). The changes in fracture modes observed for

heat-treated marble specimens were also observed for the specimens exposed to the laser. Microscopic examinations of these specimens showed (Figures 59,60) the reason for the weakening: the development of cracks due to the temperature gradient, as well as some granular weakening.

3. CRACK PROPAGATION OBSERVATIONS

Analysis of time lapsed photographs correlated with the stress-strain curves from the testing machine, show that the crack becomes visible when the specimen deforms a few thousandths of an inch beyond the point at which the ultimate load is sustained, as shown in Figure 61. This is due to the fact that the cracks formed at ultimate load are micro-cracks which must be extended to become visible with the camera. If the mid-span deflection rate of .02 inches per minute is used, the crack patterns obtained are similar to those at the .002 inch rate. Since testing the specimens at the higher rate has time advantages, it was used throughout this phase of the study. Typical results obtained from these observations are shown in Tables 2, 3, 4, and 5.

Analysis of the data obtained from untreated specimens of granite with notch depths 0.25", 0.5", and 0.75" revealed that as the notch depth is increased the cracks tend to have less branching and also follow shorter paths to the top of the specimens as shown in Figures 62, 63, and 64. The paths of the cracks are mostly intergranular, seldom transgranular and frequently pass through the mica segments of the cross section. In the specimens with a small notch depth, a high value for fracture surface energy is obtained and also a larger amount of branching occurs in the specimens. This indicates that some of the energy required to fracture the specimens is consumed in crack branching.

The heat-treated granite specimens showed cracking patterns generally similar to that of untreated specimens, however, the number of transgranular cracks increased due to the treatment. A typical specimen is shown in Figure 65. The crack propagation patterns in specimens that were exposed to laser radiation were similar to the heat-treated specimens.

The failure of the untreated marble specimens was accompanied by a diminution in transparency in a narrow region at the center of the specimens as shown in Figure 66. It is believed this is due to the weakening and/or rupture of the grain boundaries, under the applied stress. In the heat-treated marble specimens the grain boundaries are much more distinct. Failure in these specimens is accompanied by a crack which follows those created by the prior heat treatment, as shown in Figure 67.

The crack patterns in the marble specimens exposed to the laser were similar to those in the heat-treated specimens.

VII. CONCLUSIONS AND SUGGESTIONS FOR FUTURE WORK

Based on the data collected and observations made during the course of this study, the following conclusions seem valid:

1. The energy required to propagate a crack and to create new surfaces can be easily and conveniently measured using a bending method of testing.

2. The value of fracture surface energy is a property of the material and does not change with changes in geometry or orientation.

3. To avoid incorporation of excess energy in the value of fracture surface energy, a specimen geometry should be selected such that a stable fracture is produced, and also the lowest mid-span deflection rate should be used.

4. The value of fracture surface energy for granite is increased with increasing deflection rate due to the formation of additional microcracks.

5. The value of fracture surface energy for marble is not changed with increasing deflection rate.

6. The application of heat to granite causes a decrease in the ultimate flexural load and a decrease in the value of fracture surface energy.

7. The application of heat to marble causes a decrease in the ultimate flexural load although the value of fracture surface energy remains essentially unchanged.

8. The application of heat to marble and granite causes weakening and/or rupture of the grain boundaries and also the development of transgranular cracks.

9. The exposure of rocks to laser radiation has the same effects as does heat treatment, though in much shorter periods of time.

10. The major mechanisms by which rocks are weakened by laser radiation are the development of thermal stresses due to a severe temperature gradient, and the development of intergranular and transgranular cracks.

The results of this study show that the following areas are of interest and may warrant investigation:

1. The variation of fracture surface energy and ultimate flexural strength in marble and granite over a broader range of deflection rates should be examined. This should include heat-treated specimens and specimens exposed to laser irradiation.

2. A study to find the effect of temperature level and duration on the fracture surface energies and the ultimate flexural strengths of rock should be done.

3. The effect of laser power level and duration of exposure on the fracture surface energies and ultimate flexural strengths of rock should be explored. This should include the determination of weight loss and chemical changes and character of microcracks created by the temperature gradients encountered.

Property	Danby Marble [1]	Chelmsford Granite [2]
Principal Constituents	Calcite	Feldspar Quartz Muscovite Biotite
Color	White	Light Gray
Density lbs./cu. ft.	170.9	163
Porosity	0.48	1.51-1.62
Absorption by Weight 48 Hours	0.102	0.32
Thermal Conductivity BTU/in./hr./sq. ft./°F.	15.0	
Minimum Abrasive Hardness Coefficient	10.6	
Compressive Strength psi	10,550	24,460 ^[3] 27,500 ^[4]
Modulus of Rupture psi Minimum Maximum	1,450	1,460 ^[5] 2,500 ^[5]
Modulus of Elasticity psi Minimum Maximum	7.4 x 10 ⁶	1.7 x 10 ⁶ 3.3 x 10 ⁶
Shear Strength psi Minimum	2,300	

- 1) Data obtained from the Vermont Marble Company
- 2) Data obtained from Kessler et. al. (Reference [22])
- 3) Perpendicular to Rift
- 4) Parallel to Rift
- 5) Obtained from beam specimens

TABLE 1

Properties of the Rocks Used in this Study


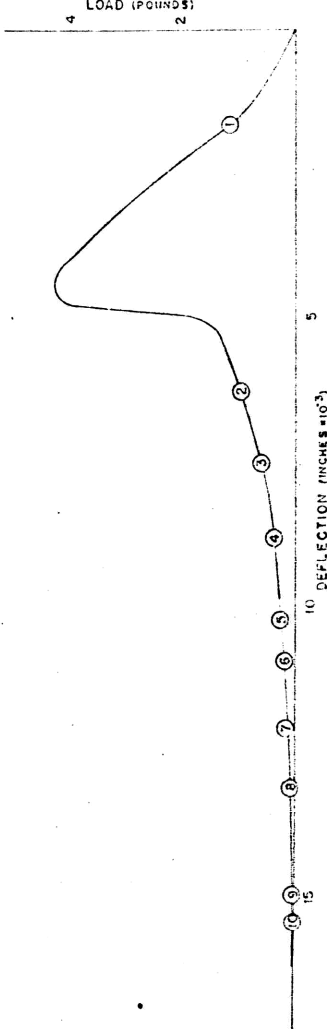
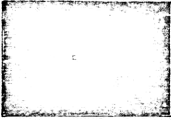



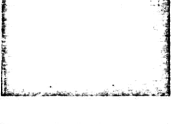


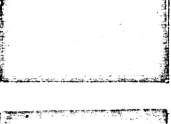
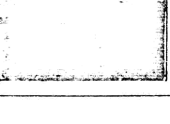
PICTURE NUMBER	MIDSPAN DEFLECTION (INCHES)	ELAPSED TIME (SECONDS)	CRACK LENGTH (INCHES)	APPEARANCE OF SPECIMEN	LOAD-DEFLECTION CURVE
1	.0023	6.90	.75		
2	.0062	18.60	.75		
3	.0075	22.60	.75		
4	.0089	26.60	.75		
5	.0102	30.60	.80		
6	.0109	32.60	.80		
7	.0122	36.60	.82		
8	.0132	39.60	.84		
9	.0149	44.60	.86		
10	.0154	46.20	.86		

TABLE 2
 THE CRACK PROPAGATION
 PATTERN FOR AN UNHEATED
 GRANITE SPECIMEN


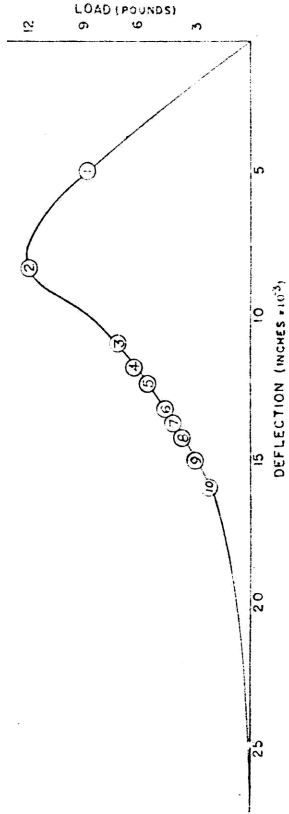
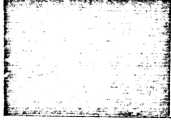

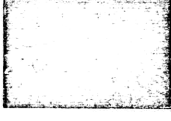

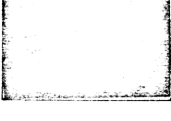
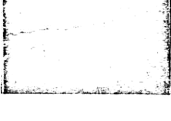
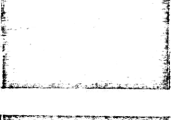
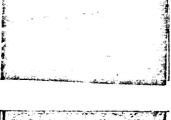
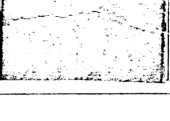
PICTURE NUMBER	MIDSPAN DEFLECTION (INCHES)	ELAPSED TIME (SECONDS)	CRACK LENGTH (INCHES)	APPEARANCE OF SPECIMEN	LOAD- DEFLECTION CURVE
1	.0056	1680	.25		
2	.0087	26.10	.45		
3	.0108	32.40	.50		
4	.0118	35.40	.52		
5	.0122	36.60	.65		
6	.0128	38.40	.75		
7	.0135	40.50	.85		
8	.0141	42.30	.85 ⁺		
9	.0150	45.00	.85 ⁺		
10	.0163	48.90	.85 ⁺		

TABLE 3

THE CRACK PROPAGATION
PATTERN FOR A HEATED
GRANITE SPECIMEN


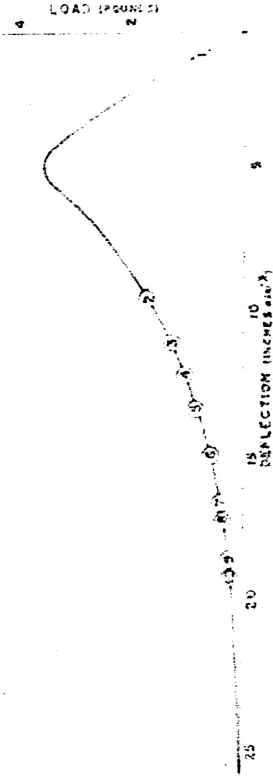




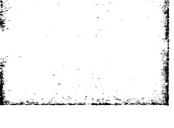
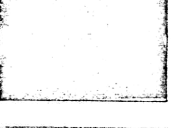
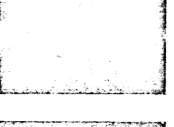
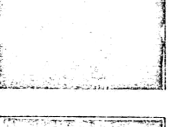
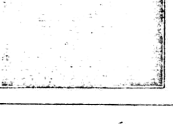
PICTURE NUMBER	MIDSPAN DEFLECTION (INCHES)	ELAPSED TIME (SECONDS)	CRACK LENGTH (INCHES)	APPEARANCE OF SPECIMEN	LOAD-DEFLECTION CURVE
1	.0016	4.80	.25		
2	.0097	29.30	.35		
3	.0109	32.60	.40		
4	.0123	37.00	.43		
5	.0136	40.80	.45		
6	.0149	44.80	.62		
7	.0166	49.80	.70		
8	.0173	51.80	.70		
9	.0186	55.80	.72		
10	.0191	57.40	.72		

TABLE 4

THE CRACK PROPAGATION
PATTERN FOR A HEATED
MARBLE SPECIMEN


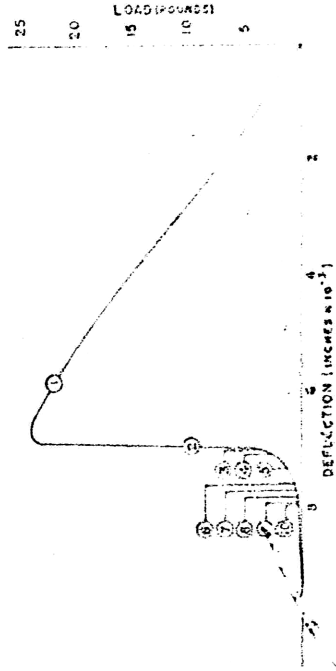








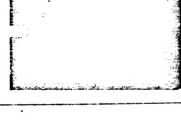
PICTURE NUMBER	MIDSPAN DEFLECTION (INCHES)	ELAPSED TIME (SECONDS)	CRACK LENGTH (INCHES)	APPEARANCE OF SPECIMEN	LOAD-DEFLECTION CURVE
1	.0058	17.40	—		
2	.0068	20.40	—		
3	.0070	20.90	—		
4	.0071	21.10	—		
5	.0073	22.00	—		
6	.0076	22.80	—		
7	.0077	23.20	—		
8	.0078	23.40	—		
9	.0079	23.60	—		
10	.0079	23.70	—		

TABLE 5

THE CRACK PROPAGATION
PATTERN FOR AN UNHEATED
MARBLE SPECIMEN

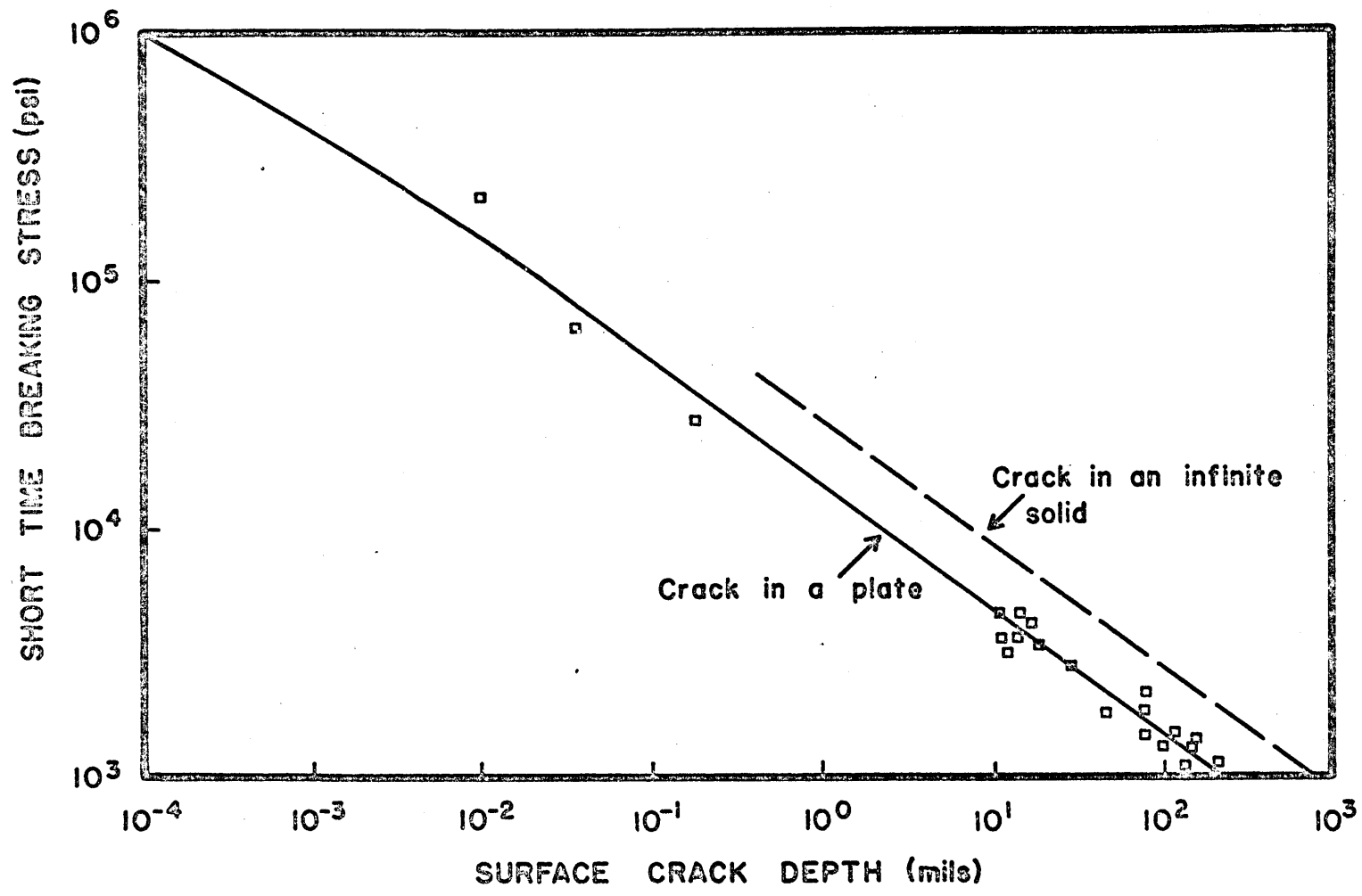


Figure 1 Fracture strength vs. size of crack, for glass [Ref. 2]

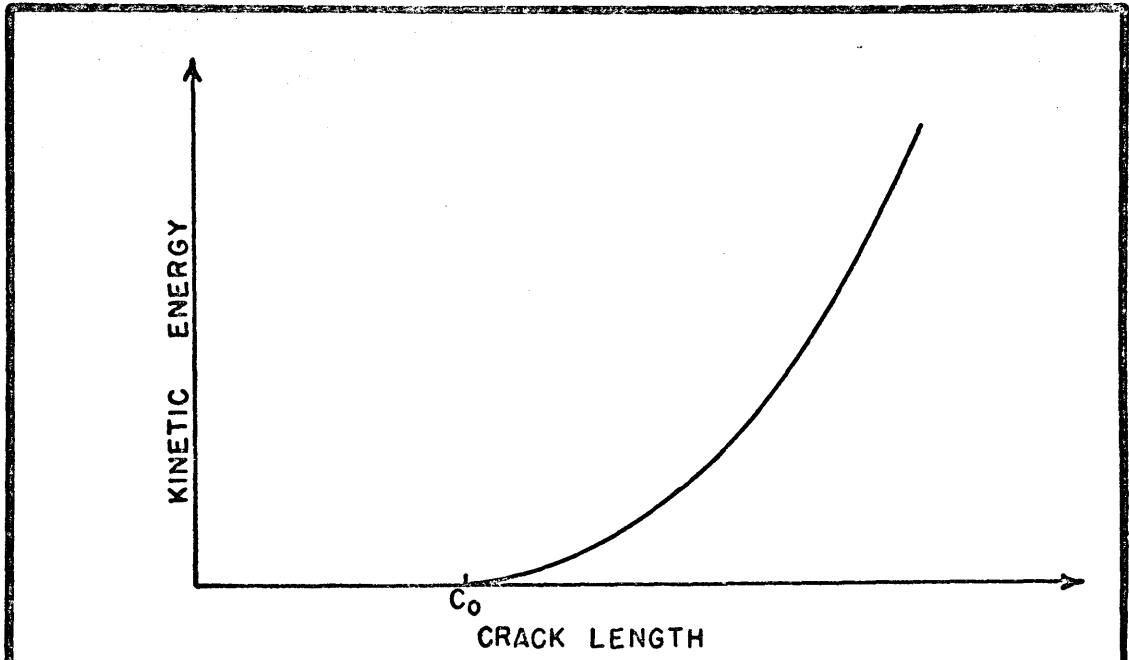


Figure 2 Kinetic energy vs. crack half length [Ref. 3]

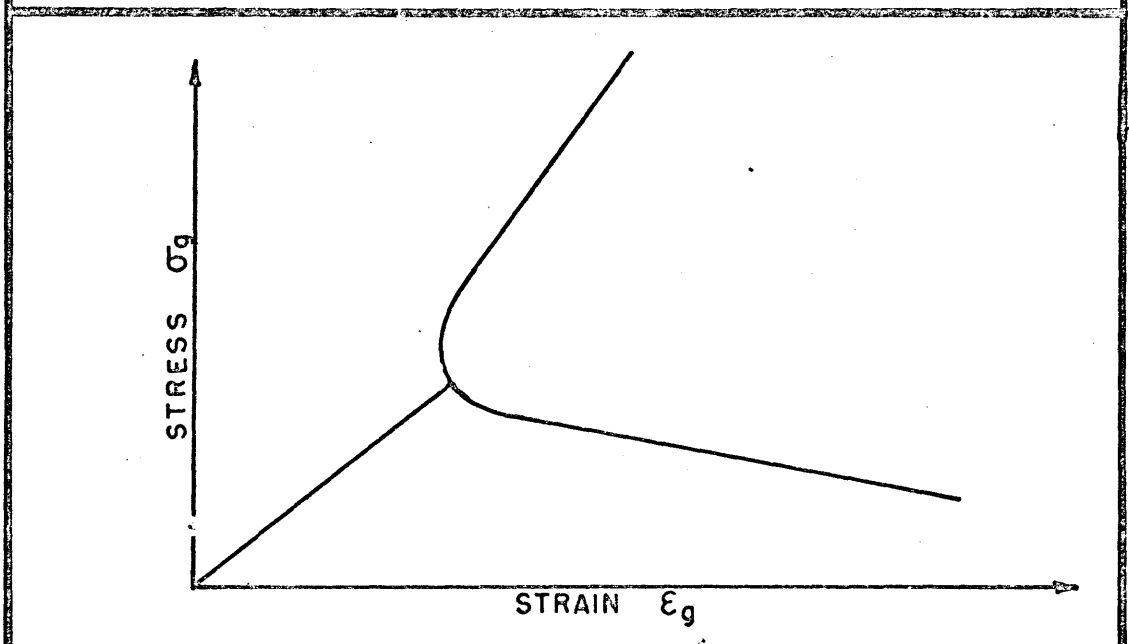


Figure 3 Stress - Strain relation based on Griffith criterion [Ref. 3]

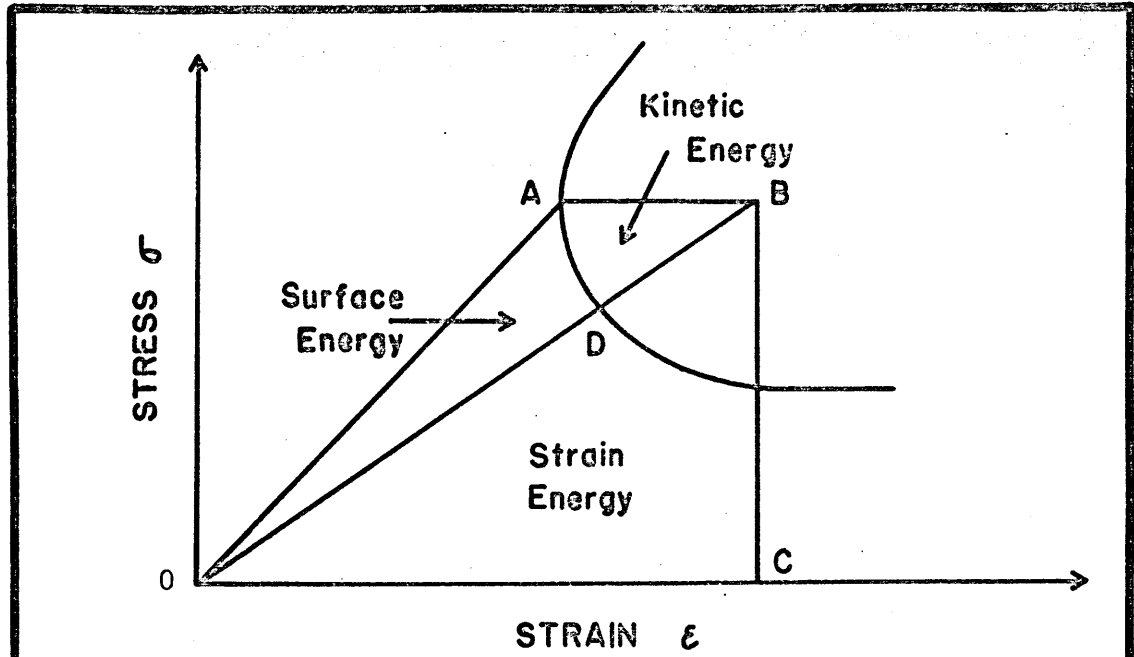


Figure 4 Graphical determination of fracture surface energy and kinetic energy [Ref. 3]

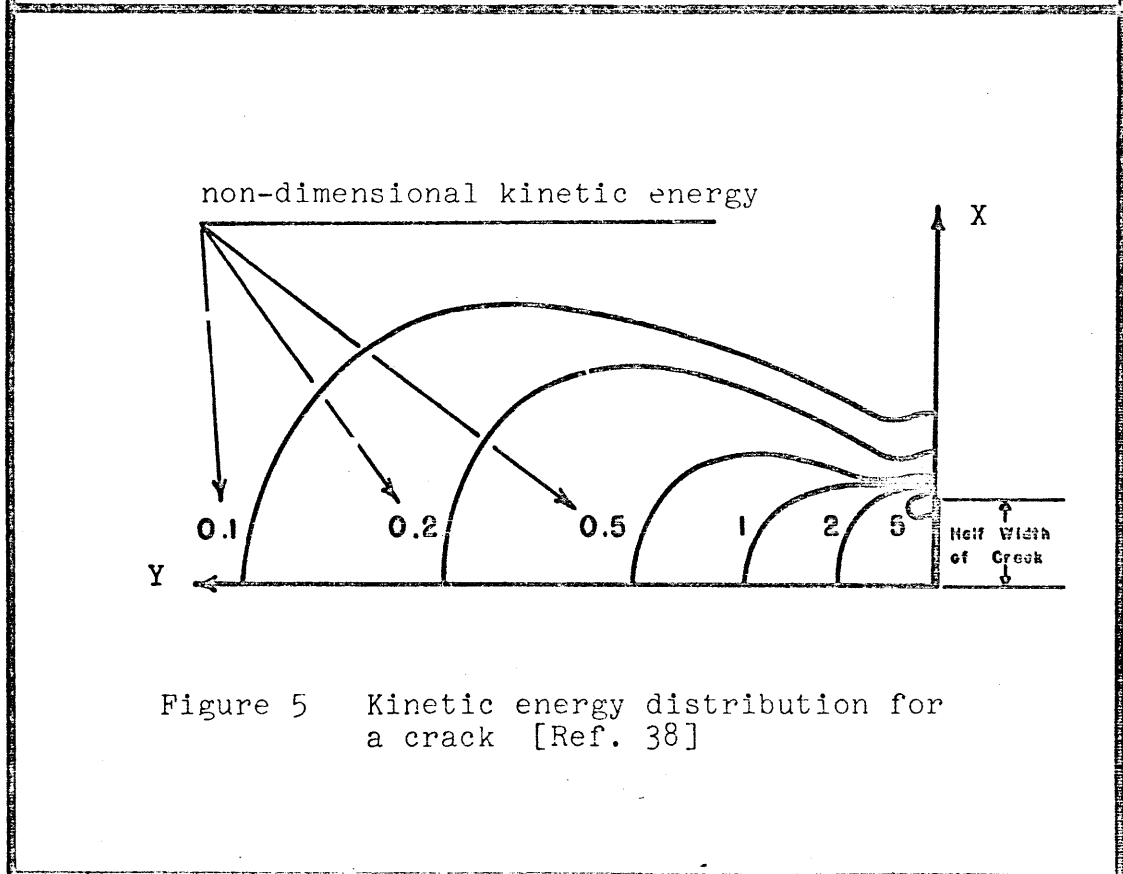


Figure 5 Kinetic energy distribution for a crack [Ref. 38]

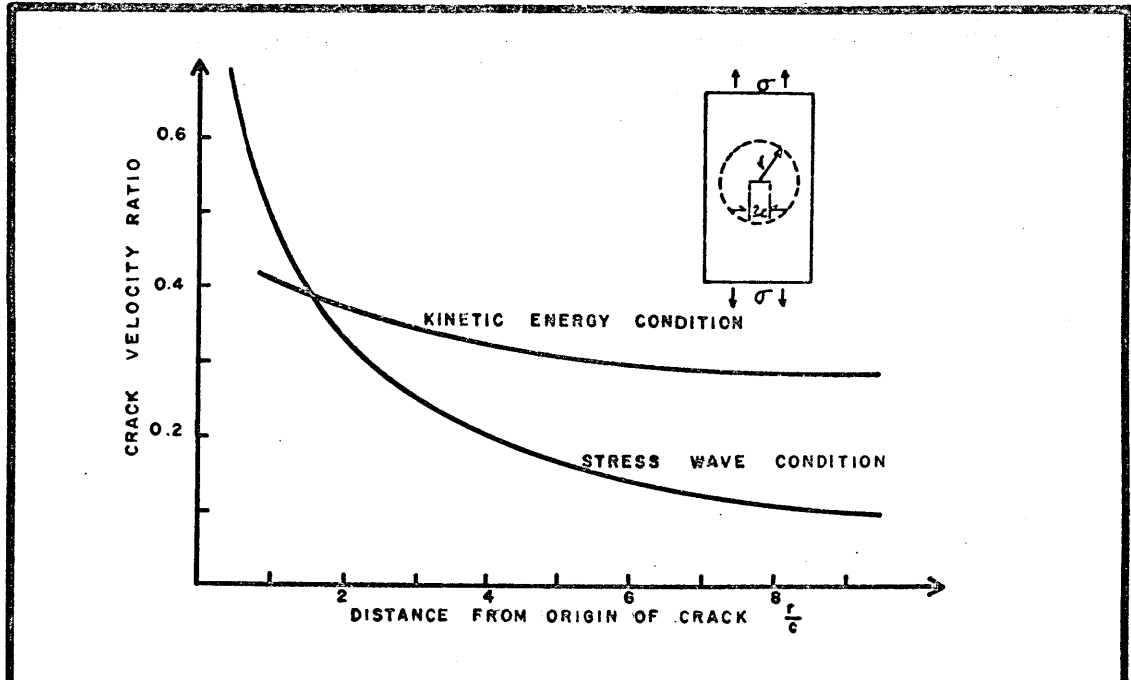


Figure 6 Effect of stress wave propagation on crack velocity [Ref. 38]

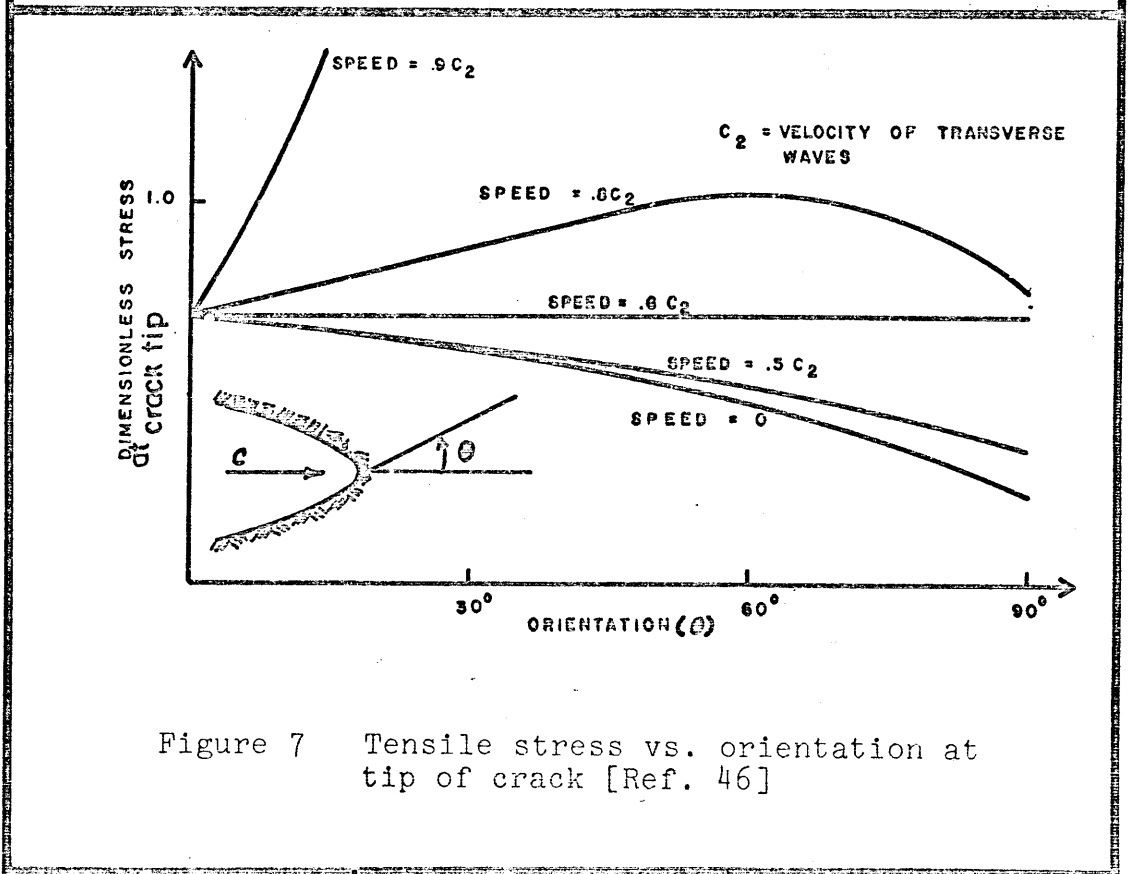
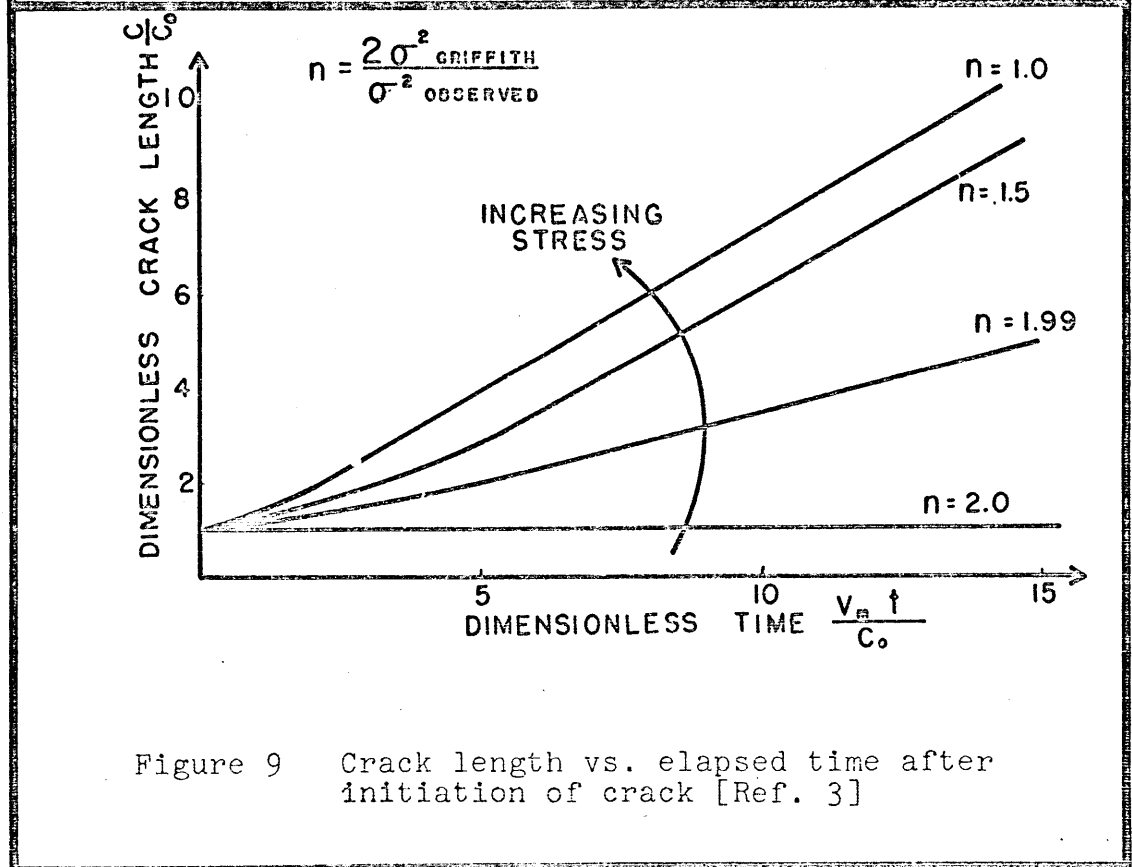
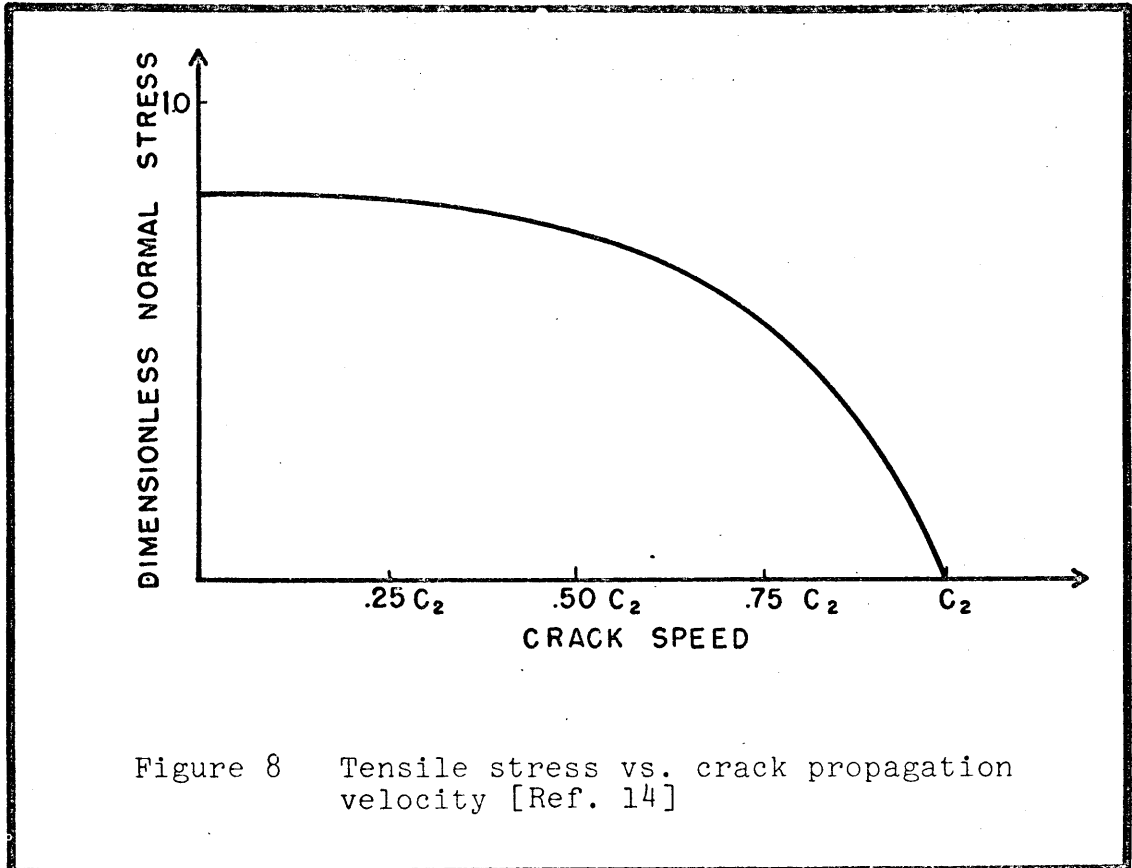


Figure 7 Tensile stress vs. orientation at tip of crack [Ref. 46]



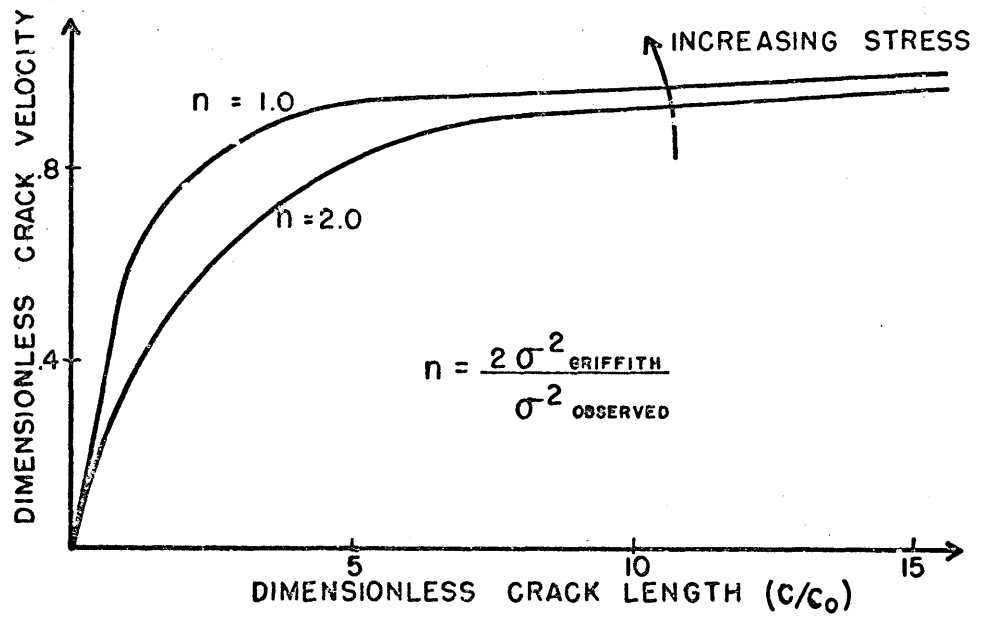


Figure 10 Crack propagation velocity vs. crack length [Ref. 3]

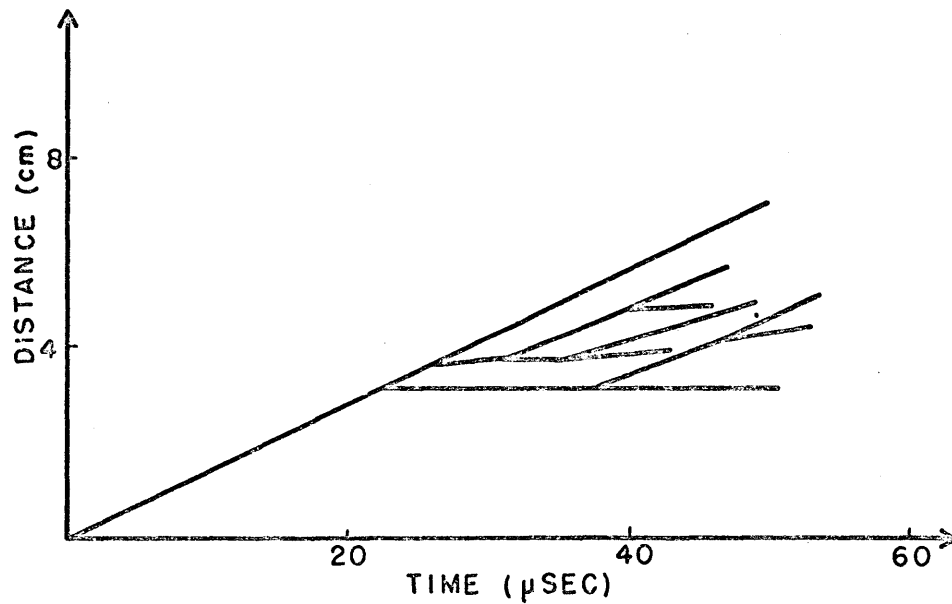


Figure 11 Distance travelled by crack tip vs. elapsed time, for glass [Ref. 43]

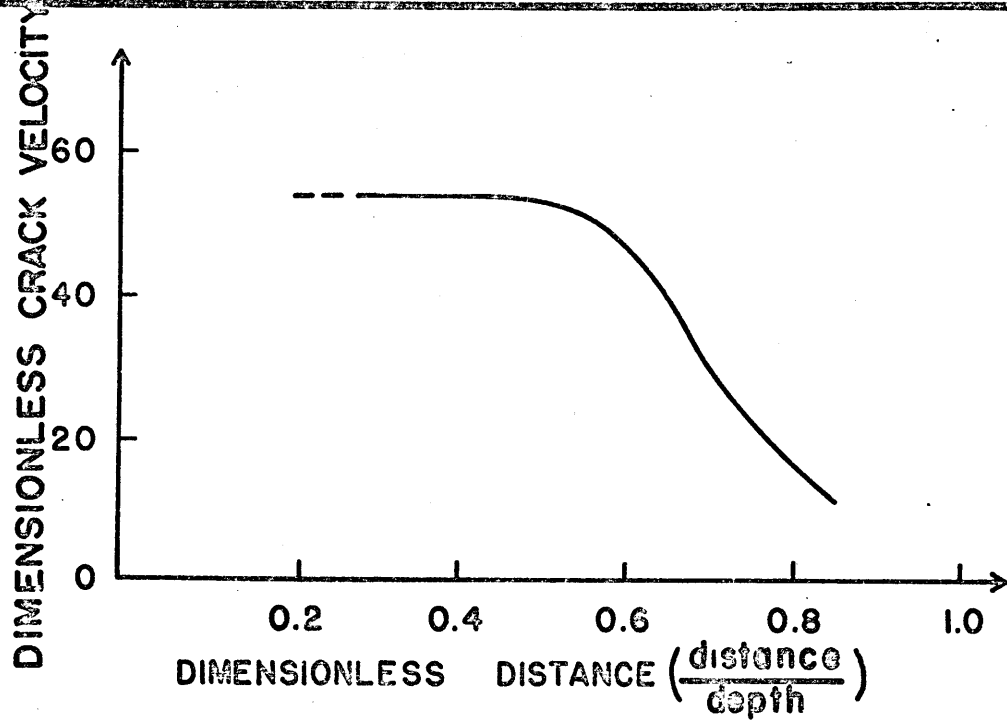


Figure 12 Fracture Velocity vs. Depth for a Glass Bar in Bending [Ref. 40]

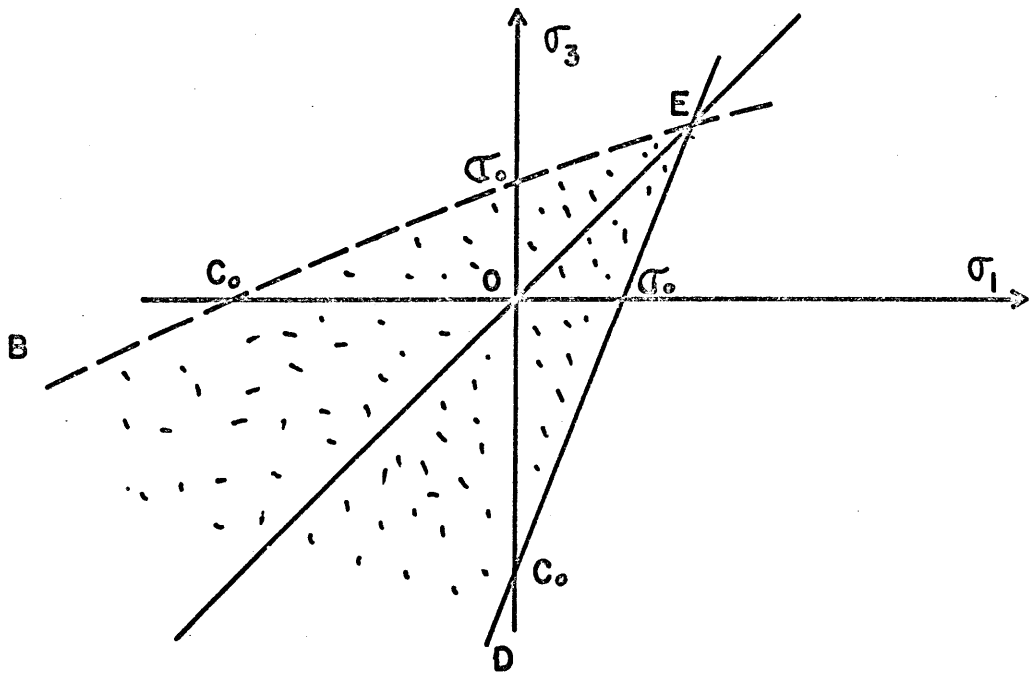


Figure 13 Coulomb-Navier Criterion for Two Normal Stresses [Ref. 29]

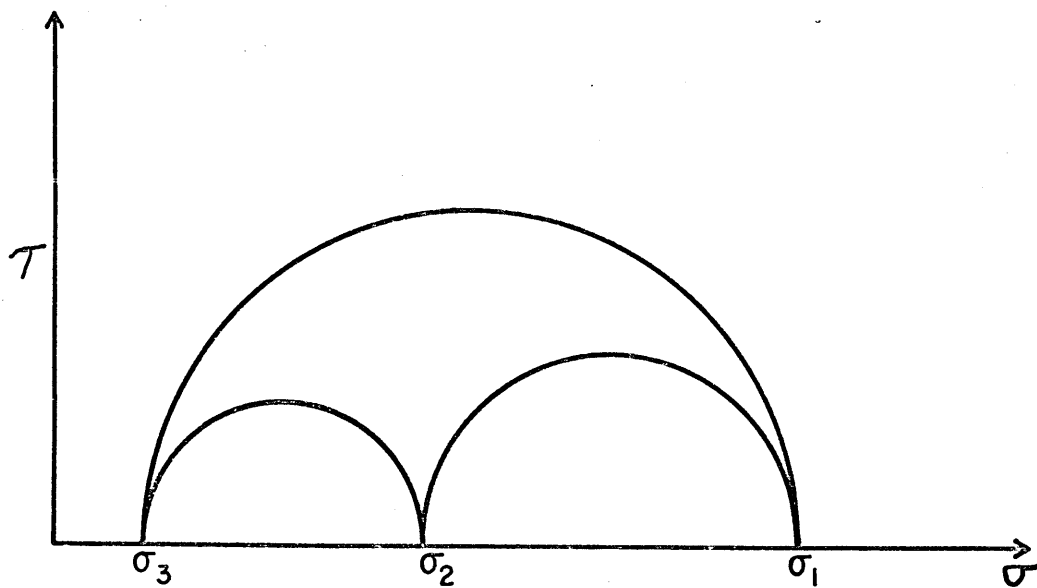


Figure 14 Mohr circle for graphical representation of stress states in terms of applied stresses [Ref. 45]

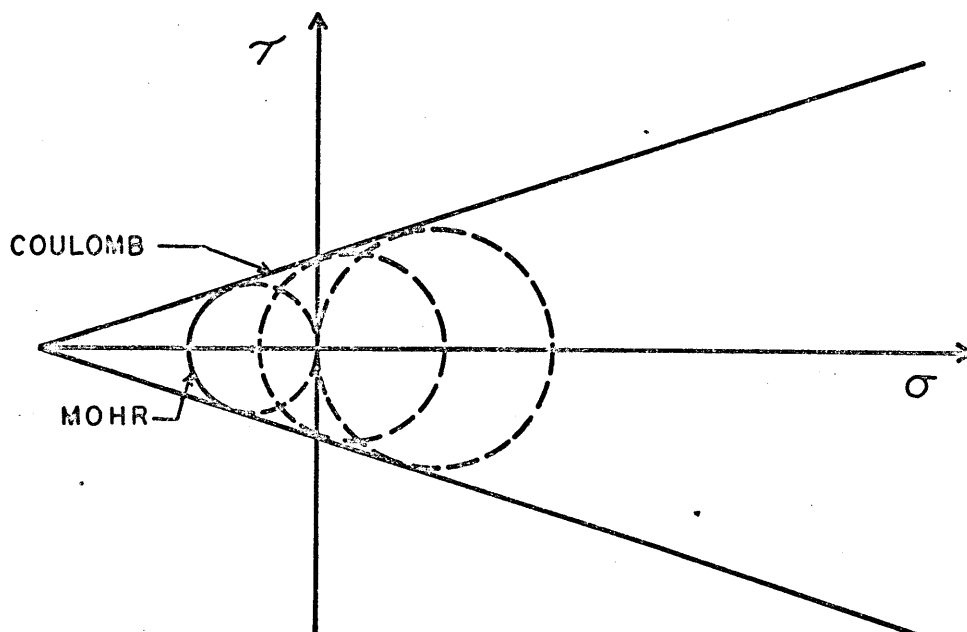


Figure 15 Failure envelopes as suggested by Coulomb and Mohr [Ref. 32]

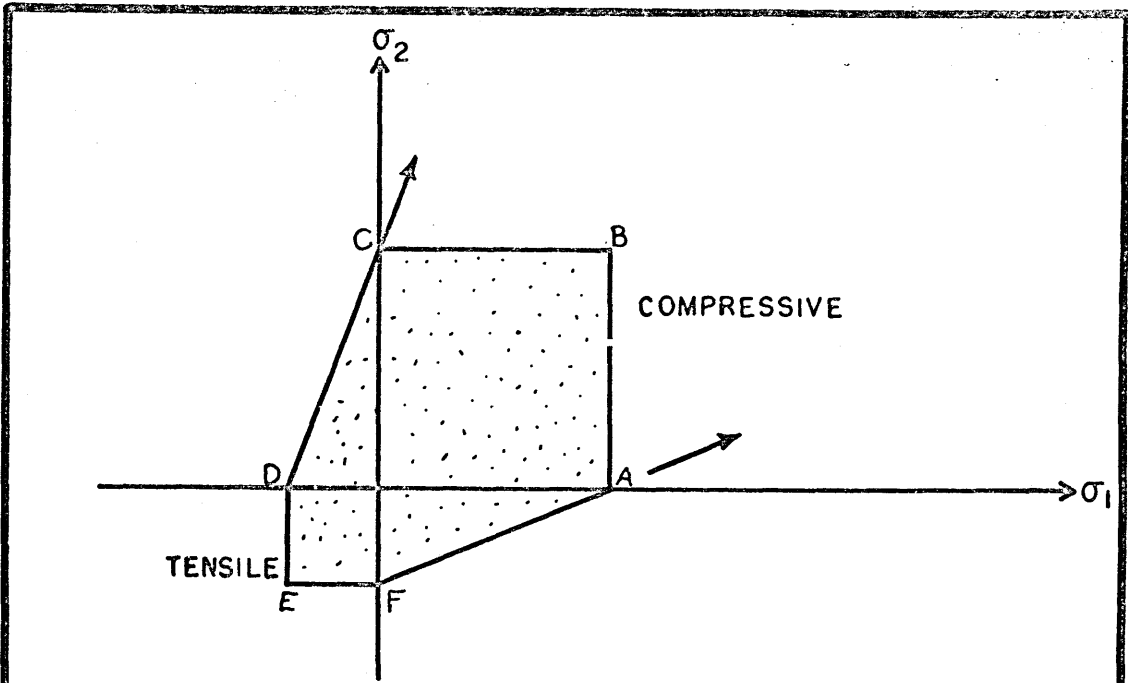


Figure 16 Graphical representation of Mohr Theory for two normal stresses [Ref. 32]

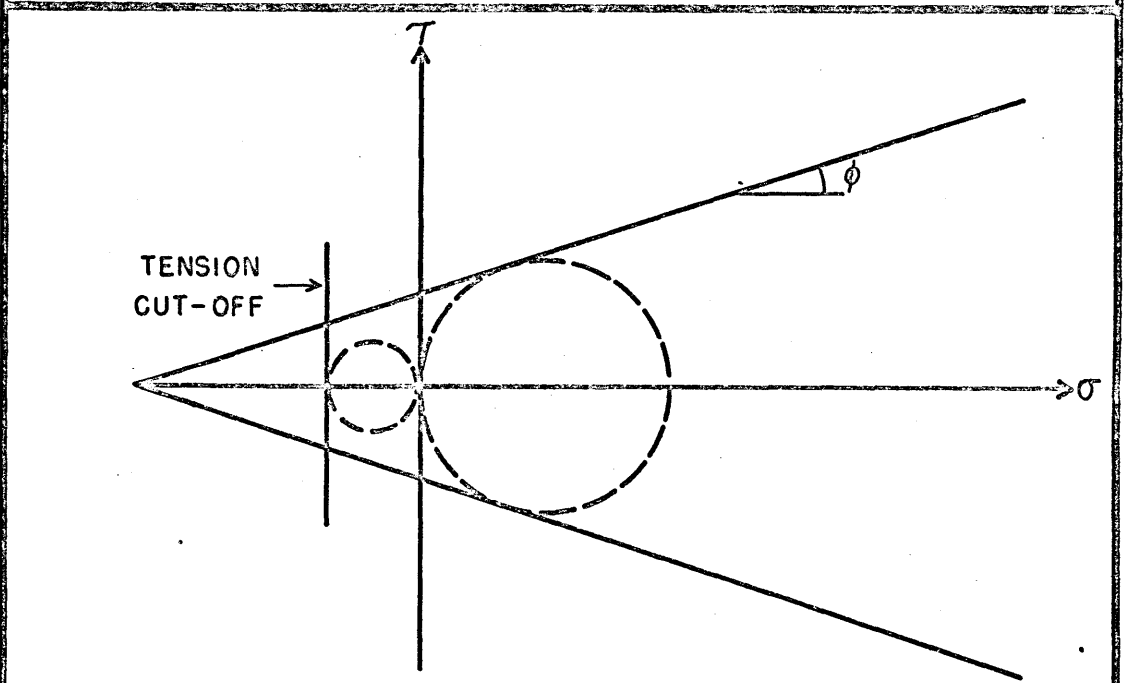


Figure 17 Modification of Coulomb - Navier - Mohr failure criterion [Ref. 32]

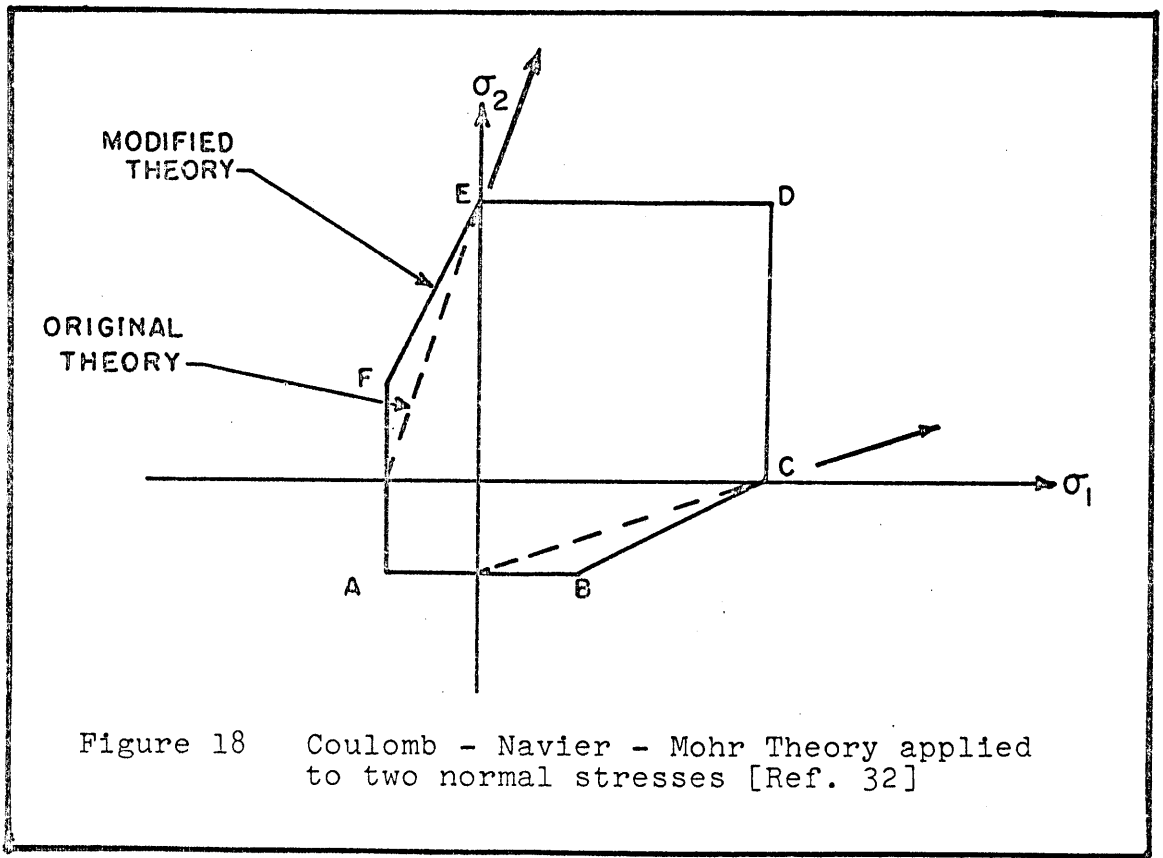


Figure 18 Coulomb - Navier - Mohr Theory applied to two normal stresses [Ref. 32]

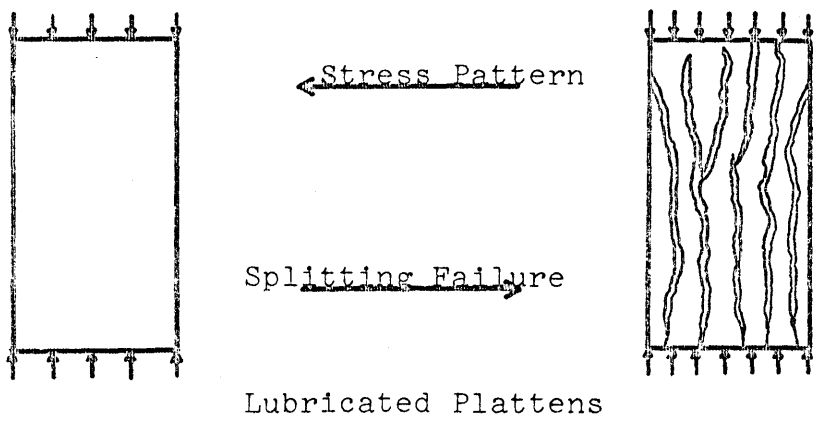
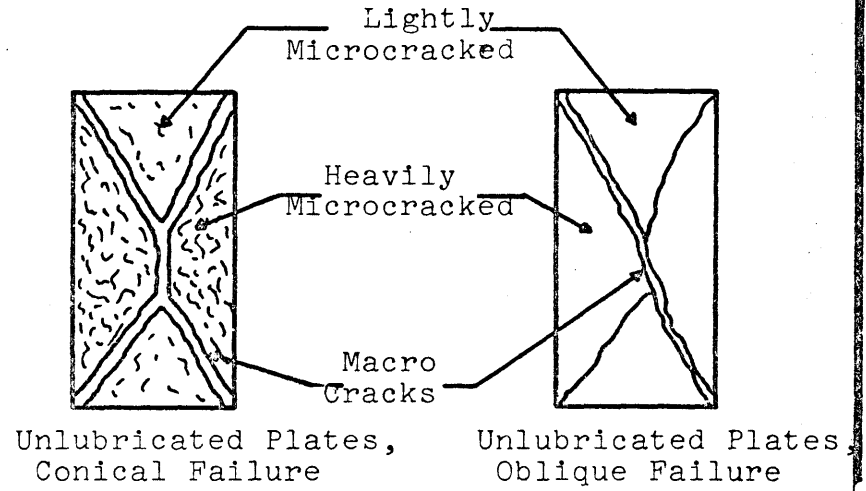
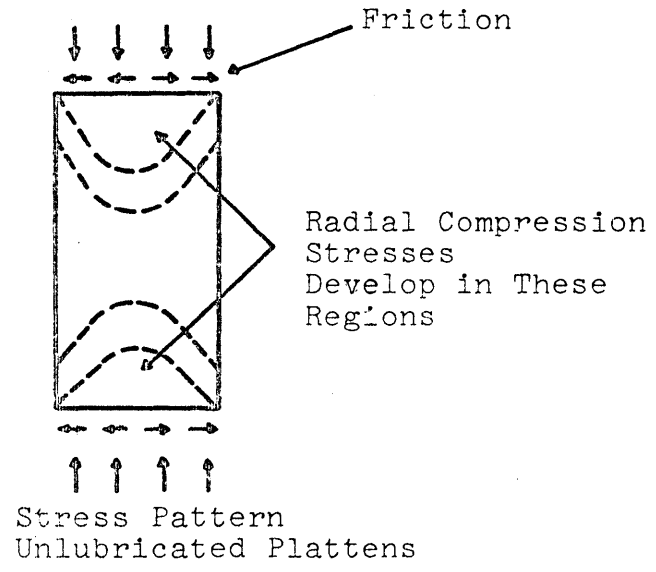


Figure 19
Effect of Lubrication of
End Plates on the
Failure Mode of Compression
Specimens [Ref. 33]

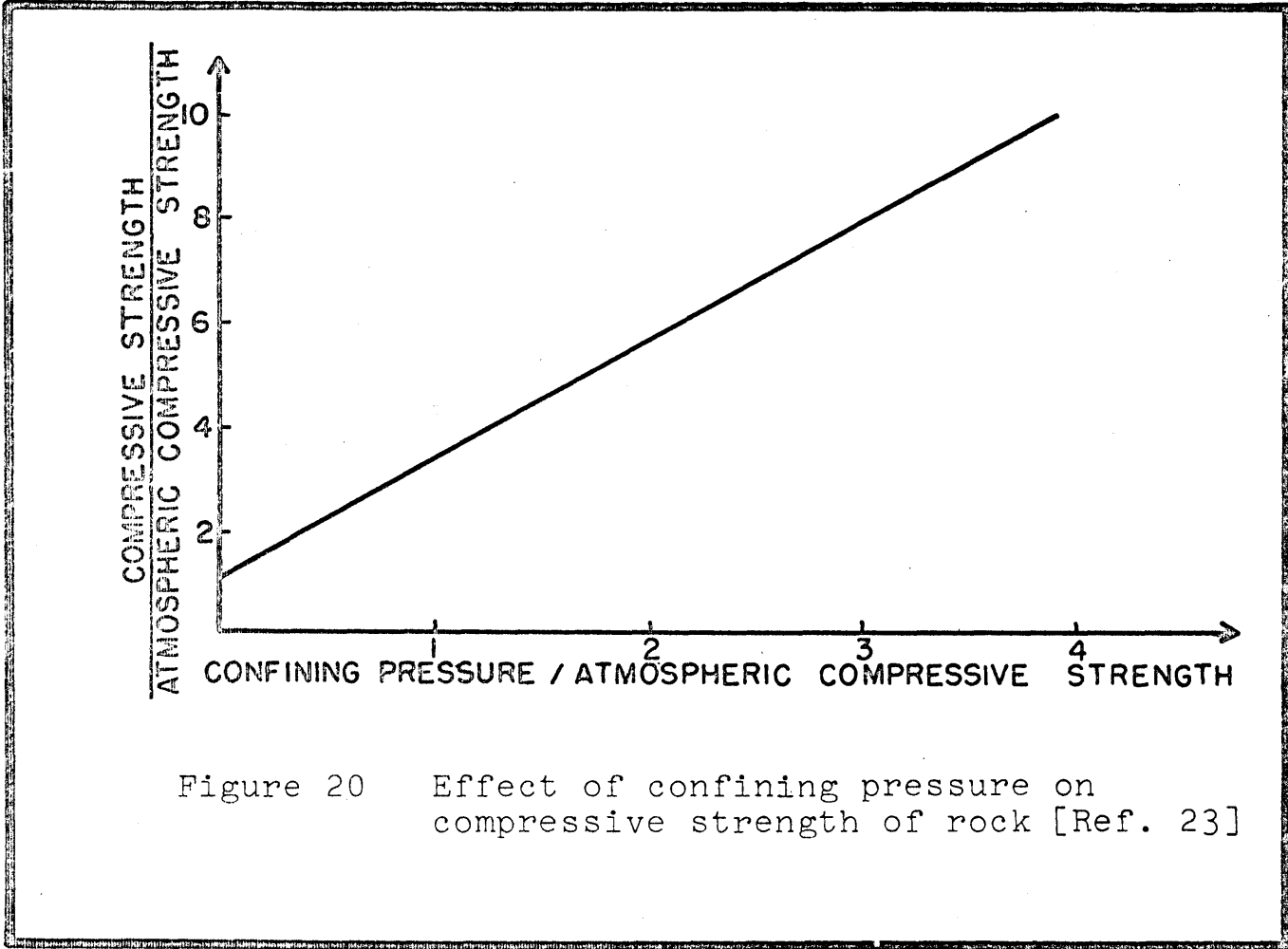
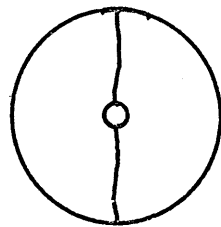
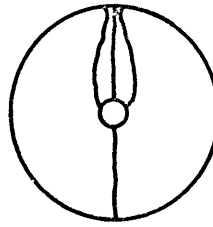


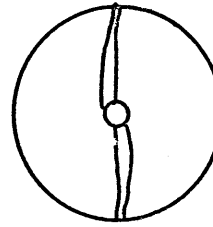
Figure 20 Effect of confining pressure on compressive strength of rock [Ref. 23]



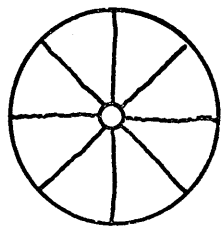
SINGLE



BRANCHED



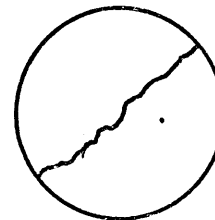
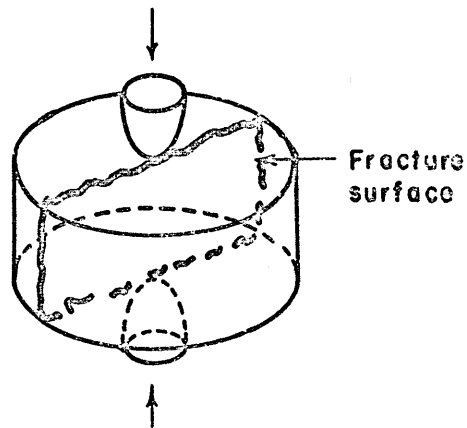
S-SHAPED



CROSS
SHAPED

Figure 21

Major Types of Fracture
Occurring in Transverse
Compression of Disks
[Ref. 37]



Orientation of
Fracture

Figure 22 Direction of Fracture of Disks
under Point Load Stresses [Ref. 24]

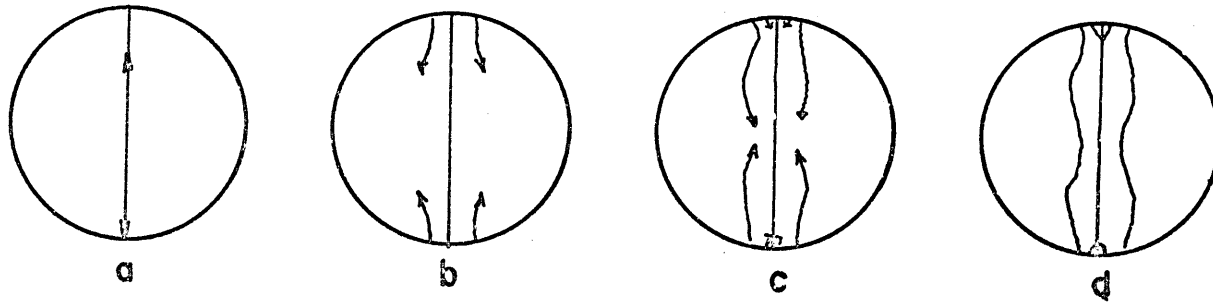


Figure 23 Stages of failure in Brazilian test [Ref. 9]

- a) primary fracture initiation
- b) secondary fracture cracks near the surfaces
- c) tertiary fracture initiation
- d) final stage of fracture

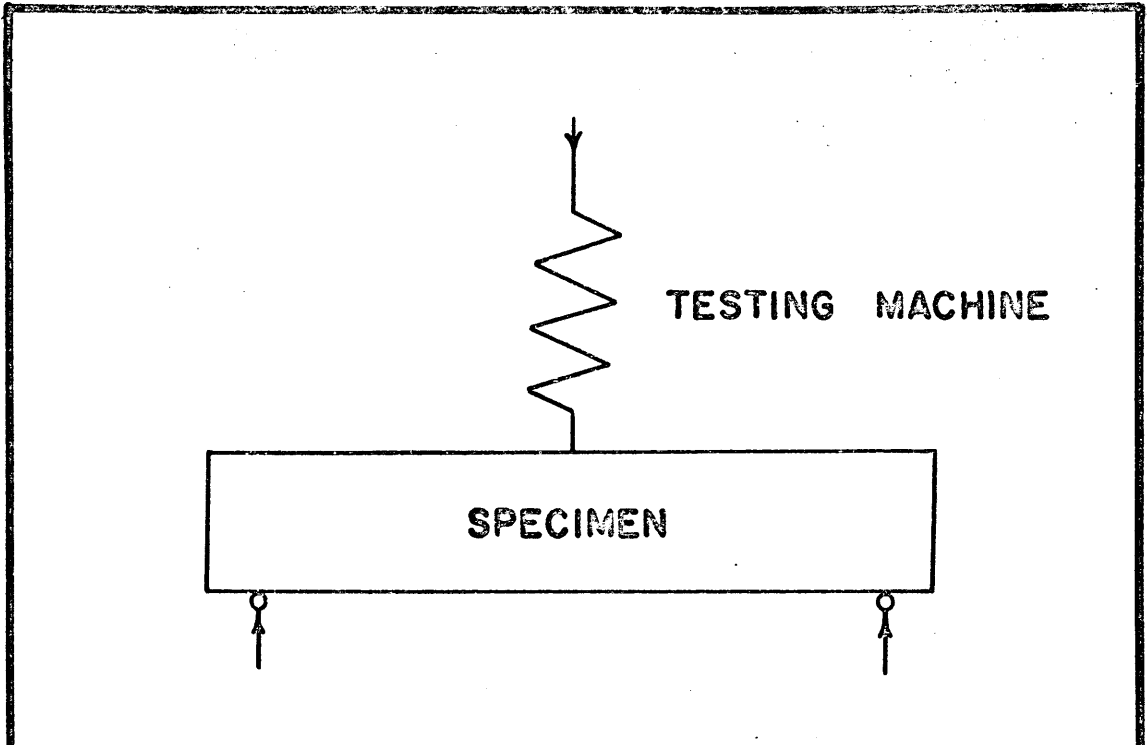


Figure 24 Schematic of Bending Test [Ref. 28]

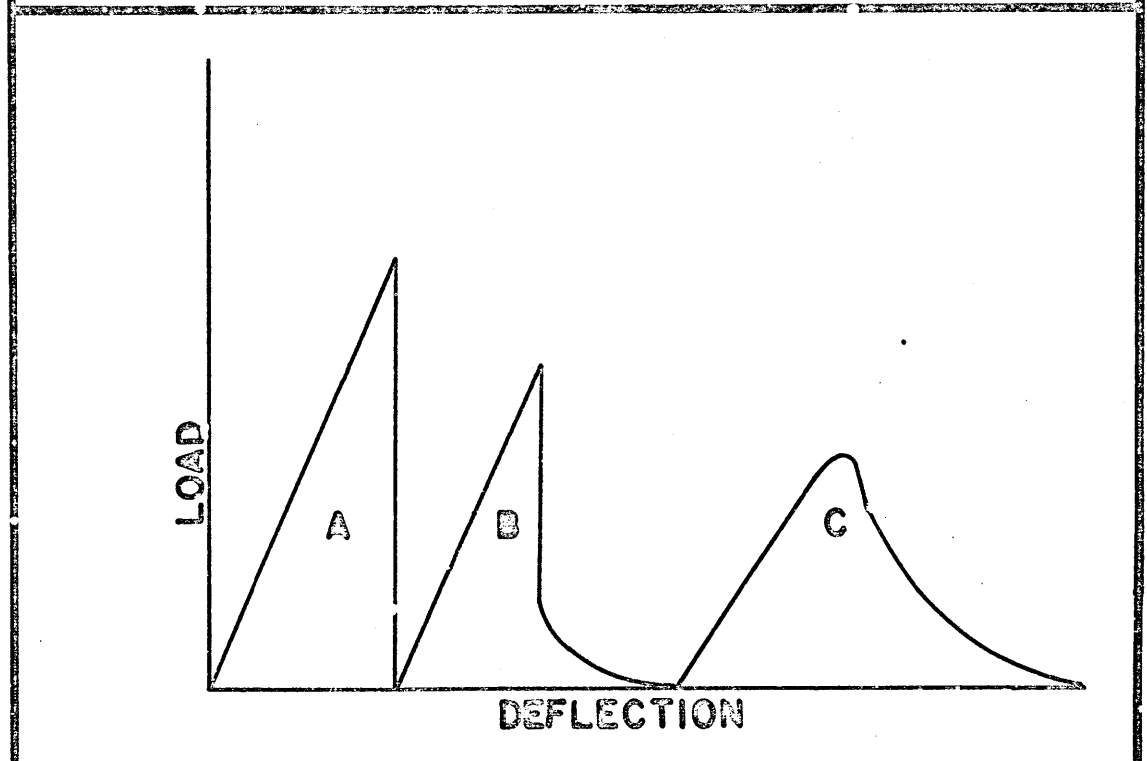


Figure 25 Typical Load Deflection Curves [Ref. 28]
 A - unstable, B - semistable, C - stable

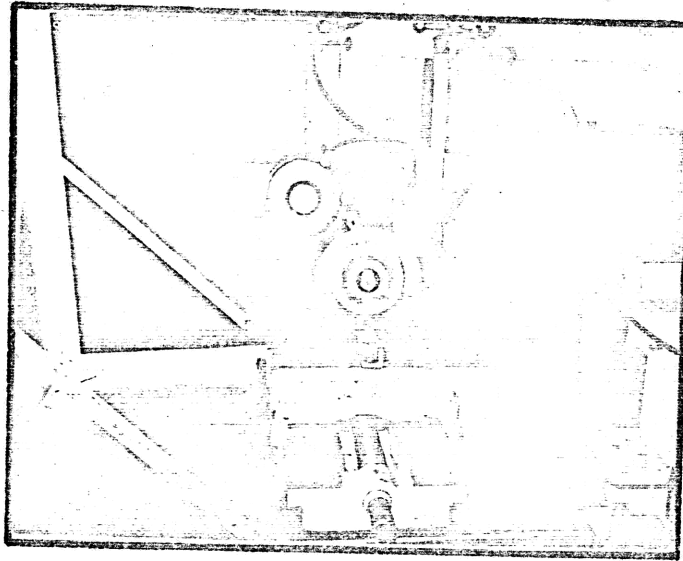


Figure 26 The Modified Shaper Used to Prepare the Specimens

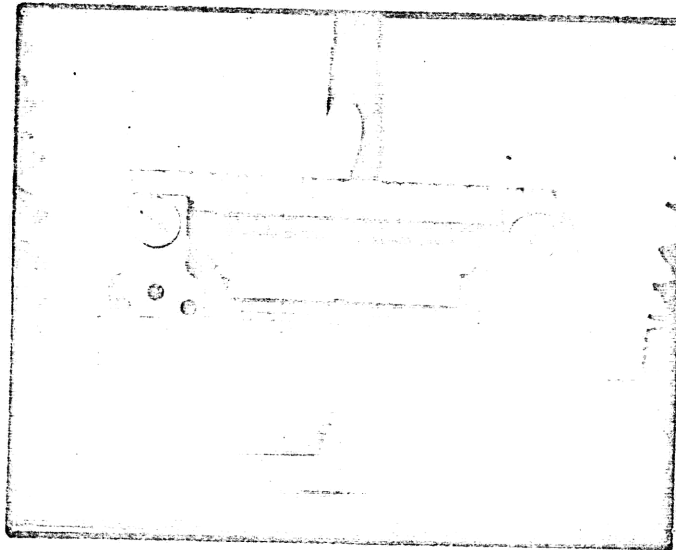


Figure 27 The Loading System for Type A (1x1x12) Beams

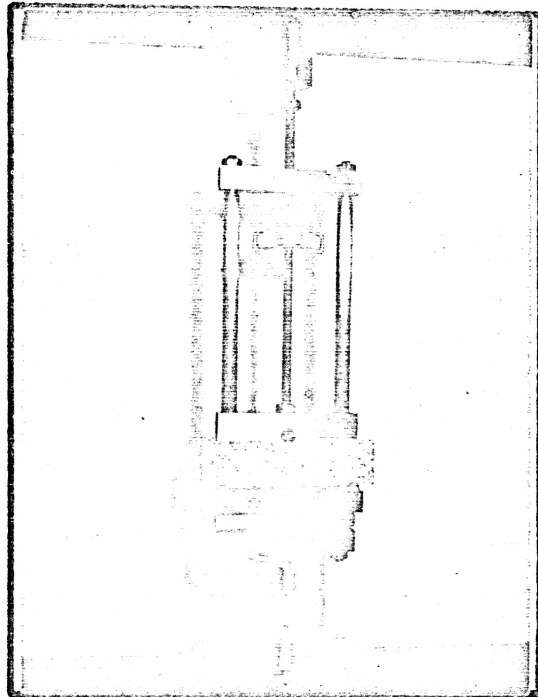
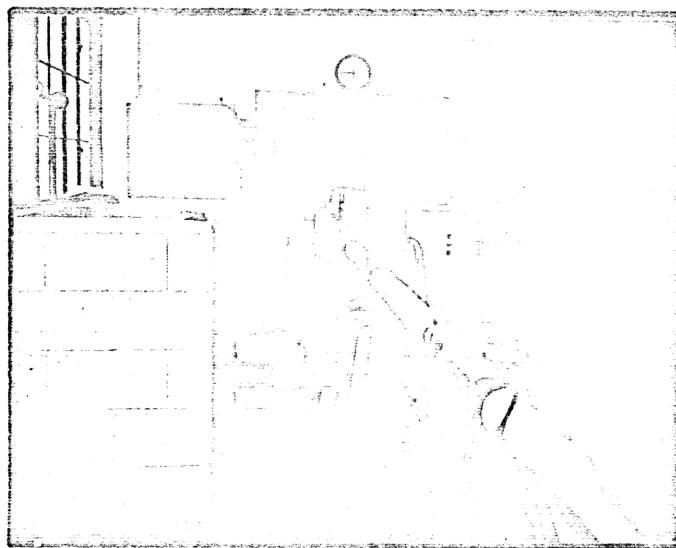


Figure 28 The Loading System for
Type D (.1x1x4) Beams

Figure 29 The 1000 Watt Continuous Gas Laser



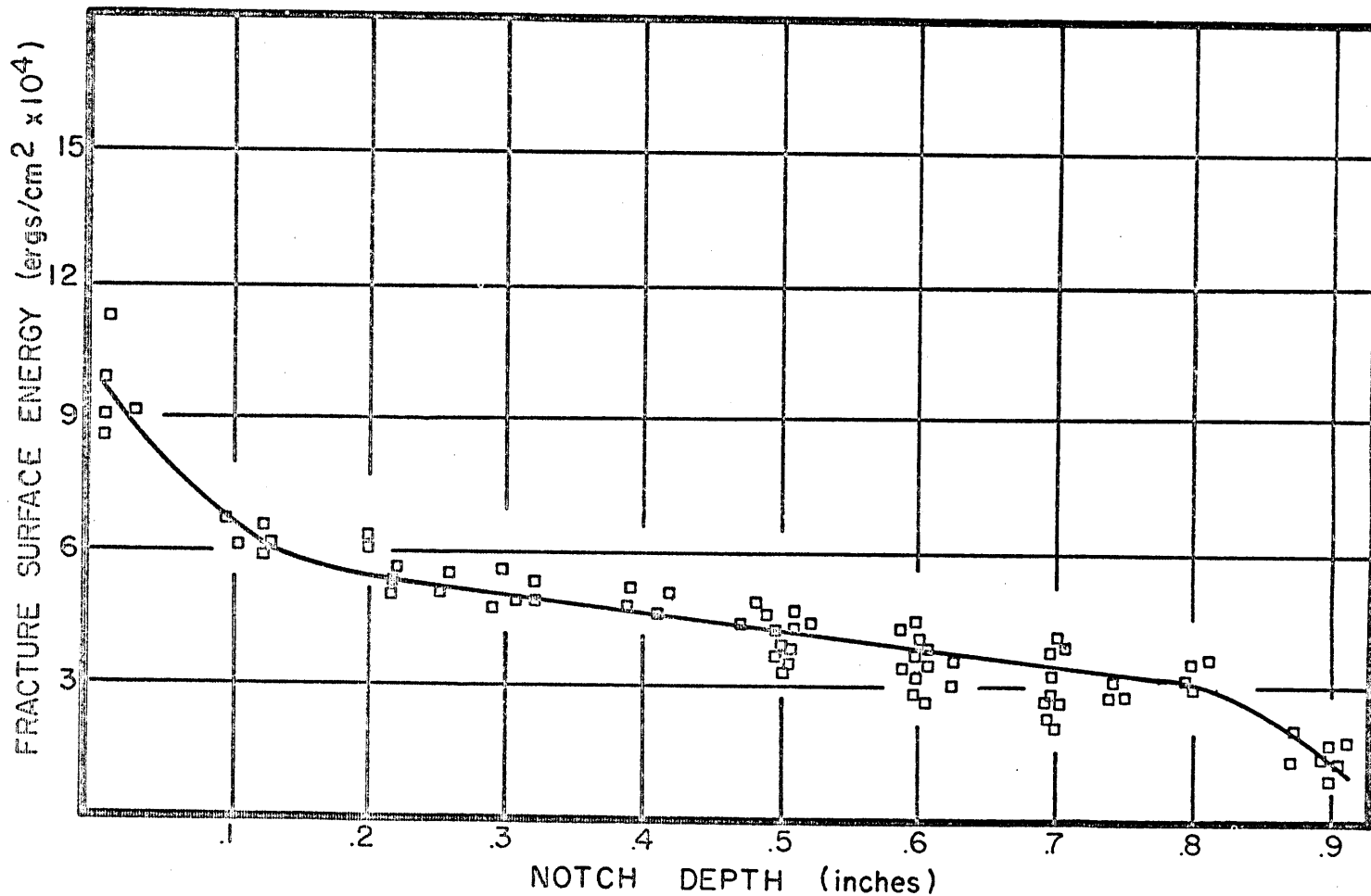


Figure 30 Fracture Surface Energy vs. Notch Depth, for Untreated Granite, Specimen Size 1"x1"x12", Mid-Span Deflection Rate .002 inches per minute

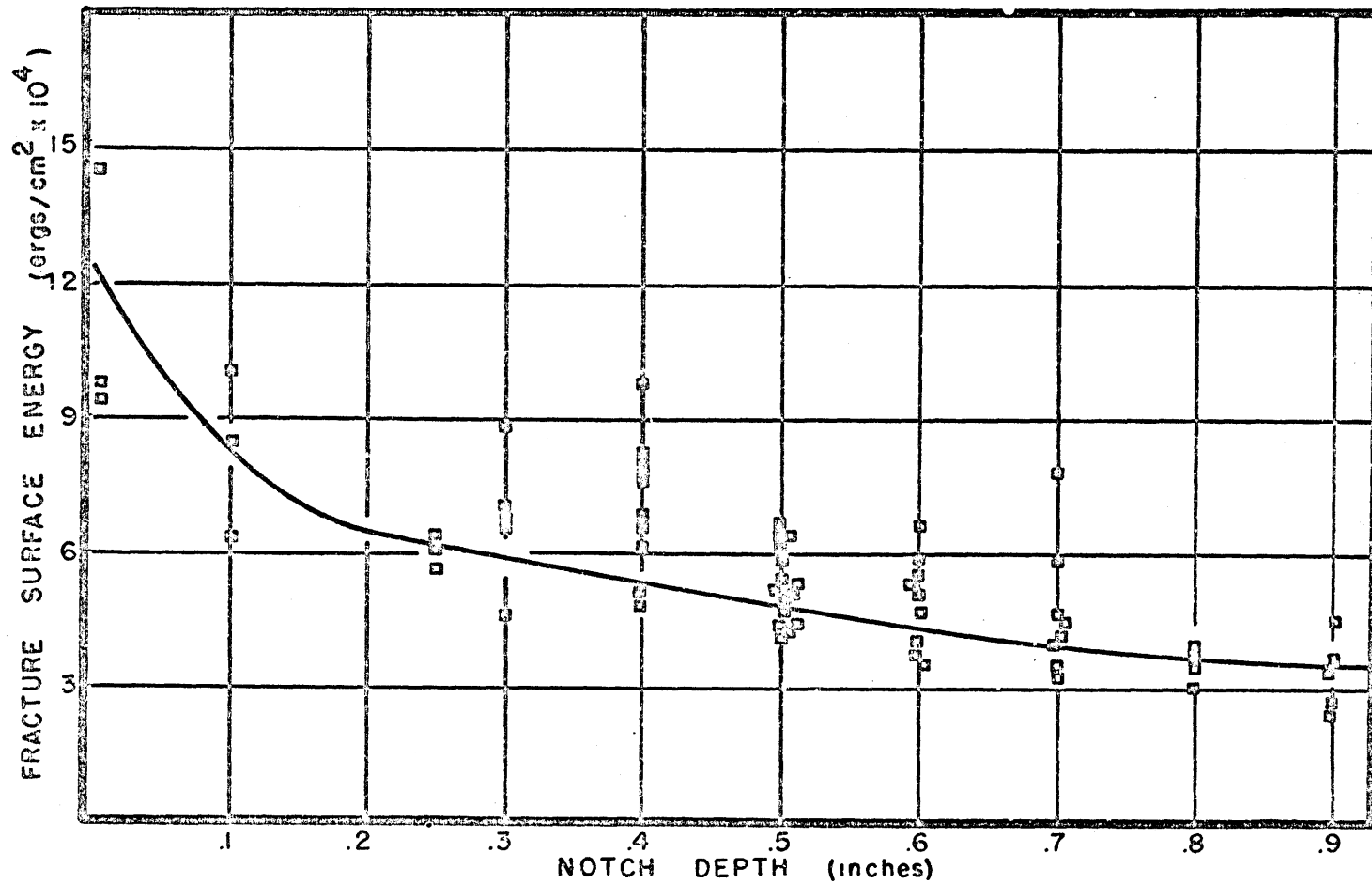


Figure 31 Fracture Surface Energy vs. Notch Depth, for Untreated Granite Specimen Size $.1 \times 1 \times 4$, Mid-Span Deflection Rate .002 inches per minute

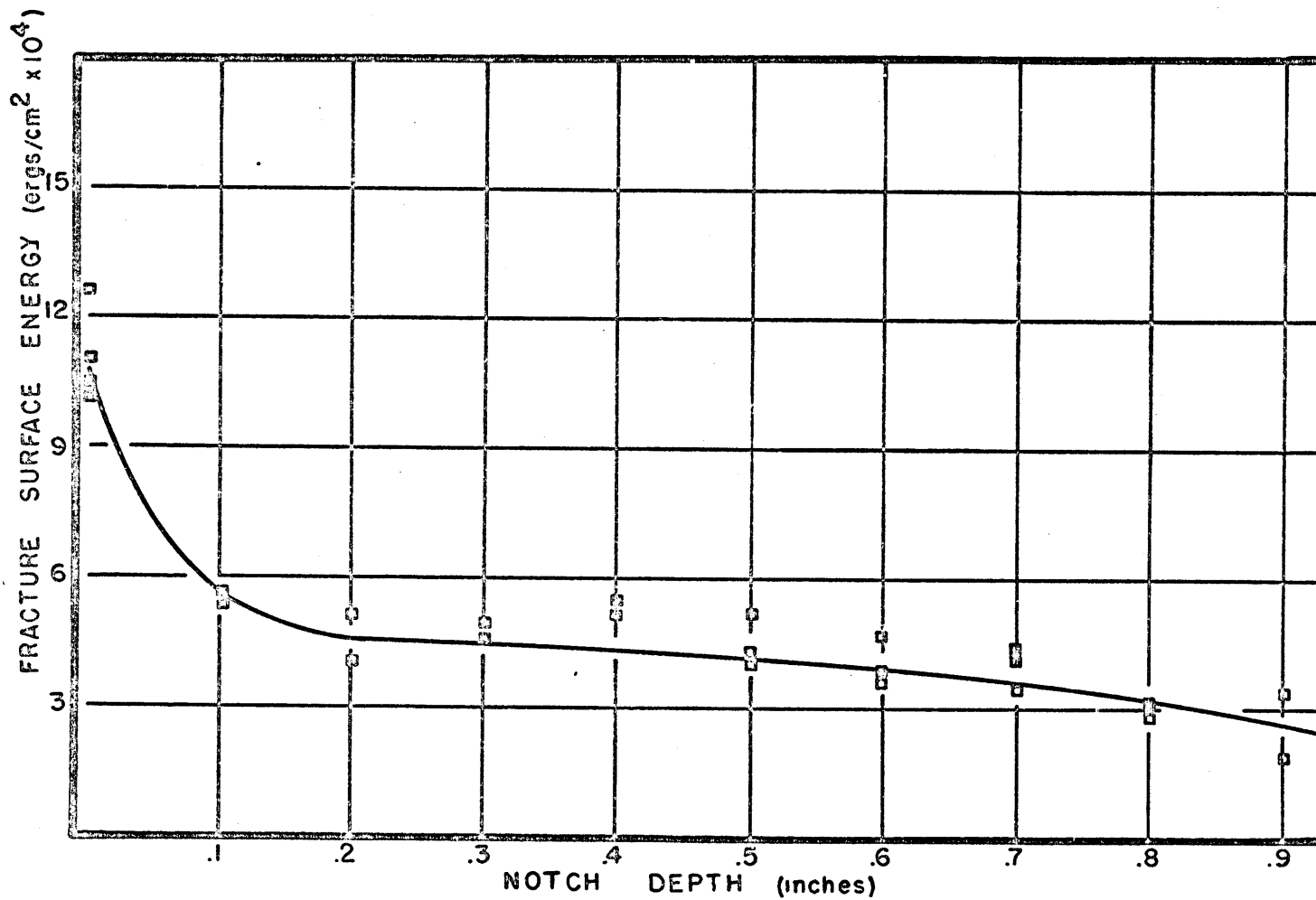


Figure 32 Fracture Surface Energy vs. Notch Depth, for Untreated Granite Specimen Size 1x1x4, Mid-Span Deflection Rate .002 inches per minute

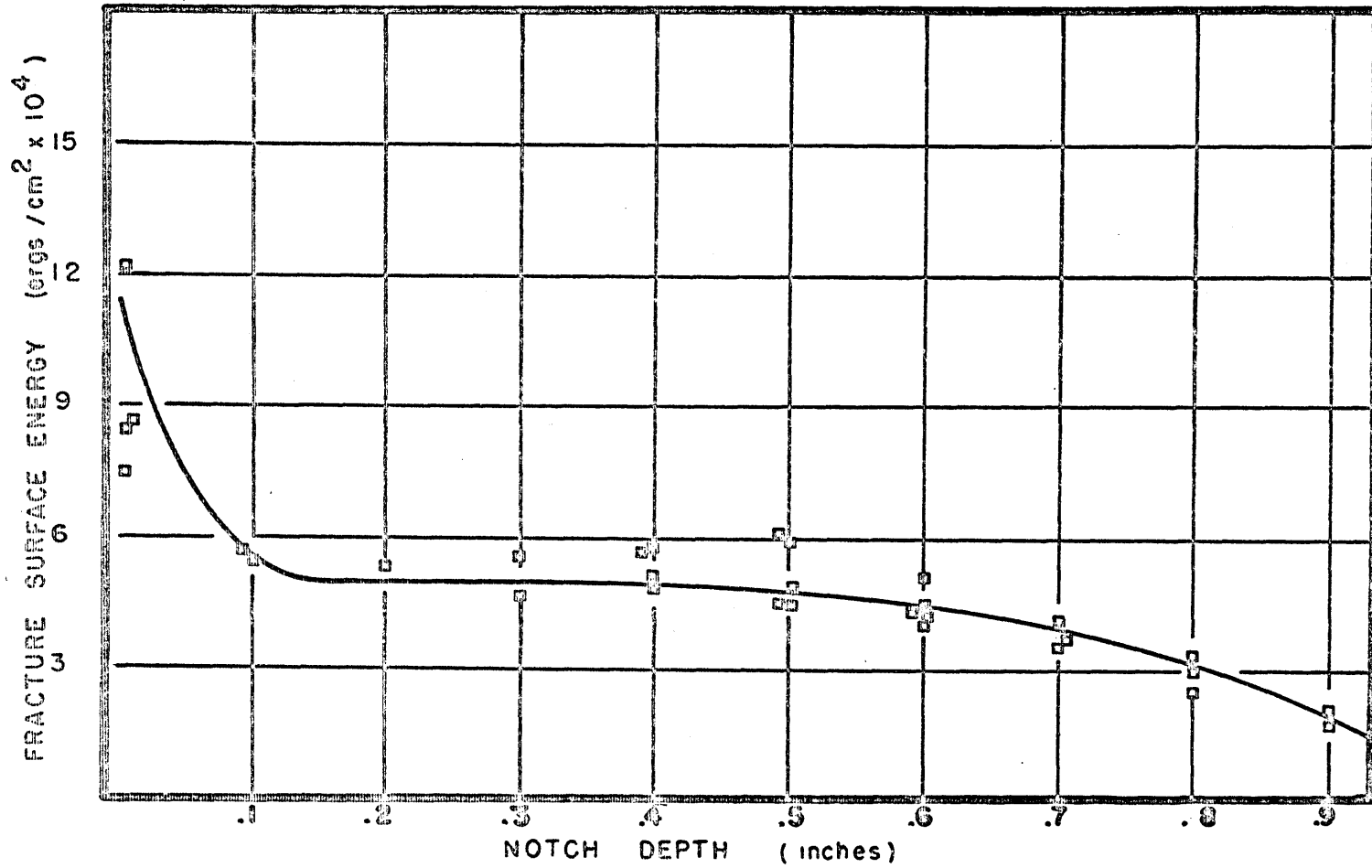


Figure 33 Fracture Surface Energy vs. Notch Depth, for Untreated Granite Specimen Size .5"x1"x4", Mid-Span Deflection Rate .002 inches per minute

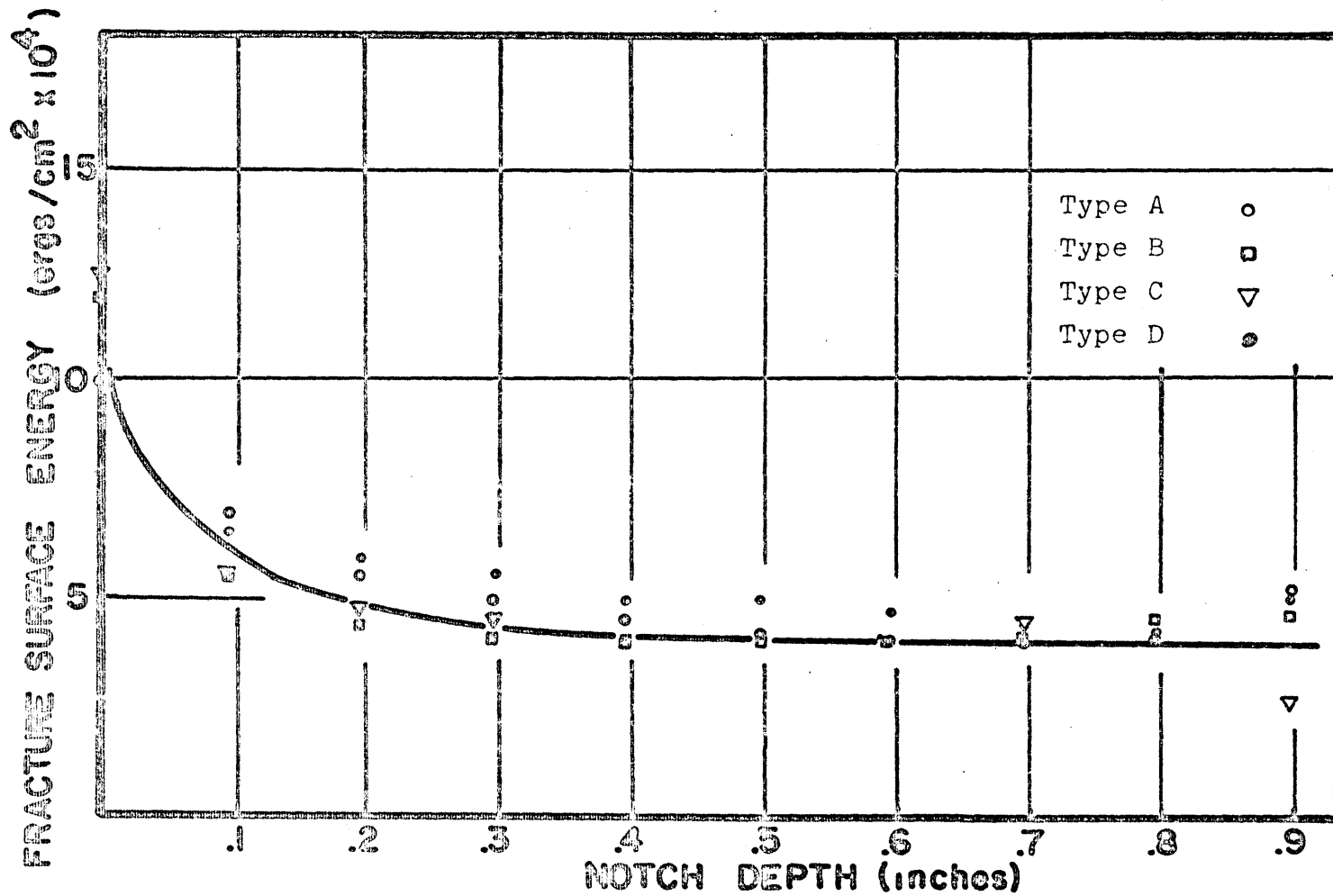


Figure 34 Fracture Surface Energy vs. Notch Depth for Untreated Granite All Sizes, Mid-Span Deflection Rate .002 inches per minute

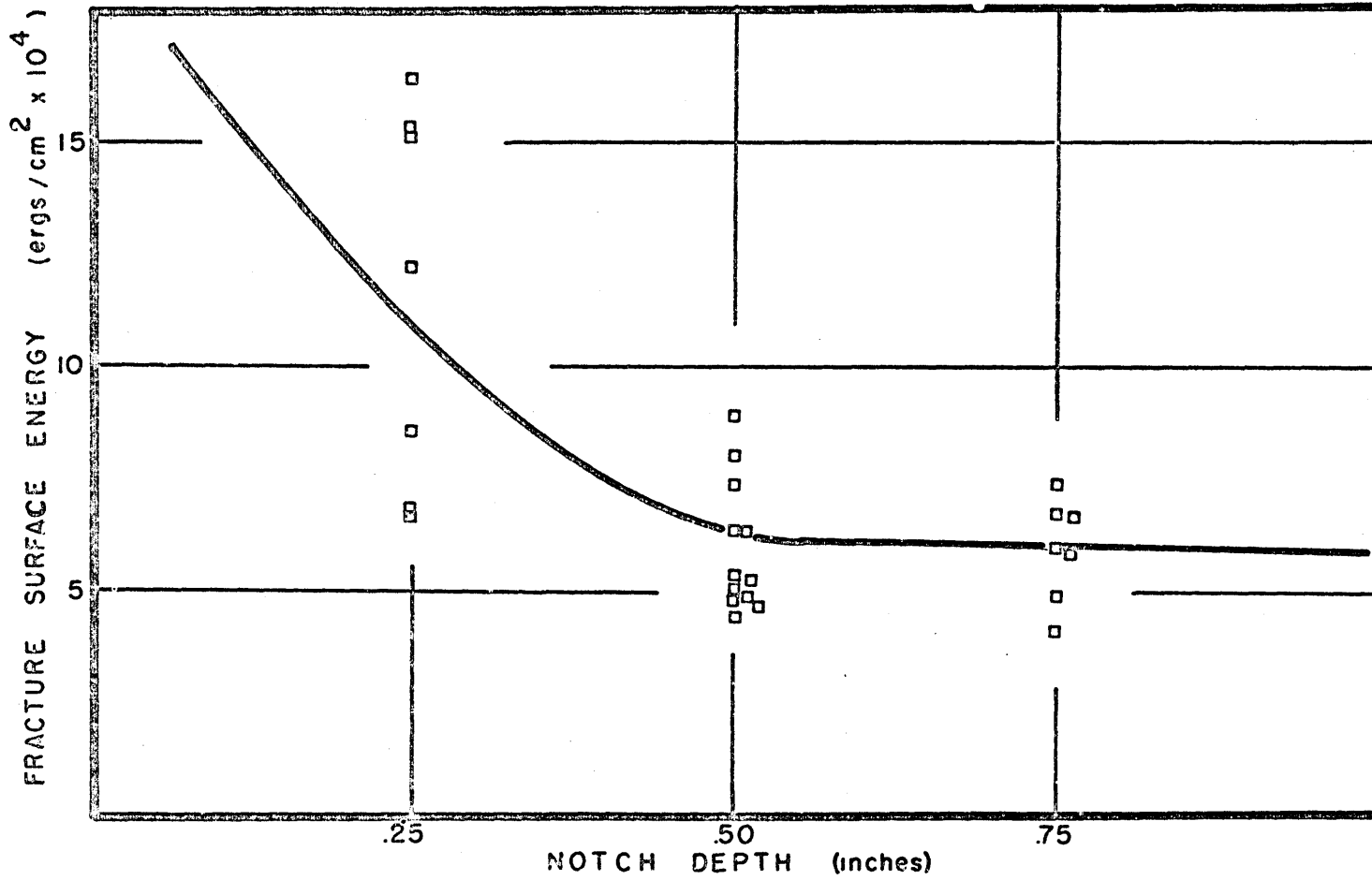


Figure 35 Corrected Fracture Surface Energy vs. Notch Depth, for Untreated Granite, Specimen Size .1"x1"x4", Mid-Span Deflection Rate .02 inches per minute

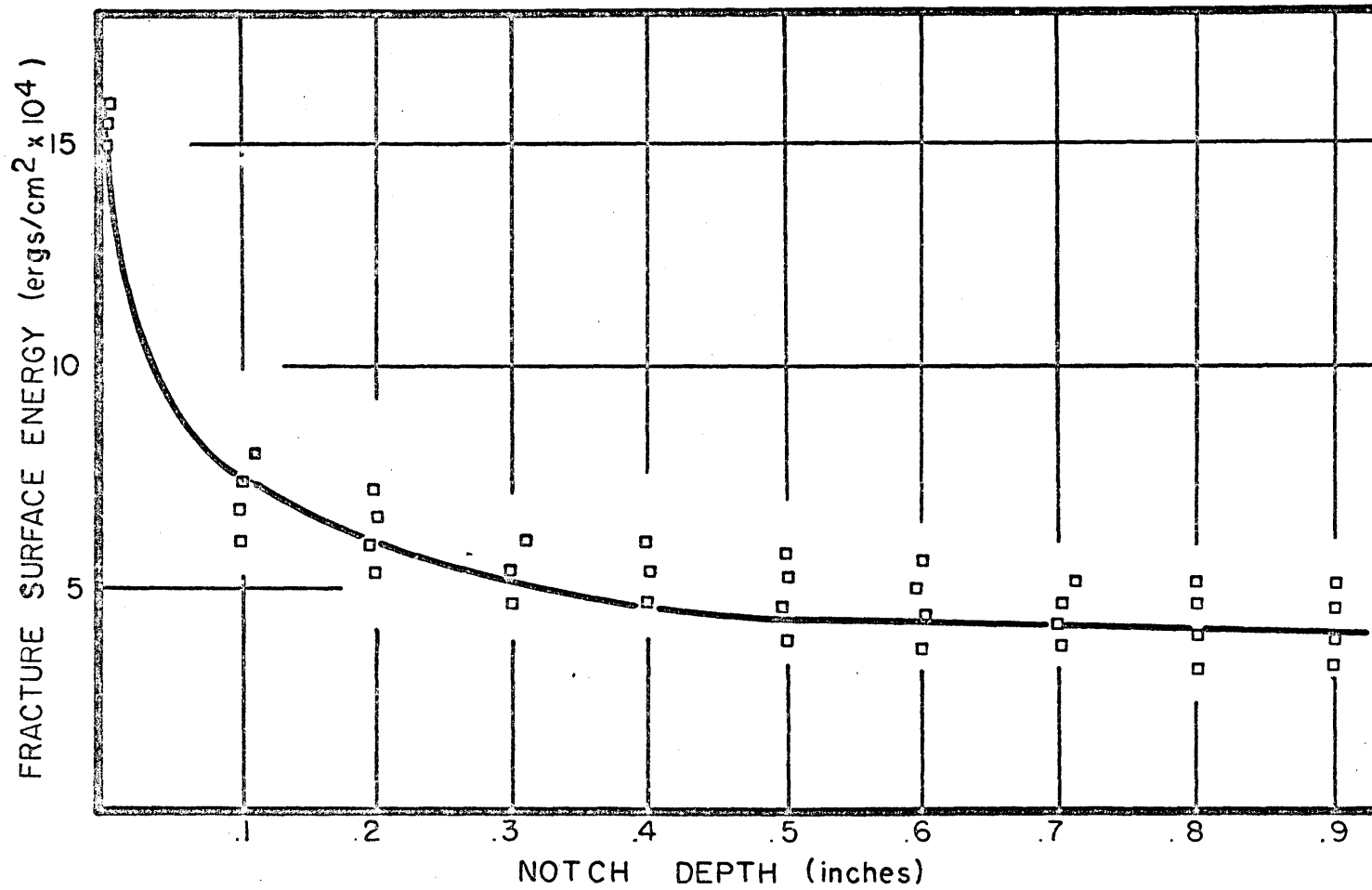


Figure 36 Corrected Fracture Surface Energy vs. Notch Depth, for Untreated Marble, Specimen Size 1"x1"x12", Mid-Span Deflection Rate .002 inches per minute

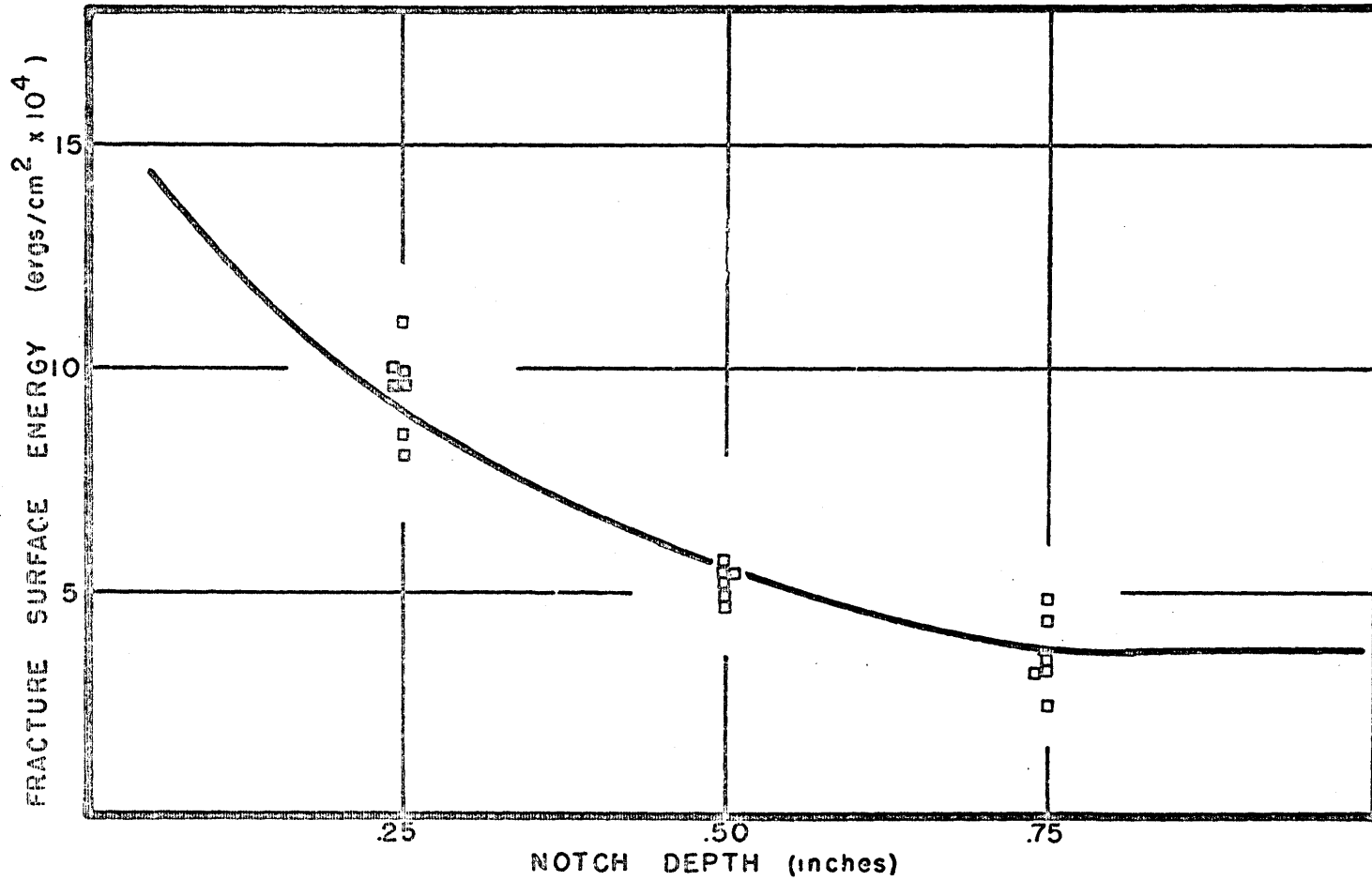


Figure 37 Corrected Fracture Surface Energy vs. Notch Depth, for Untreated Marble, Specimen Size .1"x1"x4", Mid-Span Deflection Rate .02 inches per minute

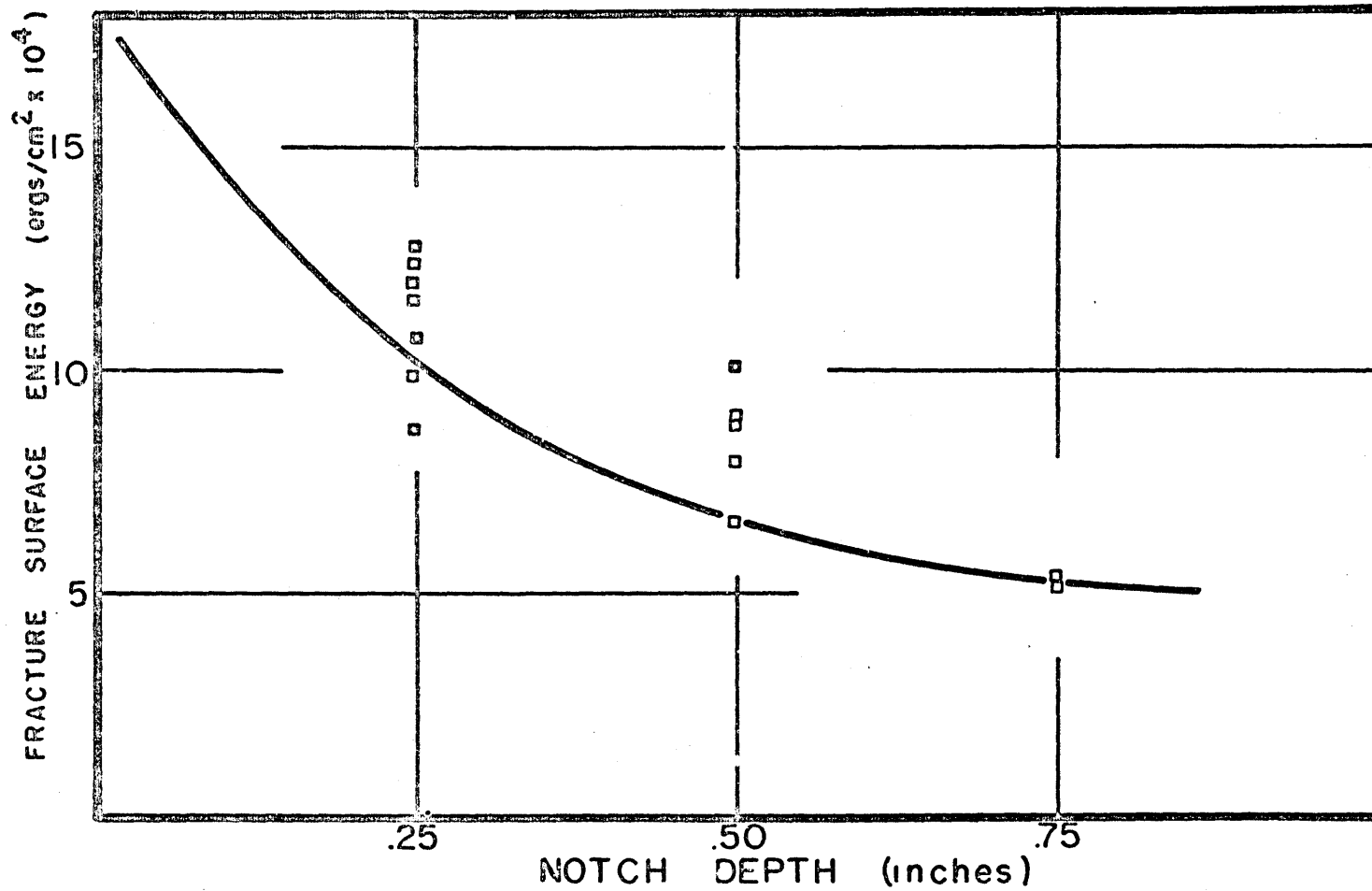


Figure 38 Corrected Fracture Surface Energy vs. Notch Depth, for Heat-Treated Granite, Specimen Size .1"x1"x4", Mid-Span Deflection Rate .02 inches per minute

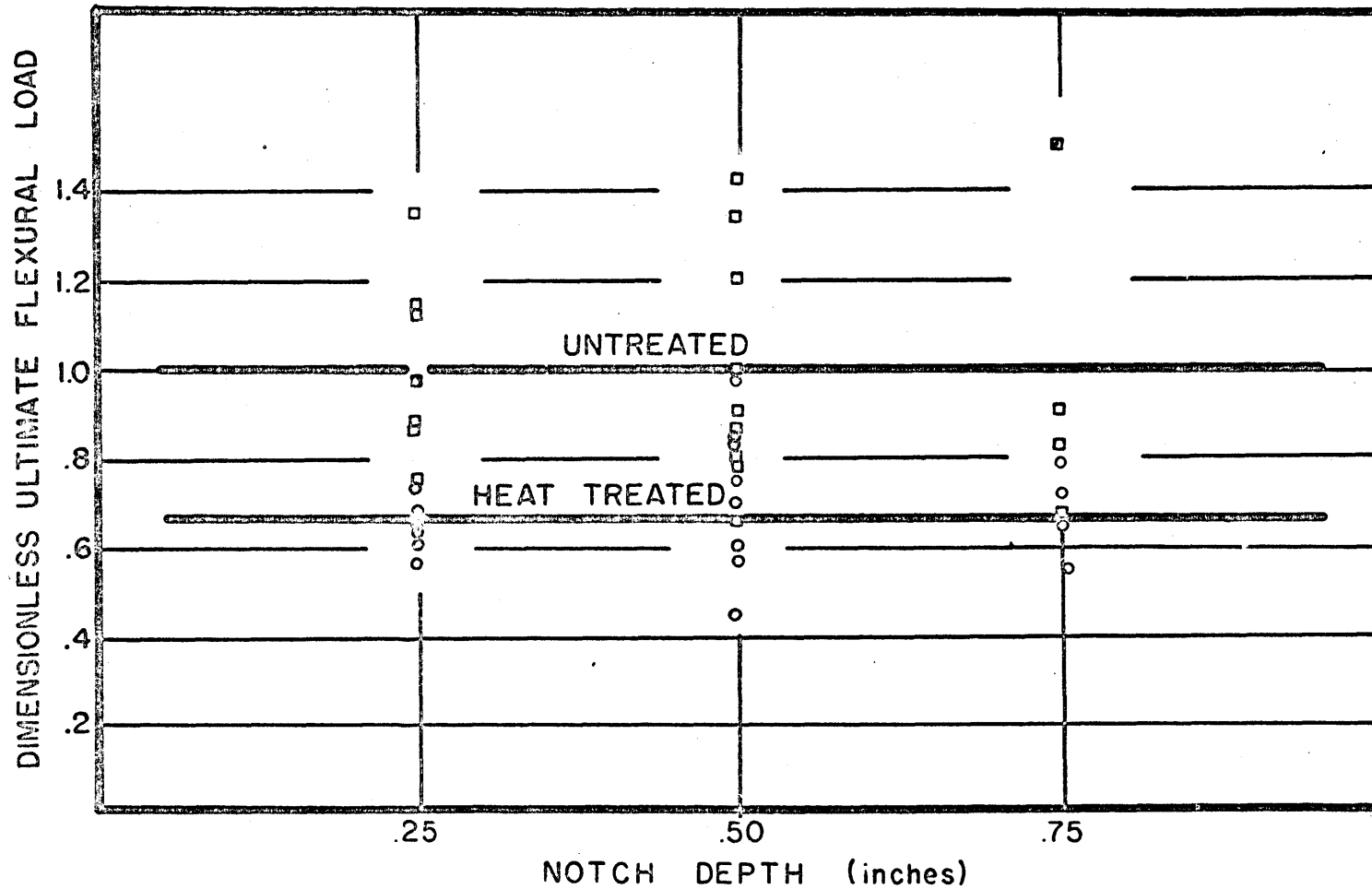


Figure 39 Dimensionless Ultimate Flexural Load vs. Notch Depth, for Untreated and Heat-Treated Granite, Specimen Size .1"x1"x4", Mid-Span Deflection Rate .02 inches per minute

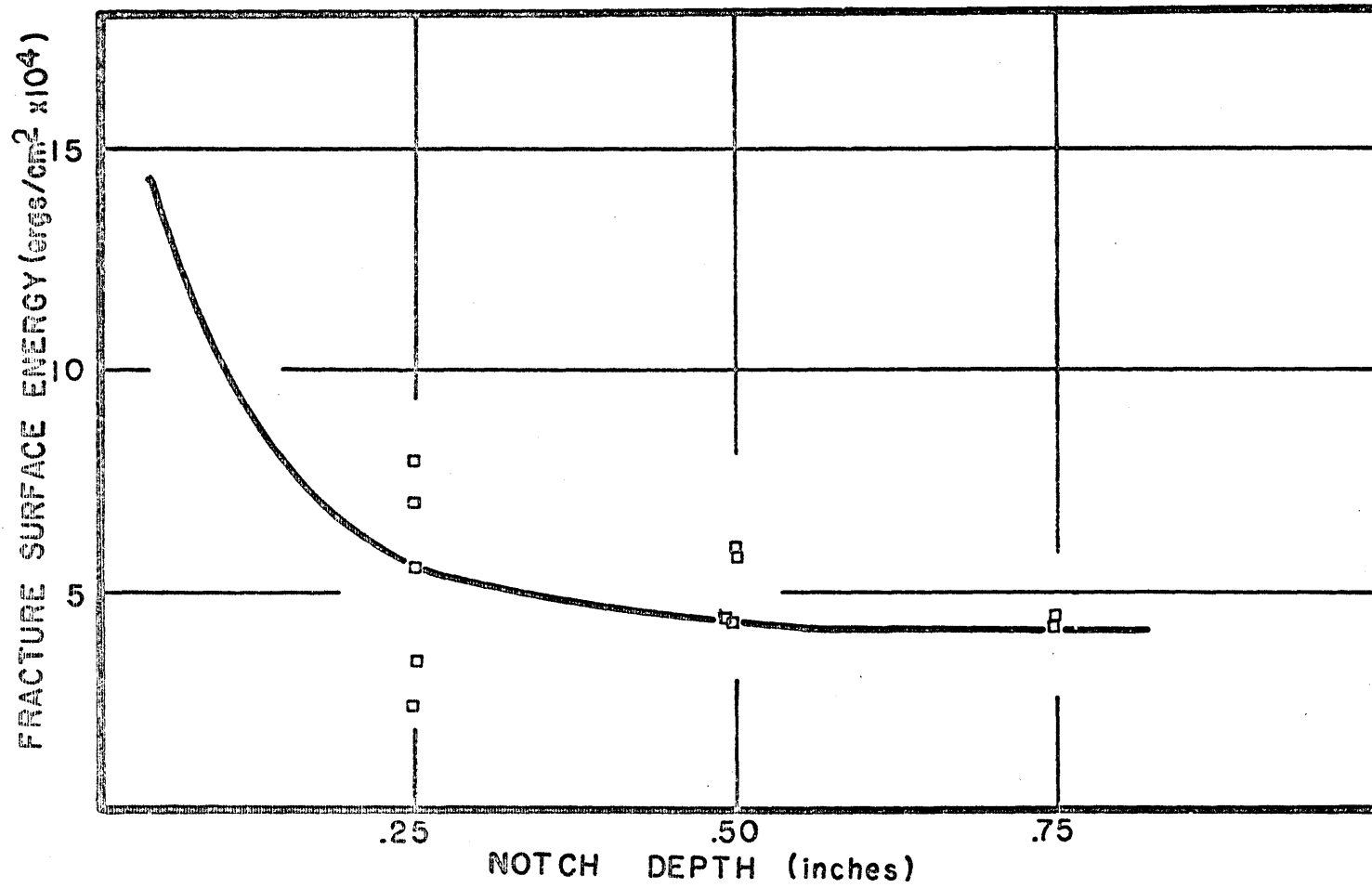


Figure 40 Corrected Fracture Surface Energy vs. Notch Depth, for Heat-Treated Marble, Specimen Size .1"x1"x4", Mid-Span Deflection Rate .02 inches per minute

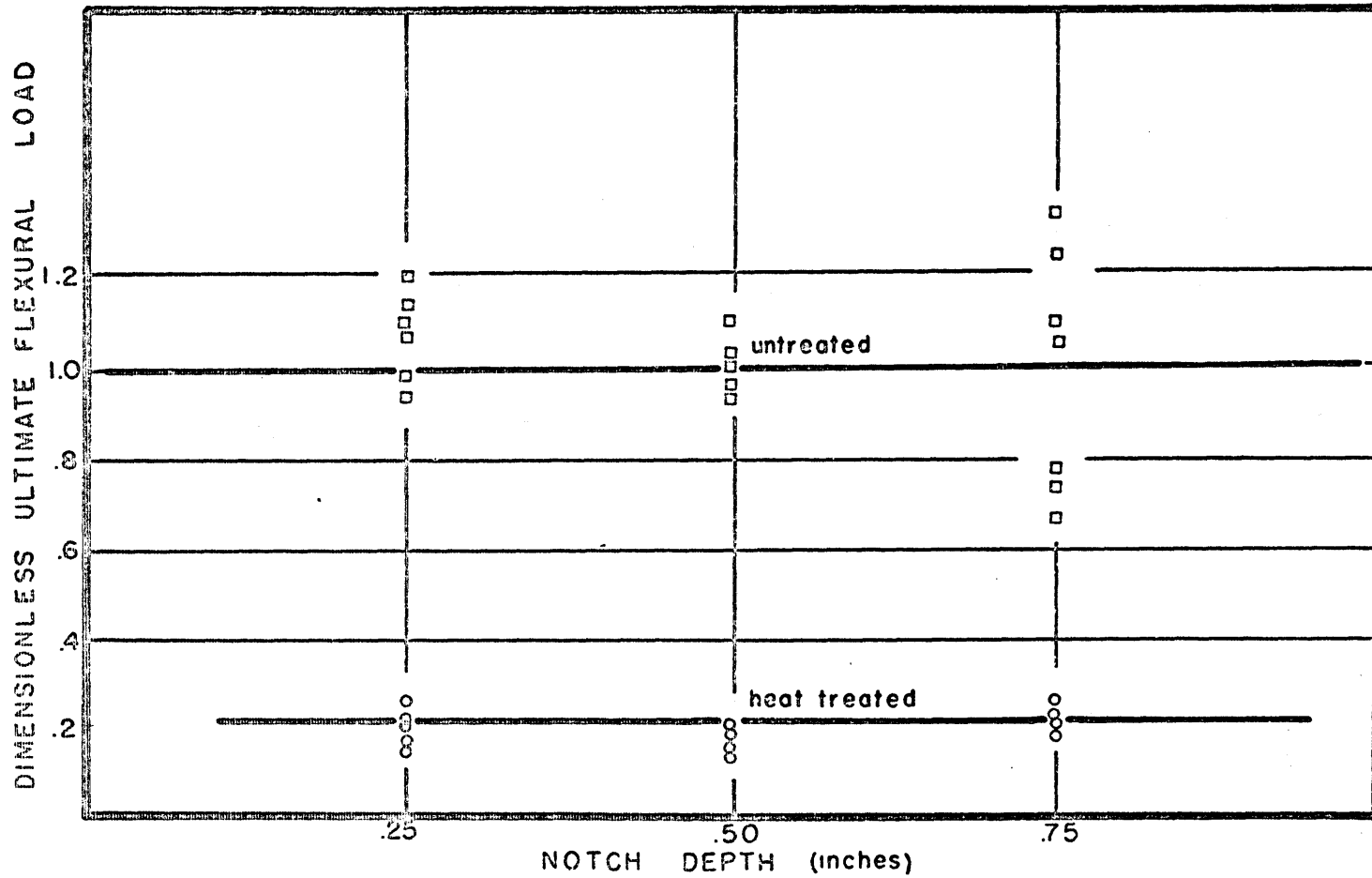


Figure 41 Dimensionless Ultimate Flexural Load vs. Notch Depth, for Untreated and Heat-Treated Marble, Specimen Size .1"x1"x4", Mid-Span Deflection Rate .02 inches per minute

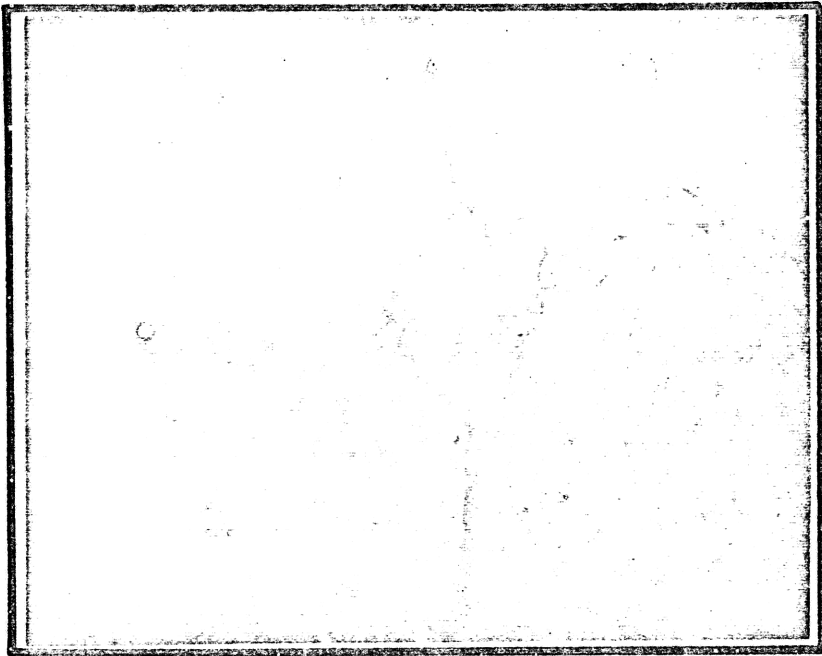


Figure 42 Untreated Granite Specimen after Failure

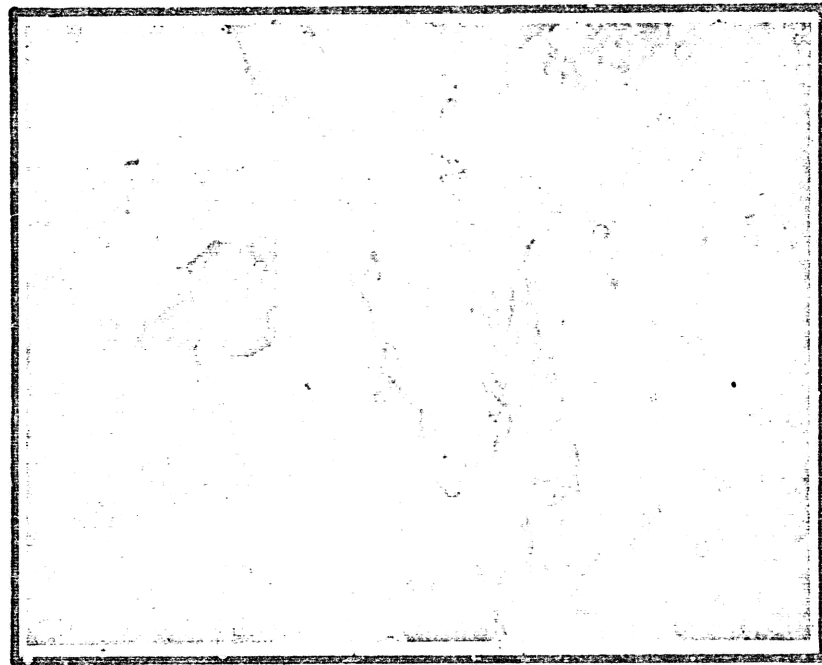


Figure 43 Untreated Granite Specimen after Failure

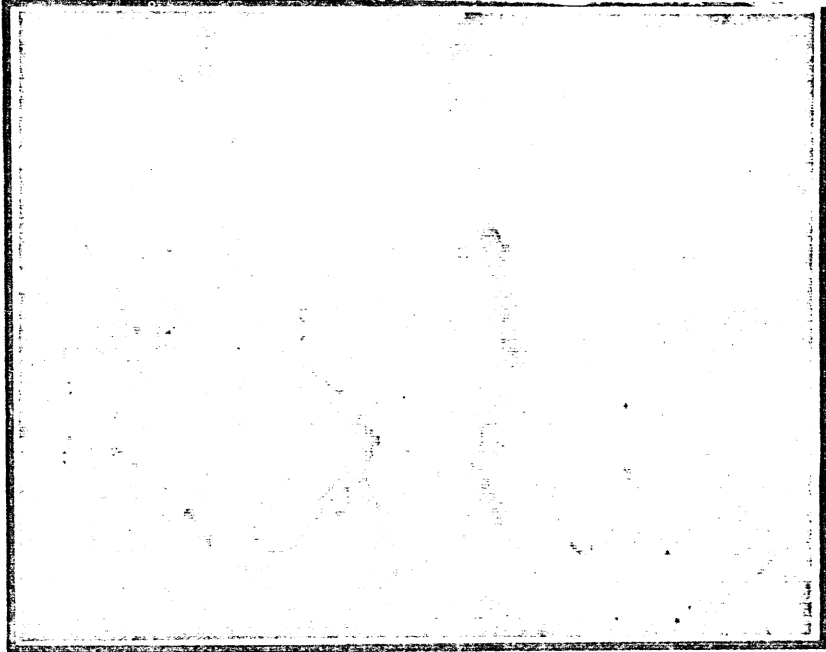


Figure 44 Untreated Granite Specimen after Failure, 50X

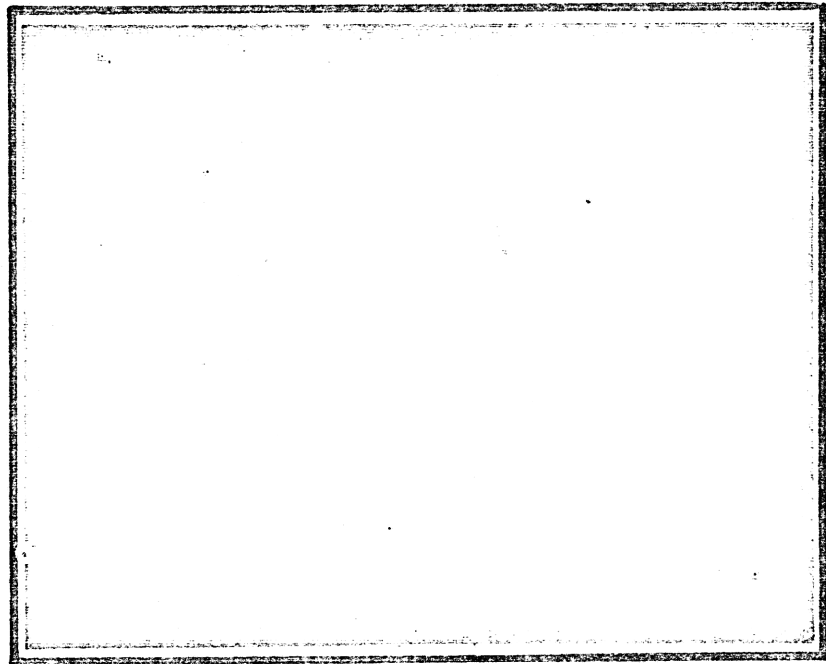


Figure 45 Untreated Marble Specimen, 50X

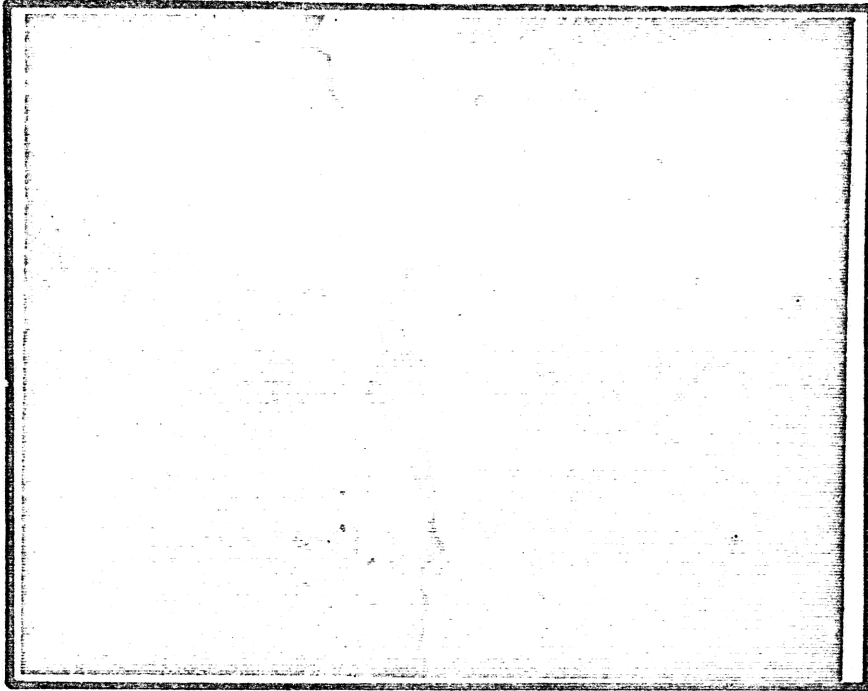


Figure 46 Untreated Marble Specimen after Failure, 50X

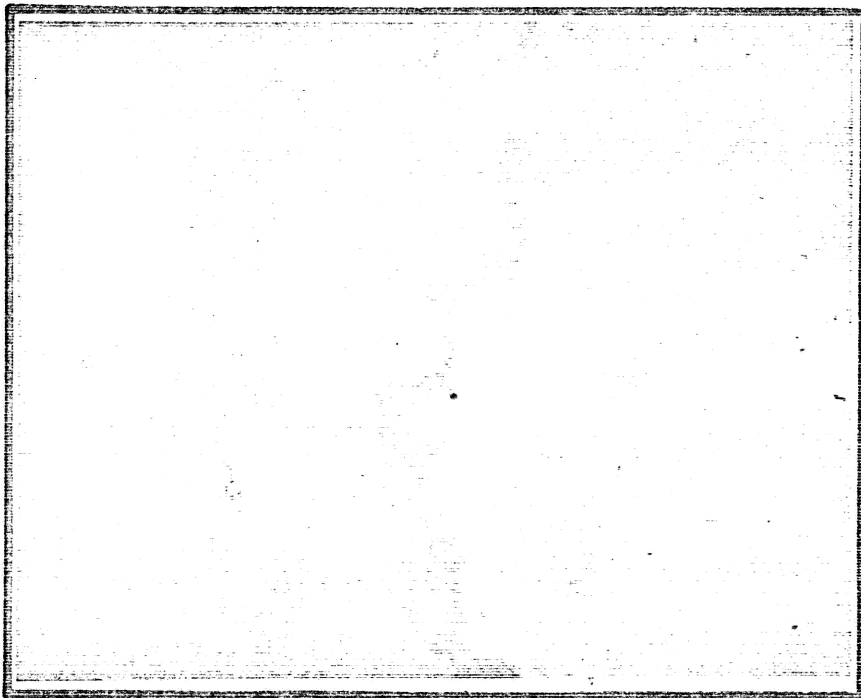


Figure 47 Heat Treated Marble Specimen after Failure, 50X

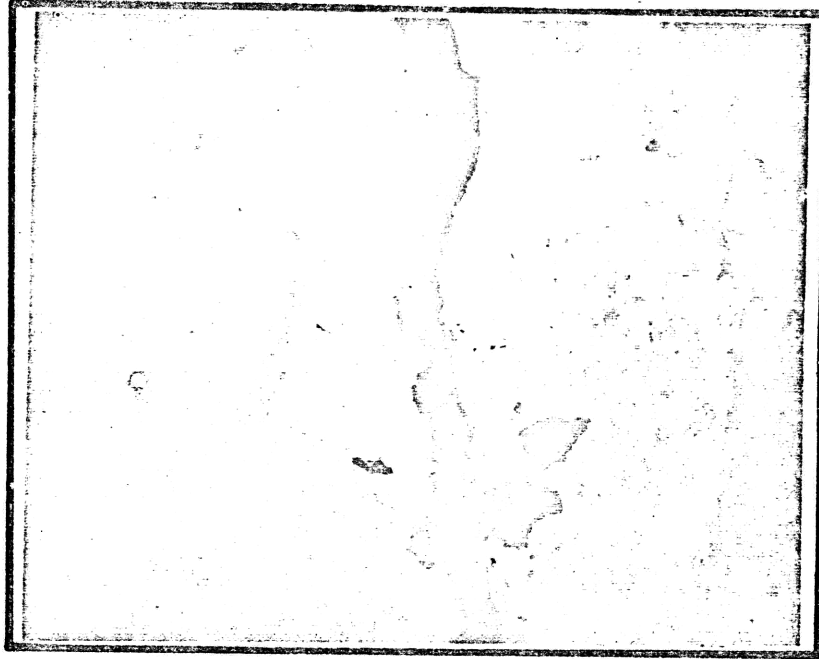


Figure 48 Heat Treated Granite Specimen, after Failure, 50X

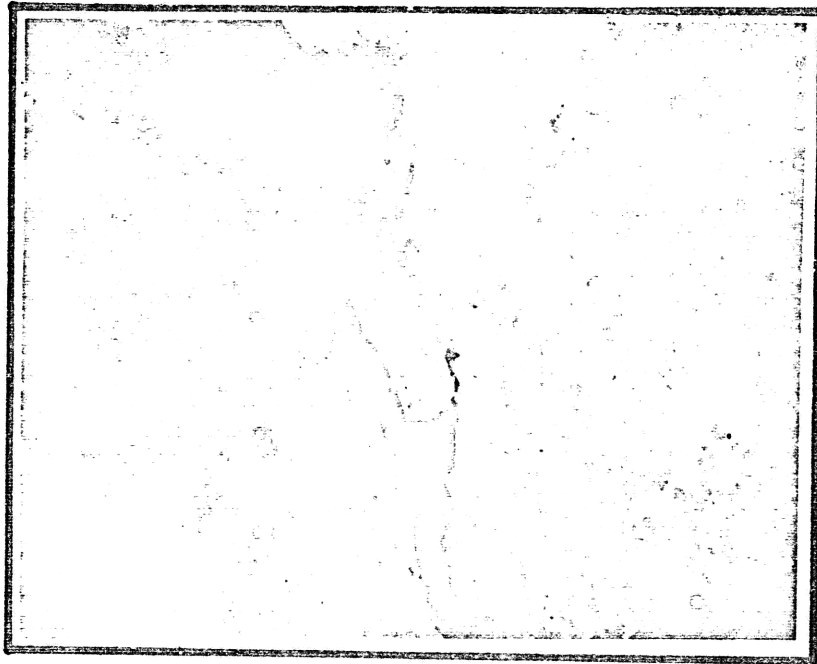


Figure 49 Heat Treated Granite Specimen, after Failure, 50X

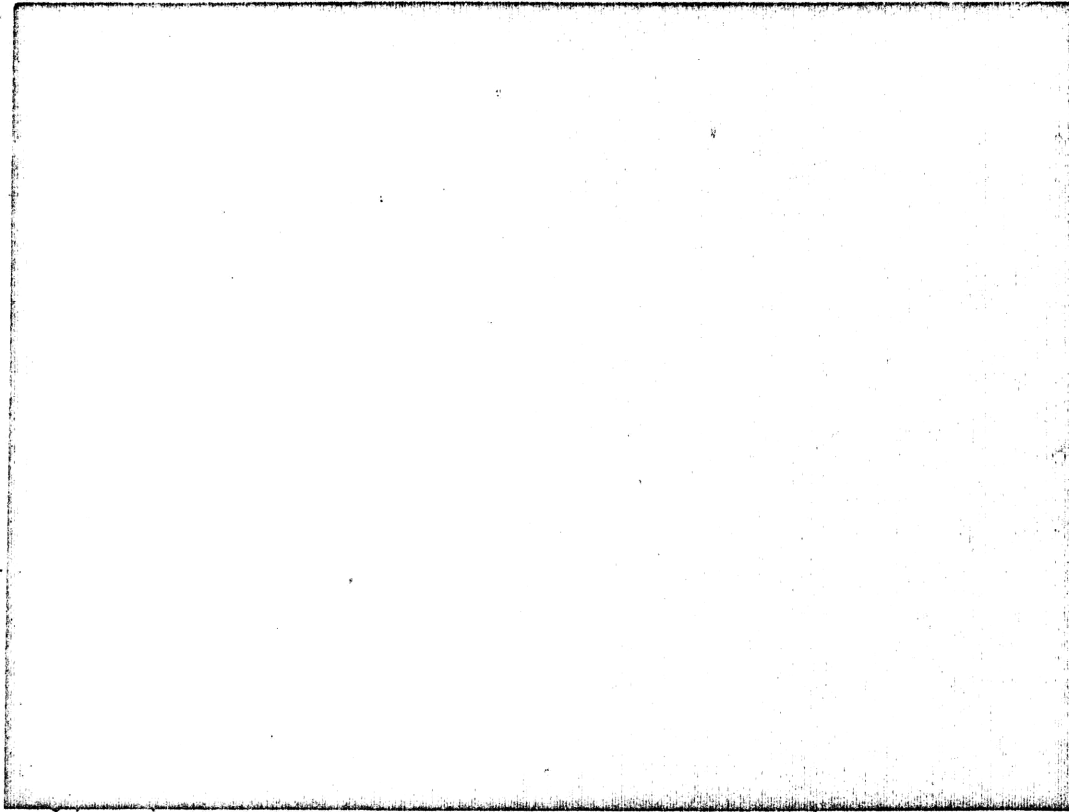


Figure 50 Heat Treated Marble Specimen, 50X

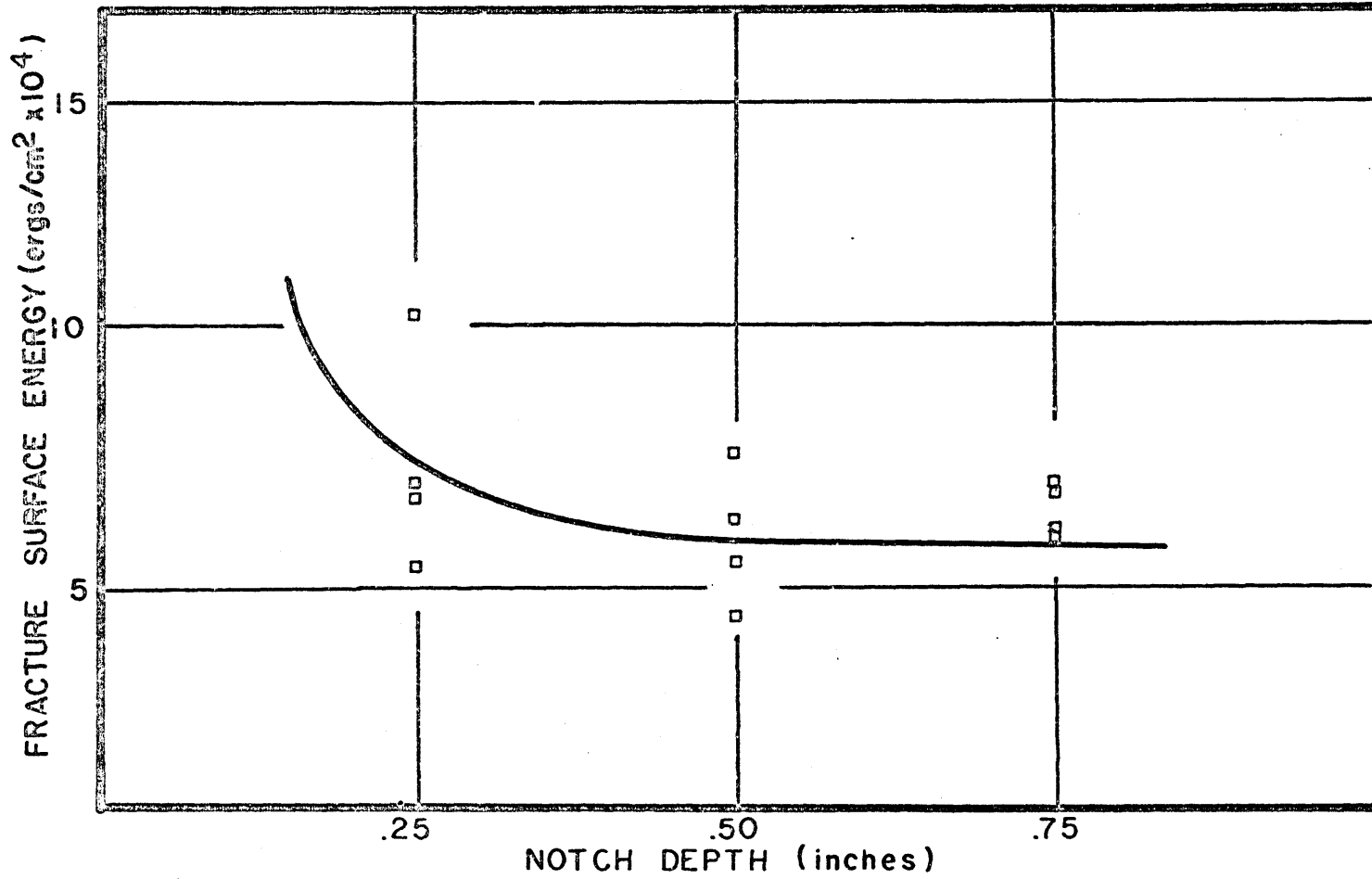


Figure 51 Corrected Fracture Surface Energy vs. Notch Depth, for Granite Specimens Exposed to Laser, Specimen Size .1"x1"x4", Mid-Span Deflection Rate .02 inches per minute

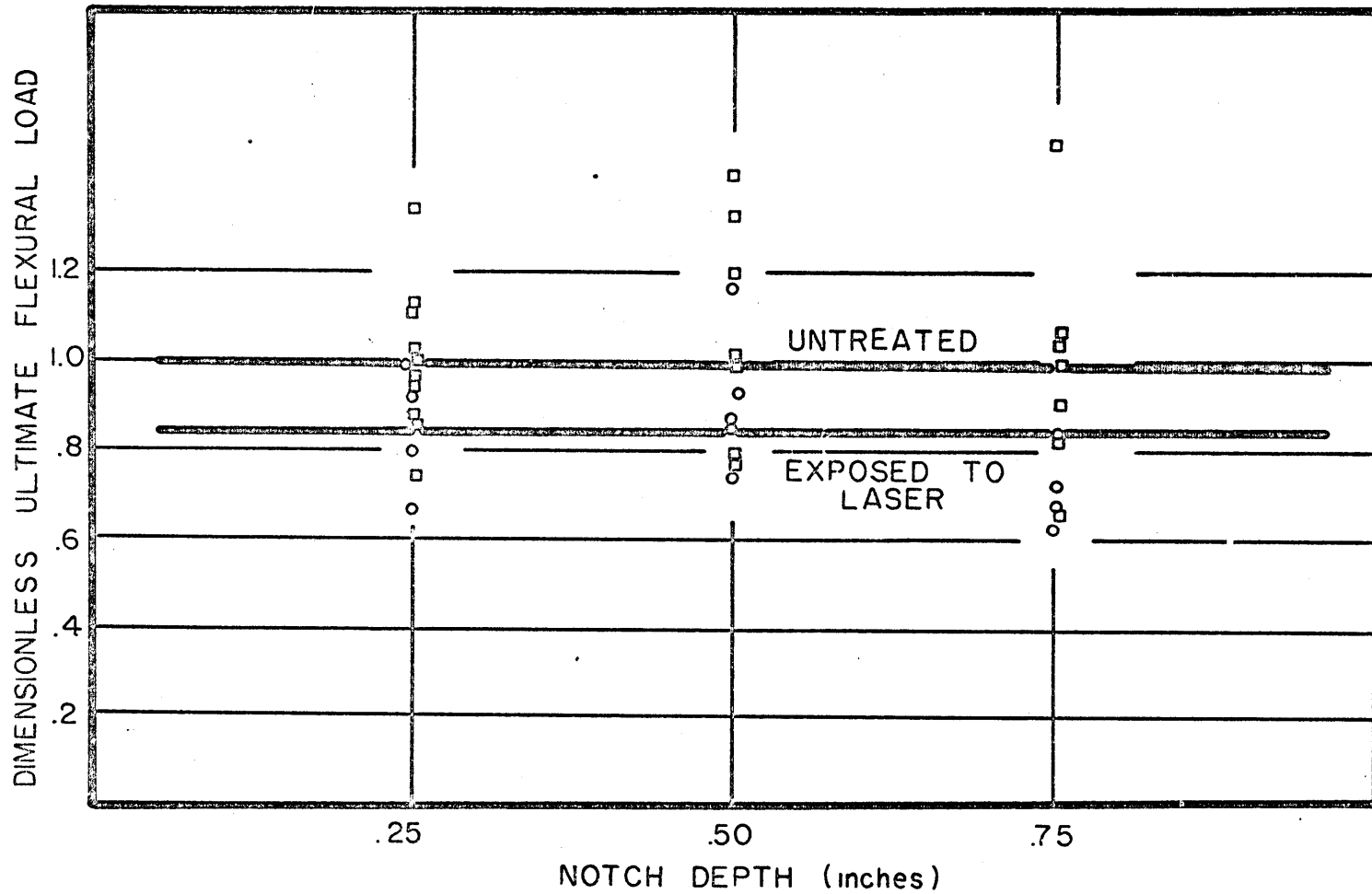


Figure 52 Dimensionless Ultimate Flexural Loads vs. Notch Depth, for Granite Specimens Exposed to Laser, Specimen Size .1"x1"x4", Mid-Span Deflection Rate .02 inches per minute

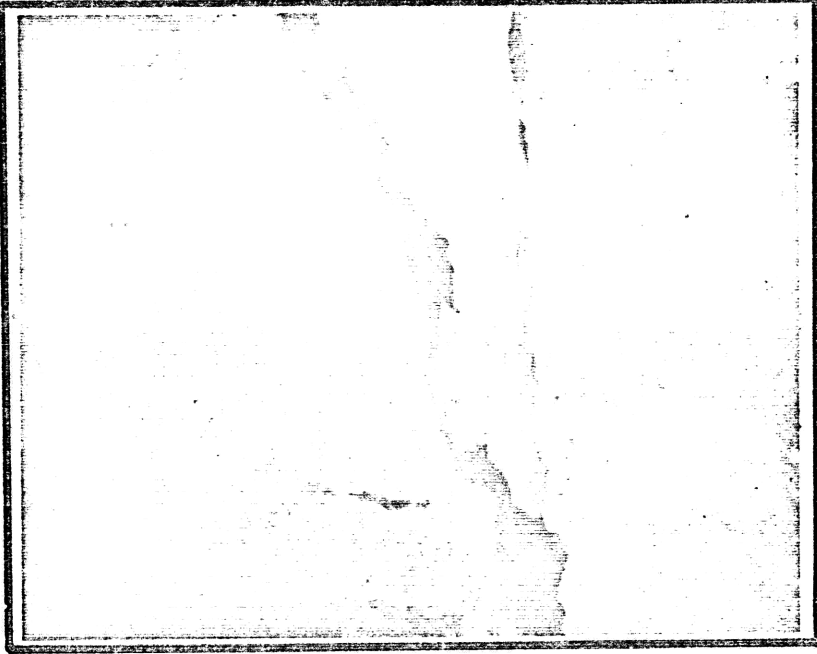


Figure 53 Granite Specimen after Exposure to Laser and after Testing, 50X

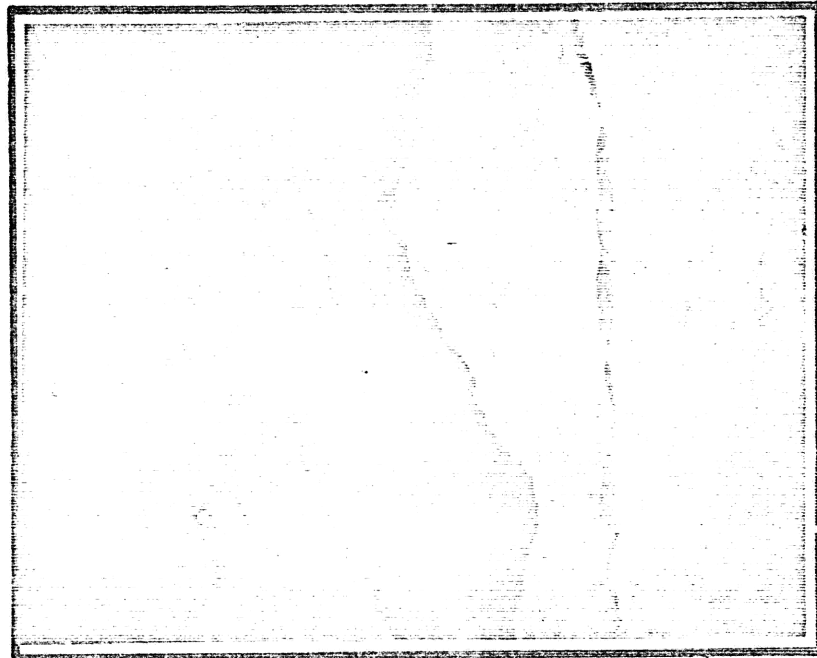


Figure 54 Granite Specimen after Exposure to Laser and after Testing, 50X

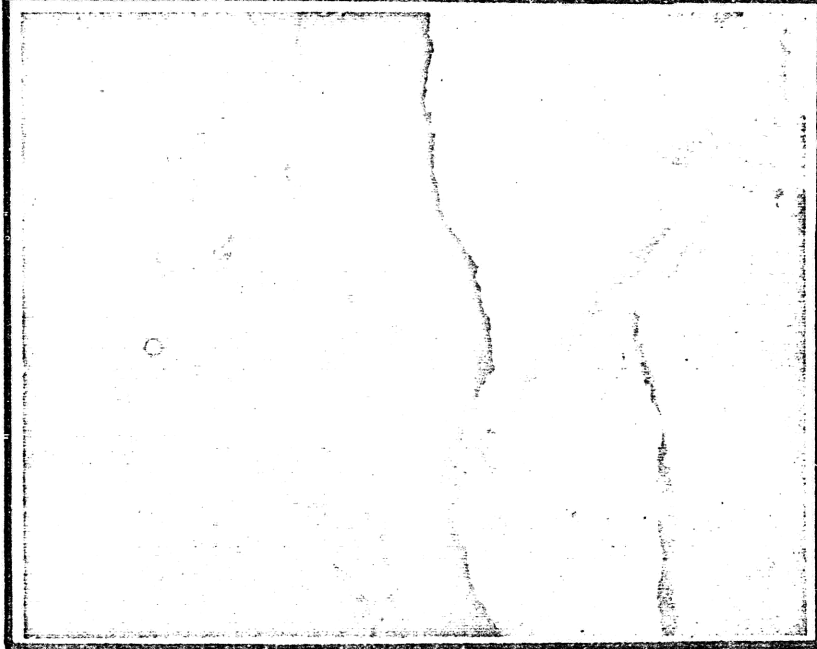


Figure 55 Granite Specimen after Exposure to Laser and after Testing, 50X

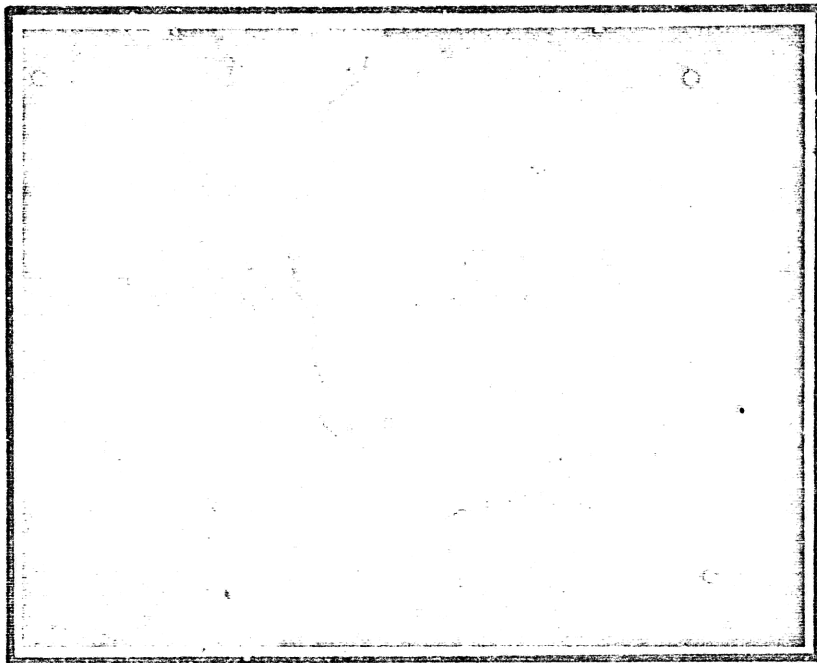


Figure 56 Granite Specimen after Exposure to Laser and after Testing, 50X

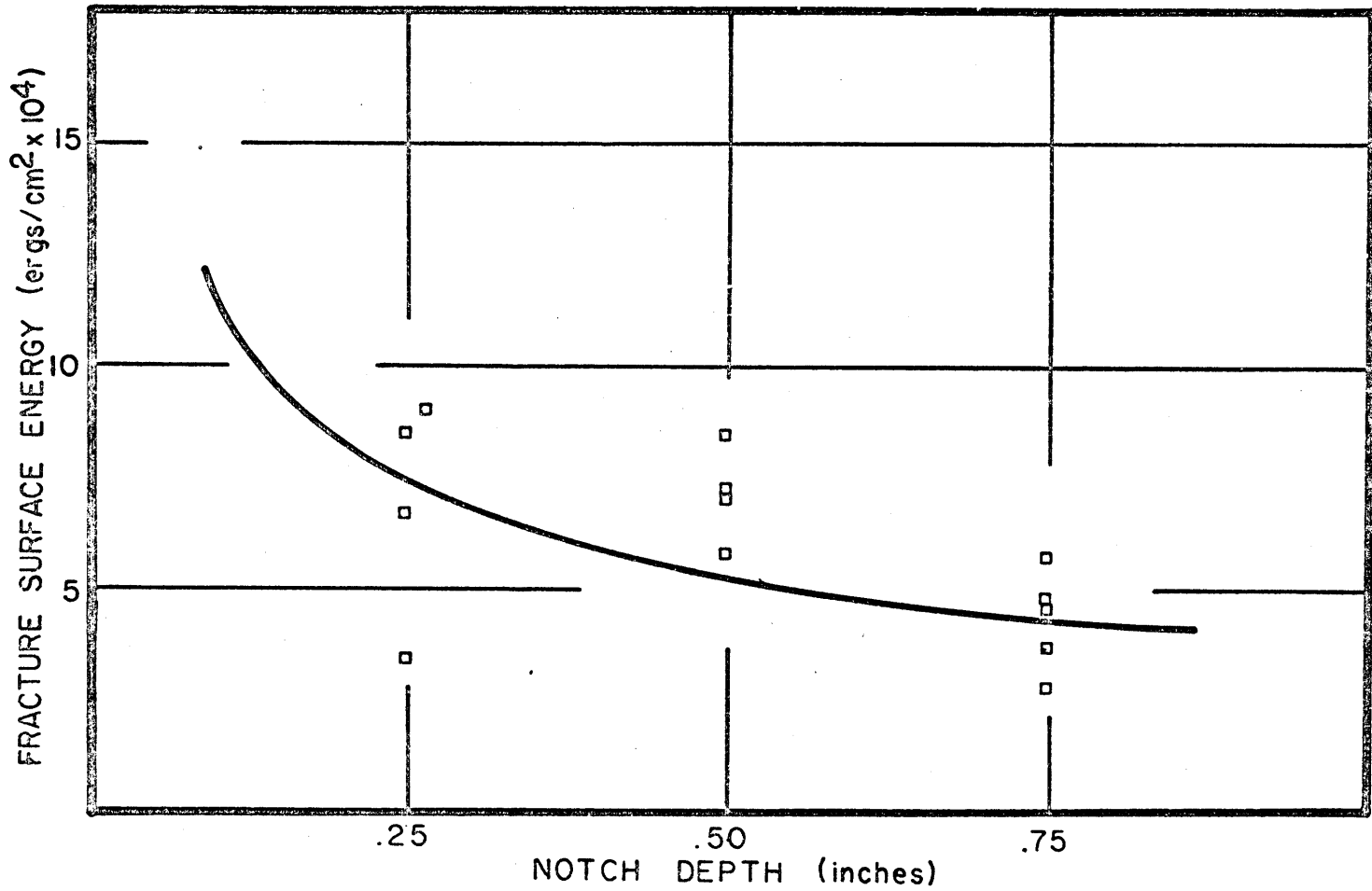


Figure 57 Corrected Fracture Surface Energy vs. Notch Depth, for Marble Specimens Exposed to Laser, Specimen Size .1"x1"x4", Mid-Span Deflection Rate .02 inches per minute

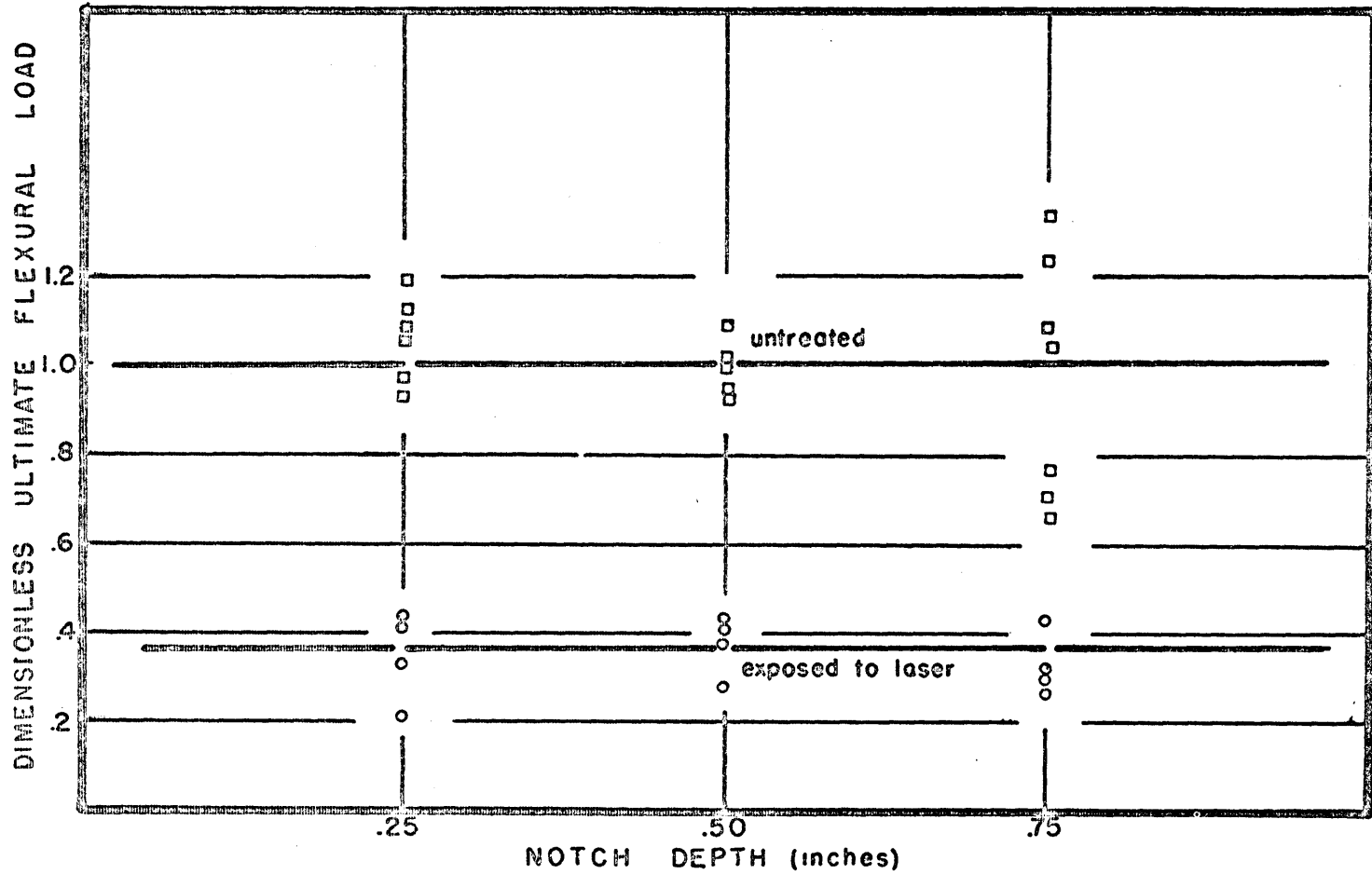


Figure 58 Dimensionless Ultimate Flexural Load vs. Notch Depth for Marble Specimens Exposed to Laser, Specimen Size .1"x1"x4", Mid-Span Deflection Rate .02 inches per minute

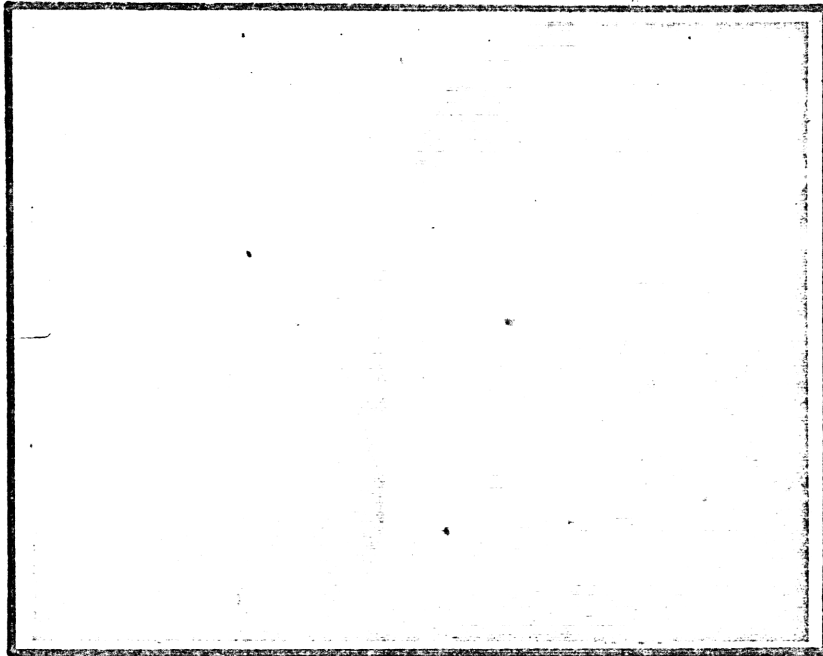


Figure 59 Marble Specimen after Exposure to Laser and after Testing, 50X

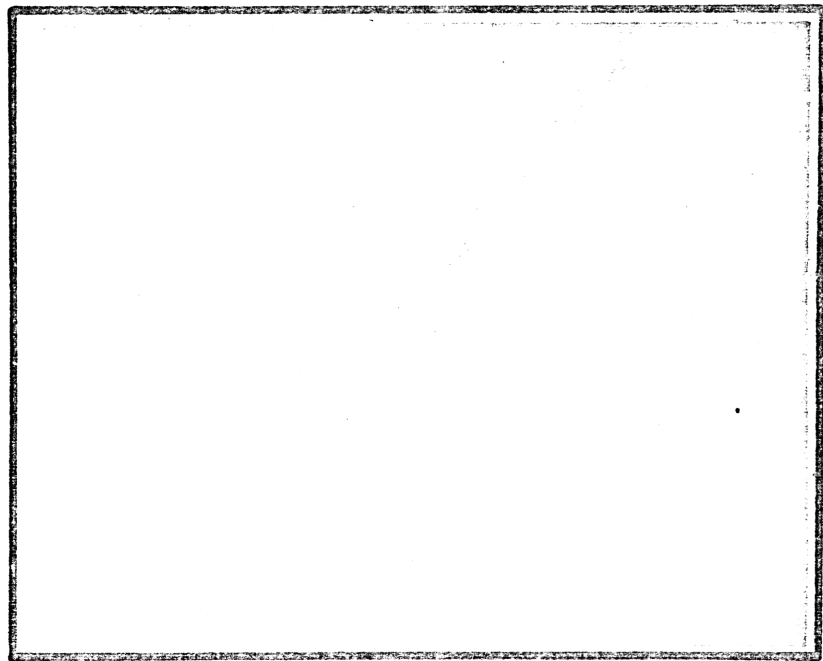


Figure 60 Marble Specimen after Exposure to Laser and after Testing, 50X

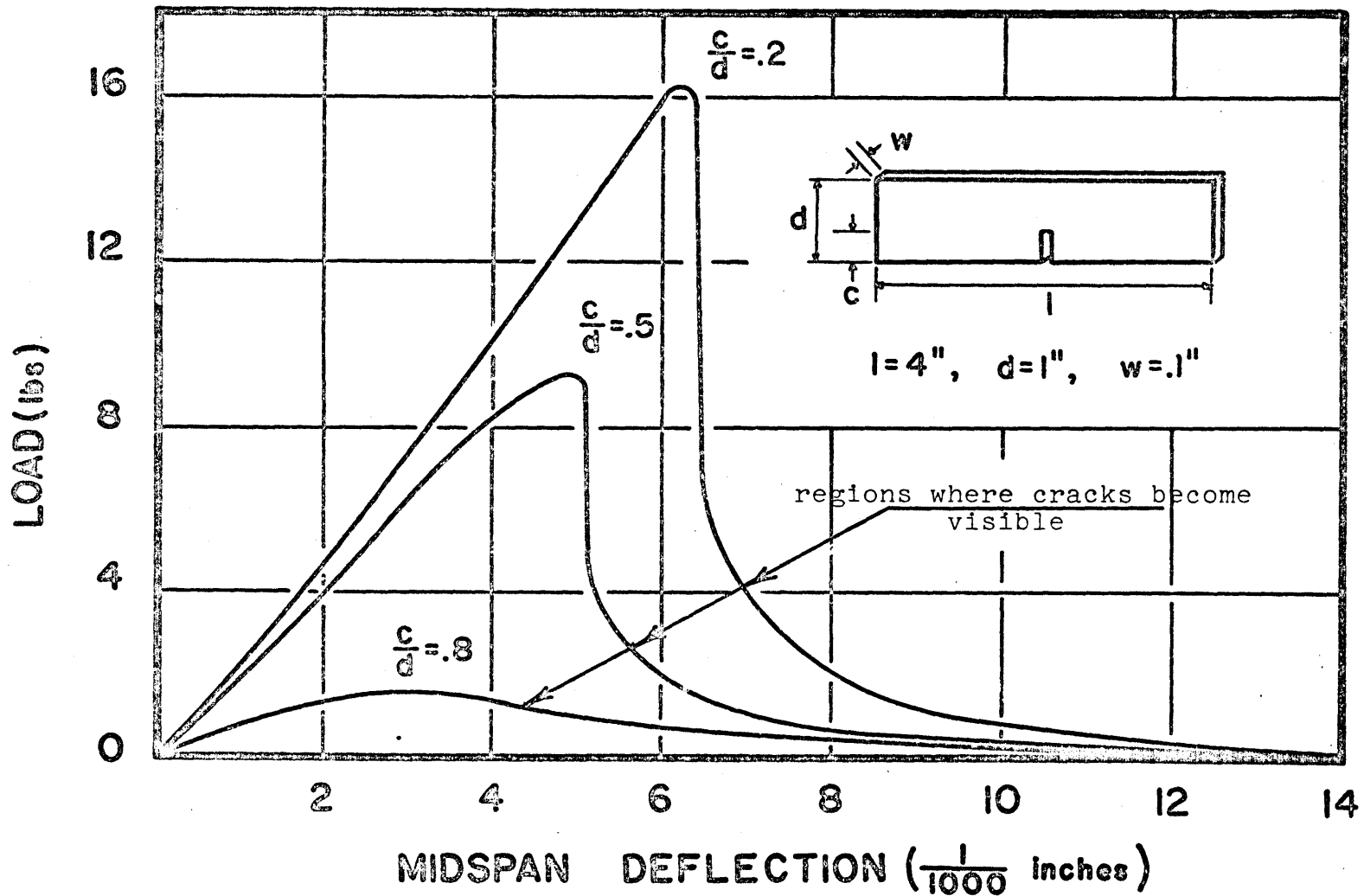


Figure 61 Typical Load Deflection Curves for Specimens

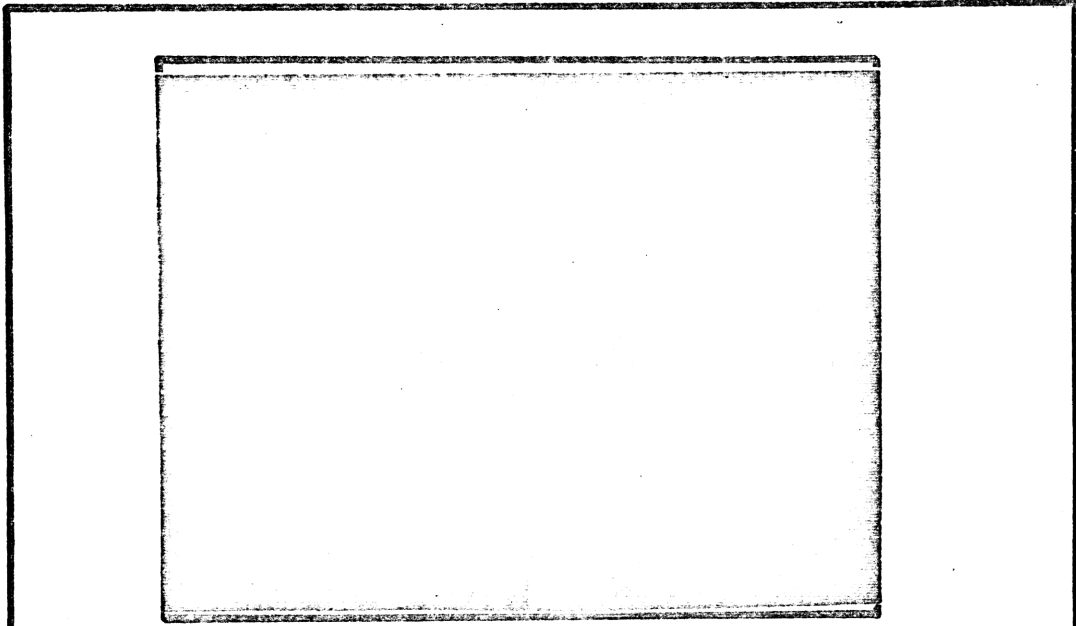


Figure 62 Crack Propagation Pattern in a Specimen of Granite with a .25" Notch, 5X

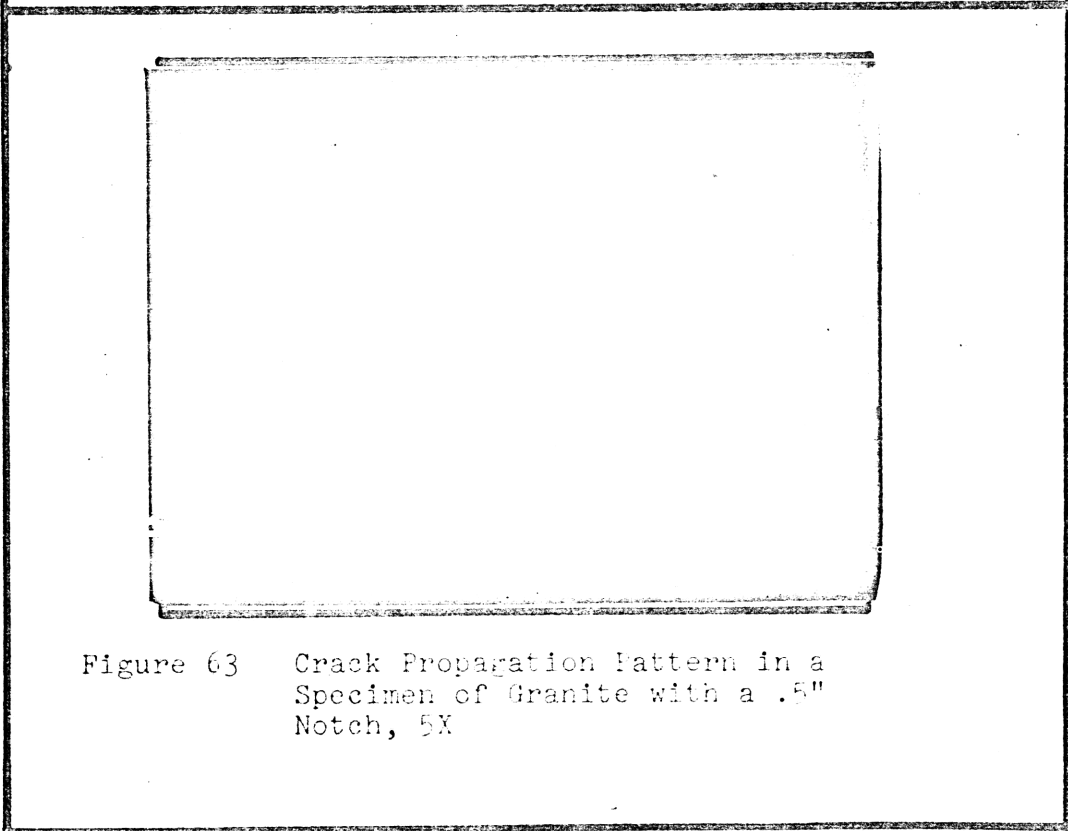


Figure 63 Crack Propagation Pattern in a Specimen of Granite with a .5" Notch, 5X

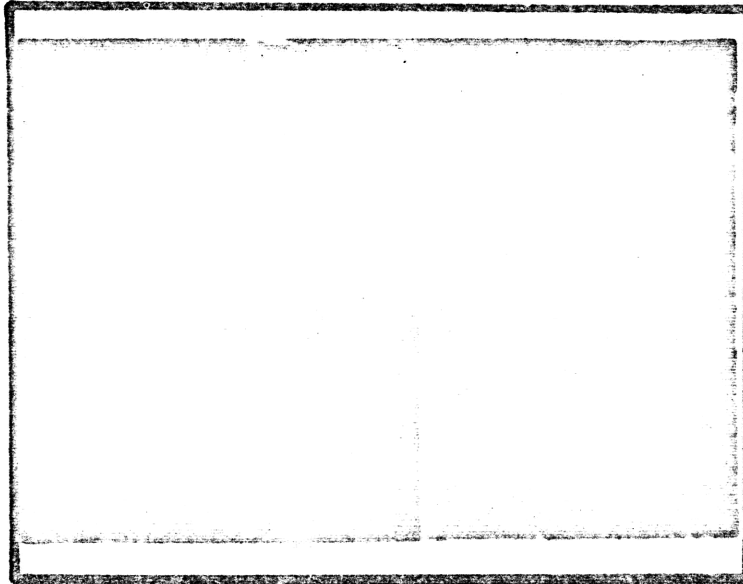


Figure 14 Crack Preparation pattern in a Specimen of Granite with a .7" Notch, IX

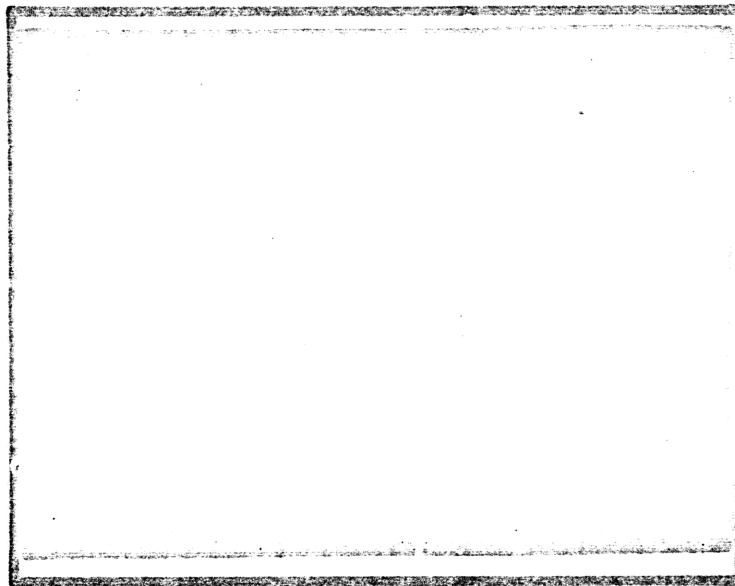


Figure 15 Crack Preparation pattern in a Specimen of Granite with a .7" Notch, X

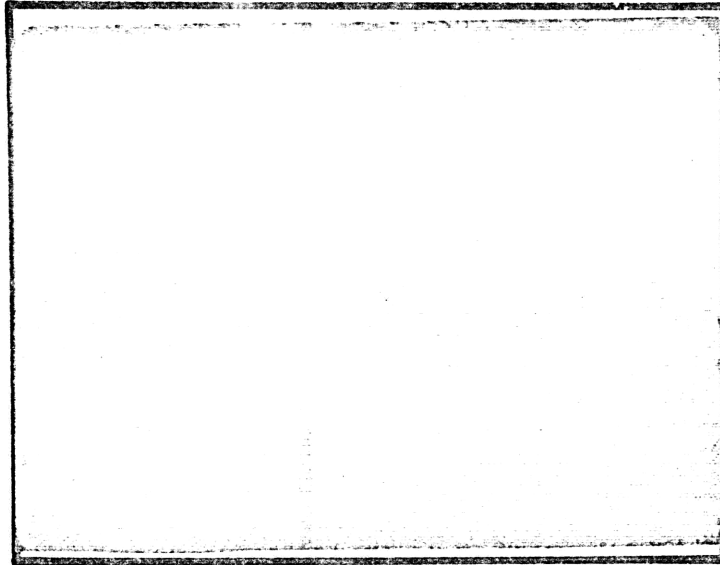


Figure 66 Crack Propagation Pattern in an Untreated Marble Specimen, 5X

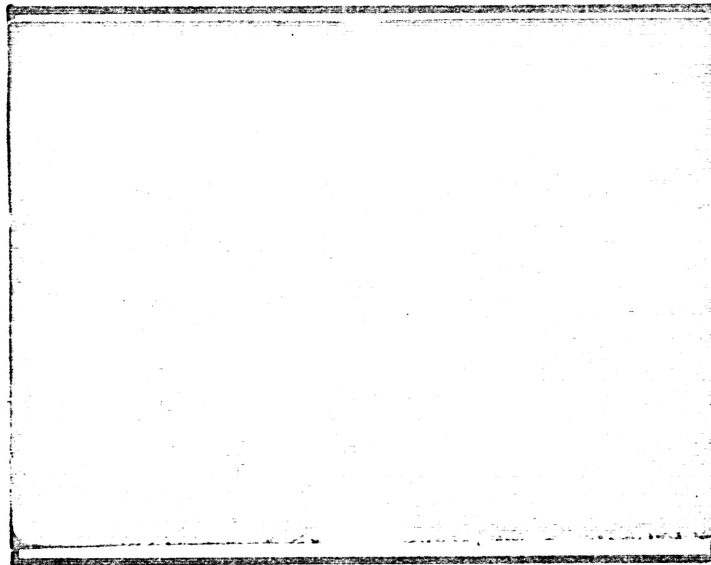


Figure 67 Crack Propagation Pattern in a Heat-Treated Marble Specimen, 5X

REFERENCES ON FRACTURE

1. Addinall, E., "Tensile Failure in Rock-Like Materials," Proc. Sixth Symposium on Rock Mechanics, University of Missouri, p. 515, 1964.
2. Anderson, O.L., "The Griffith Criterion for Glass Fracture," Fracture, Proc. International Conference, M.I.T. Press, p. 331, April 1959.
3. Berry, J.P., "Equations of Motion of Griffith Crack at Constant Force," Journal of Mech. Phys. Solids, Vol. 8, p. 194, 1960.
4. Brace, W.F., "Behavior of Quartz During Indentation," Journal of Geology, Vol. 71, p. 581, 1963.
5. Brace, W.F., "Brittle Fracture of Rocks," State of Stress in the Earth's Crust, Elsevier Press, p. 111, 1964.
6. Brace, W.F., "Recent Experimental Studies of Brittle Fracture of Rocks," Failure and Breakage of Rock, Proc. Eighth Symposium on Rock Mechanics, Soc. Min. Eng., p. 58, 1967.
7. Brace, W.F., and Walsh, J.B., "Some Direct Measurements of the Surface Energy of Quartz and Orthoclase," The American Mineralogist, Vol. 47, p. 111, September - October, 1962.
8. Broberg, K.B., "The Propagation of a Brittle Crack," Arkiv for Fysik, Vol. 18, No. 10, p. 159, 1960.
9. Colback, P.S.B., "An Analysis of Brittle Fracture Initiation and Propagation in the Brazilian Test," Proc. First Congress of the International Society of Rock Mechanics, Vol. 1, p. 385, 1966.
10. Colback, J.P., et. al., "The Influence of Moisture Content on the Compressive Strength of Rocks," Proc. Symposium on Rock Mechanics, Ottawa, p. 65, 1965.

11. Cotterell, B., "On the Nature of Moving Cracks," Trans. of ASME, Journal of Applied Mechanics, p. 12, March 1964.
12. Cottrell, A.H., "Mechanics of Fracture," Fracture, The Tewksbury Symposium, p. 1, 1963.
13. Cowan, H.J., "The Strength of Concrete under the Action of Combined Stresses," Magazine of Concrete Research, Vol. 5, p. 75, 1953.
14. Craggs, J.W., "On the Propagation of a Crack in an Elastic, Brittle Material," Journal of Mechanics and Physics of Solids, Vol. 8, p. 66, 1960.
15. Ford, H., Advanced Mechanics of Materials, Wiley, 1963.
16. Griffith, A.A., "Phenomena of Rupture and Flow in Solids," Philosophical Transactions of the Royal Society, Vol. A221, p. 163, 1920.
17. Inglis, C.E., "Stresses in a Plate due to the Presence of Cracks and Sharp Corners," Transactions Inst. Naval Architecture London, Vol. 55, p. 219, 1913.
18. Hudson, J.A., "Brittle Fracture of Rocks," Failure and Breakage of Rock, Eighth Symposium on Rock Mechanics, Society of Mining Engineers, p. 162, 1967.
19. Jaeger, J.C., "Punching Tests on Disks of Rock under Hydrostatic Pressure," Journal of Geophysical Research, Vol. 67, pp. 199, 369, 1963.
20. Jaeger, J.C., "Brittle Fracture of Rocks," Failure and Breakage of Rock, Proc. Eighth Symposium on Rock Mechanics, Society of Mining Engineers, p. 3, 1967.
21. Jaeger, J.C., "Fracture of Rocks," Fracture, The Tewksbury Symposium, p. 268, 1963.
22. Kessler, D.W., et. al., "Physical, Mineralogical, and Durability Studies on the Building and Monumental Granites of the United States," Journal of Research of the National Bureau of Standards, Vol. 25, No. 2, Paper RP1320, August 1940.

23. McClintock, F.A., et. al., "Friction on Griffith's Cracks in Rock under Pressure," Proc. Fourth U.S. National Congress on Applied Mechanics, Vol. 2, p. 1015, 1963.
24. McWilliams, J.R., "The Role of Microstructure in the Physical Properties of Rock," Fifth National Meeting of ASTM, Paper no. 102, 1965.
25. Mogi, K., "Some Precise Measurements of Fracture Strength of Rocks under Uniform Compressive Stress," Rock Mechanics and Engineering Geology, Vol. 1, No. 3, p. 41.
26. Mott, N.F., "Brittle Fracture in Mild Steel Plates," Engineering, Vol. 165, p. 16, 1948.
27. Nadai, A., Theory of Fracture and Flow of Solids, McGraw-Hill, 1950.
28. Nakayama, J., "Direct Measurements of Fracture Energies of Brittle Heterogeneous Materials," Journal of the American Ceramic Society, Vol. 48, No. 11, p. 584, November 1965.
29. Obert, L., et. al., Rock Mechanics and the Design of Structures in Rock, Wiley, 1967.
30. Orowan, E., "Fracture and Strength of Solids," The Physical Society, Vol. 12, p. 185, 1949.
31. Orowan, E., "Fundamentals of Brittle Behavior in Metals," M.I.T. Symposium, Wiley, 1967.
32. Paul, B., "Modification of the Coulomb-Mohr Theory of Fracture," Journal of Applied Mechanics, Vol. 28, p. 259, 1961.
33. Paul, B., et. al., "Initial and Subsequent Fracture Curves for Biaxial Compression of Brittle Materials," Failure and Breakage of Rock, Proc. Eighth Symposium on Rock Mechanics, Society of Mining Engineers, p. 133, 1967.
34. Poncelet, E., "Fracture," Ceramic Abstracts, p. 79d, March 1949.

35. Poncelet, E., "Fracture," Ceramic Abstracts, p. 2b, January 1952.
36. Poncelet, E., "Modern Concepts of Fracture and Flow," Poulter Research Labs Technical Report 002-65, Stanford Research Institute.
37. Price, D.G., "A Study of the Tensile Strength of Isotropic Rocks," Proc. First Congress of the International Society of Rock Mechanics, Vol. 1, p. 439, 1966.
38. Roberts, D.K., et. al., "The Velocity of Brittle Fracture," Engineering, Vol. 178, p. 820, 1954.
39. Sack, R.A., "Extension of Griffith's Theory of Rupture to Three Dimensions," Proc. Physical Society of London, Vol. 58, p. 729, 1946.
40. Shand, E.B., "Experimental Study of Fracture of Glass," Journal American Ceramic Society, Vol. 37, No. 12, p. 559, 1954.
41. Shand, E.B., "The Fracture Process for Glass," Journal American Ceramic Society, Vol. 37, No. 2, p. 52, 1954.
42. Schardin, H., "Fracture of Glass," Ceramic Abstracts, Vol. 20, No. 8, p. 191, 1941.
43. Schardin, H., "Velocity Effects in Fracture," Fracture, Proc. Int. Conf., M.I.T. Press, p. 297, April 1959.
44. Sneddon, I.N., "The Distribution of Stress in the Neighborhood of a Crack in an Elastic Solid," Proc. Royl. Soc., Vol. A187, p. 229, 1946.
45. Timoshenko, S., Strength of Materials, Part II, Van Nostrand, 1965.
46. Yoffe, E.H., "The Moving Griffith Crack," Phil. Mag., Vol. 42, p. 739, 1951.

REFERENCES ON HEAT TREATMENT

47. Austin, J.B., "Thermal Expansion of Non-Metallic Crystals," Journal of the American Ceramic Society, Vol. 35, No. 10, October 1, 1952.
48. Baroody, E.M., and Simons, E.M., and Duckworth, W.H., "Effect of Shape on Thermal Fracture," Journal of the American Ceramic Society, Vol. 38, No. 1, January 1955, p. 33.
49. Beck, A., Jaeger, J.C., and Newstead, G., "The Measurement of the Thermal Conductivities of Rock by Observations in Boreholes," Australian Journal of Physics, Vol. 9, No. 2, pp. 286-296, June 1956.
50. Birch, F., and Clark, H., "The Thermal Conductivity of Rocks and Its Dependence Upon Temperature and Composition," Part I, American Journal of Science, Vol. 238, No. 8, p. 37, August 1940.
51. Birch, F., and Clark, H., "The Thermal Conductivity of Rocks and Its Dependence Upon Temperature and Composition," Part II, American Journal of Science, Vol. 238, No. 9, p. 43, September 1940.
52. Brown, J.H., "Intergranular Comminution," Sc.D. Thesis, Department of Metallurgy, M.I.T., May 1958.
53. Brown, J.H., Gaudin, A.M., and Loeb, C.M., Jr., "Intergranular Comminution by Heating," Transactions A.I.M.E., Mining Engineering, p. 490, April 1956.
54. Buessem, W.R., "Thermal Shock Testing," Journal of the American Ceramic Society, Vol. 38, No. 1, p. 15, January 1955.
55. Chang, H.C., and Grant, N.J., "Mechanism of Inter-crystalline Fracture," Journal of Metals, Transactions A.I.M.E., p. 544, May 1956.
56. Cheng, C.M., "Resistance to Thermal Shock," Journal of the American Rocket Society, Vol. 21, No. 0, p. 147, November 1951.

57. Crandall, W.B., and Ging, J., "Thermal Shock Analysis of Spherical Shapes," Journal of the American Ceramic Society, Vol. 38, No. 1, p. 44, January 1955.
58. Coble, R.L., and Kingery, W.D., "Effect of Porosity on Thermal Stress Fracture," Journal of the American Ceramic Society, Vol. 38, No. 1, p. 33, January 1955.
59. Freeman, D.C., Jr., Sawdye, J.A., and Mumpton, F.A., "The Mechanism of Thermal Spalling in Rocks," Quarterly of the Colorado School of Mines, Vol. 58, No. 4, p. 235, October 1963.
60. Hasselman, D.P.H., "Elastic Energy at Fracture and Surface Energy as Design Criteria for Thermal Shock," Journal of the American Ceramic Society, Vol. 46, No. 11, p. 535, November 1963.
61. Holman, B.W., "Heat Treatment as an Agent in Rock Breaking," Inst. of Mining and Met., London, Vol. 36, p. 219, 1927.
62. Ke, T.S., "A Grain Boundary Model and the Mechanism of Viscous Intercrystalline Slip," Journal of Applied Physics, Vol. 20, p. 274, March 1949.
63. Kingery, W.D., "Factors Affecting Thermal Stress Resistance of Ceramic Materials," Journal of the American Ceramic Society, Vol. 38, No. 1, p. 3, January 1955.
64. Lecznar, F.J., "Severance of Quartz Grains from Reduced Iron Ore by Thermal Shock," Journal of Scientific and Industrial Research, Vol. 21D, p. 119, April 1962.
65. Manson, S.S., "Theory of Thermal Shock Resistance of Brittle Materials Based on Weibull's Theory of Strength," Journal of the American Ceramic Society, Vol. 38, No. 1, January 1955.
66. Manson, S.S., "Thermal Stresses and Thermal Shock," Mechanical Behavior of Materials at Elevated Temperature, edited by J.E. Dorn, McGraw-Hill, p. 393.
67. Manson, S.S., and Smith, R.W., "Quantitative Evaluation of Thermal Shock Resistance," Transactions of A.S.M.E., Vol. 78, No. 3, April 1956.

68. Marovelli, R.L., and Chen, T.S., "Thermal Fragmentation of Rock," Transactions, Society of Mining Engineers, March 1966.
69. Marovelli, R.L., and Veith, K.F., "Thermal Conductivity of Rock Measurements by the Transient Line Source Method," U.S. Bureau of Mines, Report of Investigations 6604, 1965.
70. Mott, N.F., "Slip at Grain Boundaries and Grain Growth in Metals," Proc. of Physical Society, Vol. 60, p. 391, 1948.
71. Nakayama, J., and Ishizuka, M., "Experimental Evidence for Thermal Shock Damage Resistance," Ceramic Bulletin, Vol. 45, No. 7, p. 666-669, 1966.
72. Puttick, K.E., and King, R., "Boundary Slip in Bicrystals of Tin," Journal of the Institute of Metals, Vol. 30, p. 537, 1951-2.
73. Yates, A., "Effect of Heating and Quenching Cornish Tin Ores before Crushing," Institute of Mining and Metals, London, Vol. 36, p. 41, 1927.
74. Scientific and Technological Applications Forecast, Office of Research and Development, Department of the Army, p. 2,6,1.

REFERENCES ON LASER

75. Adams, C.M., Jr., and Hardway, G.A., "Fundamentals of Laser Beam Machining and Drilling," I.E.E.E. Transactions on Industry and General Applications, p. 90, March-April 1965.
76. Anderson, J.E., Jackson, J.E., "Theory and Application of Pulsed Laser Welding," Welding Journal, Vol. 44, No. 12, p. 1018, December 1965.
77. Brewer, R.G., "Growth of Optical Plane Waves in Stimulated Brillouin Scattering," Physical Review, Vol. 140, No. 3A, p. A800, November 1, 1965.
78. Brewer, R.G., and Rieckhoff, K.E., "Stimulated Brillouin Scattering in Liquids," Physical Review Letters, Vol. 13, No. 11, p. 334, September 14, 1965.
79. Bruma, M.S., "Laser Machining," Quantum Electronics, Proc. of the Third International Congress, Paris, p. 1333.
80. Buddenhagen, D.A., "Lasers and Their Applications," Society of Automotive Engineers, Automotive Engineering Congress, Detroit, Michigan, Report No. 819A, January 13-17, 1964.
81. Bullough, R., and Gilman, J.J., "Elastic Explosions in Solids Caused by Radiation," Journal of Applied Physics, Vol. 37, No. 6, p. 2283, May 1966.
82. Chiao, R., "Brillouin Scattering and Coherent Phonon Generation," PhD Thesis, M.I.T., May 1965.
83. Chiao, R.Y., and Townes, C.H., "Stimulated Brillouin Scattering and Coherent Generation of Intense Hypersonic Waves," Physical Review Letters, Vol. 12, No. 21, p. 592, May 25, 1964.
84. Ciccarello, I.S., and Bransfeld, K., "Ultrasonic Absorption at Microwave Frequencies and at Low Temperatures in MgO and Al_2O_3 ," Physical Review, Vol. 134, No. 6A, p. A1517, June 15, 1964.

85. Cook, Nathan H., Manufacturing Analysis, M.I.T. Press, p. 138, 1966.
86. Cullom, J.H., and Waynant, R.W., "Determination of Laser Damage Threshold for Various Glasses," Applied Optics, Vol. 3, No. 8, p. 989, August 1964.
87. Cunningham, F.E., "The Use of Lasers for Machining," B.Sc. Thesis, M.I.T., 1963.
88. Earvolino, L.P., and Kennedy, J.R., "Laser Welding of Aerospace Structural Alloys," Welding Journal, Vol. 45, No. 3, p. 127S, March 1966.
89. Fairbanks, R.H., Sr., and Adams, C.M., Jr., "Laser Beam Fusion Welding," Supplement to the Welding Journal, p. 97S, March 1964.
90. Fleck, J.A., Jr., "Quantum Theory of Laser Radiation, I. Many Atom Effects," Physical Review, Vol. 149, No. 1, p. 309, September 9, 1966.
91. Giuliano, C.R., "Laser-Induced Damage to Transparent Di-Electric Materials," Applied Physics Letters, Vol. 5, No. 7, p. 137, October 1, 1964.
92. Harper, D.W., "Laser Damage in Glasses," British Applied Physics, Vol. 16, p. 751, 1965.
93. Hercher, M., "Laser Induced Damage in Transparent Media," Journal of Optical Society of America, Vol. 54, p. 563, 1964.
94. Ingebrigtsen, K.A., and Tønning, A., "Numerical Data for Acoustic Surface Waves in α -Quartz and Cadmium Sulfide," Applied Physics Letters, Vol. 9, No. 1, P. 16, July 1, 1966.
95. Katzman, et. al., "Laser Excitation of Modes in X-cut Quartz," Proc. of I.E.E.E., Vol. 53, No. 10, p. 1635.
96. Knecht, W.L., "Surface Temperature of Laser Heated Metal," Proc. of the I.E.E.E., p. 692, April 1966.
97. Kroll, N.M., "Excitation of Hypersonic Vibration by Means of Photoelastic Coupling of High Intensity Light Waves to Elastic Waves," Journal of Applied Physics, Vol. 36, No. 1, p. 34, January 1965.

98. Miller, K.J., Nunnikhoven, J.D., "Production Laser Welding for Specialized Applications," Welding Journal, Vol. 44, No. 6, p. 480, June 1965.
99. Olness, D., "Laser Damage Threshold in NaCl Crystals," Applied Physics Letters, Vol. 8, No. 11, p. 283, June 1, 1966.
100. Penner, S.S., and Sharma, O.P., "Interaction of Laser Radiation with an Absorbing Semi-Infinite Solid Bar," Journal of Applied Physics, Vol. 37, No. 6, p. 2304, May 1966.
101. Pfluger, A.R., and Maas, P.M., "Laser Beam Welding Electronic-Component Leads," Welding Journal, Vol. 44, No. 6, p. 264S, June 1965.
102. Ready, J.F., "Effects Due to Absorption of Laser Radiation," Journal of Applied Physics, Vol. 36, No. 2, p. 462, February 1965.
103. Ready, J.F., "Effects Due to Absorption of Laser Radiation," Journal of Optical Society of America, Vol. 53, p. 514, April 1963.
104. Schmidt, A.O., Ham, I., Hoshi, T., "An Evaluation of Laser Performance in Microwelding," Welding Journal, Vol. 44, No. 11, p. 481S, November 1965.
105. Shapiro, S.M., et. al., "Brillouin Scattering Spectra of Crystalline Quartz, Fused Quartz and Glass," Applied Physics Letters, Vol. 9, No. 4, p. 157, August 1966.
106. Sirons, J., "Lasers for Aeroscope Weaponry," Technical Documentary Report No. ASD-TDR-62-440, May 1962.
107. Tomiyasu, K., "Laser Bibliography," I.E.E.E. Journal of Quantum Electronics, Vol. QE-2, No. 6, p. 124, June 1966.

APPENDIX I

List of Figures

- Figure 1 Fracture Strength vs. Size of Crack, for Glass [Ref. 2]
- Figure 2 Kinetic Energy vs. Crack Half Length [Ref. 3]
- Figure 3 Stress-Strain Relation based on Griffith Criterion [Ref. 3]
- Figure 4 Graphical Determination of Fracture Surface Energy and Kinetic Energy [Ref. 3]
- Figure 5 Kinetic Energy Distribution for a Crack [Ref. 38]
- Figure 6 Effect of Stress Wave Propagation on Crack Velocity [Ref. 38]
- Figure 7 Tensile Stress vs. Orientation at Tip of the Crack [Ref. 46]
- Figure 8 Tensile Stress vs. Crack Propagation Velocity [Ref. 14]
- Figure 9 Crack Length vs. Elapsed Time after Initiation of Crack [Ref. 3]
- Figure 10 Crack Propagation Velocity vs. Crack Length [Ref. 3]
- Figure 11 Distance Travelled by Crack Tip vs. Elapsed Time, for Glass [Ref. 43]
- Figure 12 Fracture Velocity vs. Depth for a Glass Bar in Bending [Ref. 40]
- Figure 13 The Modified Coulomb-Navier-Mohr Criterion for Two Normal Stresses [Ref. 29]
- Figure 14 Mohr Circle for Graphical Representation of Stress States in Terms of Applied Stresses [Ref. 45]

- Figure 15 Failure Envelopes as Suggested by Coulomb and Mohr [Ref. 32]
- Figure 16 Graphical Representation of Mohr Theory for Two Normal Stresses [Ref. 32]
- Figure 17 Modification of Coulomb-Navier-Mohr Theory Failure Criterion [Ref. 32]
- Figure 18 Coulomb-Navier-Mohr Theory Applied to Two Normal Stresses [Ref. 32]
- Figure 19 Effect of Lubrication of End Plates on the Failure Mode of Compression Specimens [Ref. 33]
- Figure 20 Effect of Confining Pressure on Compressive Strength of Rock [Ref. 23]
- Figure 21 Major Types of Fracture Occurring in Transverse Compression of Disks [Ref. 37]
- Figure 22 Direction of Fracture of Disks under Point Load Stresses [Ref. 24]
- Figure 23 Stages of Failure in Brazilian Test [Ref. 9]
- Figure 24 Schematic of Bending Test [Ref. 28]
- Figure 25 Typical Load Deflection Curves [Ref. 28]
A - unstable, B - semistable, C - stable
- Figure 26 The Modified Shaper Used to Prepare the Specimens
- Figure 27 The Loading System for Type A (1"x1"x12") Beams
- Figure 28 The Loading System for Type D (.1"x1"x4") Beams
- Figure 29 The 1000 Watt Continuous Gas Laser
- Figure 30 Fracture Surface Energy vs. Notch Depth, for Untreated Granite, Specimen Size 1"x1"x12", Mid-Span Deflection Rate .002 inches per minute
- Figure 31 Fracture Surface Energy vs. Notch Depth, for Untreated Granite, Specimen Size .1"x1"x4", Mid-Span Deflection Rate .002 inches per minute

- Figure 32 Fracture Surface Energy vs. Notch Depth, for Untreated Granite, Specimen Size 1"x1"x4", Mid-Span Deflection Rate .002 inches per minute
- Figure 33 Fracture Surface Energy vs. Notch Depth, for Untreated Granite, Specimen Size .5"x1"x4", Mid-Span Deflection Rate .002 inches per minute
- Figure 34 Fracture Surface Energy vs. Notch Depth, for Untreated Granite, All Sizes, Mid-Span Deflection Rate .002 inches per minute
- Figure 35 Corrected Fracture Surface Energy vs. Notch Depth, for Untreated Granite, Specimen Size .1"x1"x4", Mid-Span Deflection Rate .02 inches per minute
- Figure 36 Corrected Fracture Surface Energy vs. Notch Depth, for Untreated Marble, Specimen Size 1"x1"x12", Mid-Span Deflection Rate .002 inches per minute
- Figure 37 Corrected Fracture Surface Energy vs. Notch Depth, for Untreated Marble, Specimen Size .1"x1"x4", Mid-Span Deflection Rate .02 inches per minute
- Figure 38 Corrected Fracture Surface Energy vs. Notch Depth, for Heat-Treated Granite, Specimen Size .1"x1"x4", Mid-Span Deflection Rate .02 inches per minute
- Figure 39 Dimensionless Ultimate Flexural Load vs. Notch Depth, for Untreated and Heat-Treated Granite, Specimen Size .1"x1"x4", Mid-Span Deflection Rate .02 inches per minute
- Figure 40 Corrected Fracture Surface Energy vs. Notch Depth, for Heat-Treated Marble, Specimen Size .1"x1"x4", Mid-Span Deflection Rate .02 inches per minute
- Figure 41 Dimensionless Ultimate Flexural Load vs. Notch Depth, for Untreated and Heat-Treated Marble, Specimen Size .1"x1"x4", Mid-Span Deflection Rate .02 inches per minute
- Figure 42 Untreated Granite Specimen after Failure

- Figure 43 Untreated Granite Specimen after Failure
- Figure 44 Untreated Granite Specimen after Failure, 50X
- Figure 45 Untreated Marble Specimen, 50X
- Figure 46 Untreated Marble Specimen after Failure, 50X
- Figure 47 Heat Treated Marble Specimen after Failure, 50X
- Figure 48 Heat Treated Granite Specimen after Failure, 50X
- Figure 49 Heat Treated Granite Specimen after Failure, 50X
- Figure 50 Heat Treated Marble Specimen, 50X
- Figure 51 Corrected Fracture Surface Energy vs. Notch Depth, for Granite Specimens Exposed to Laser, Specimen Size .1"x1"x4", Mid-Span Deflection Rate .02 inches per minute
- Figure 52 Dimensionless Ultimate Flexural Loads vs. Notch Depth, for Granite Specimens Exposed to Laser, Specimen Size .1"x1"x4", Mid-Span Deflection Rate .02 inches per minute
- Figure 53 Granite Specimen after Exposure to Laser and after Testing, 50X
- Figure 54 Granite Specimen after Exposure to Laser and after Testing, 50X
- Figure 55 Granite Specimen after Exposure to Laser and after Testing, 50X
- Figure 56 Granite Specimen after Exposure to Laser and after Testing, 50X
- Figure 57 Corrected Fracture Surface Energy vs. Notch Depth, for Marble Specimens Exposed to Laser, Specimen Size .1"x1"x4", Mid-Span Deflection Rate .02 inches per minute
- Figure 58 Dimensionless Ultimate Flexural Load vs. Notch Depth, for Marble Specimens Exposed to Laser, Specimen Size .1"x1"x4", Mid-Span Deflection Rate .02 inches per minute

- Figure 59 Marble Specimen after Exposure to Laser and after Testing, 50X
- Figure 60 Marble Specimen after Exposure to Laser and after Testing, 50X
- Figure 61 Typical Load Deflection Curves for Specimens
- Figure 62 Crack Propagation Pattern in a Specimen of Granite with a .25" Notch, 5X
- Figure 63 Crack Propagation Pattern in a Specimen of Granite with a .5" Notch, 5X
- Figure 64 Crack Propagation Pattern in a Specimen of Granite with a .75" Notch, 5X
- Figure 65 Crack Propagation Pattern in a Heat-Treated Granite Specimen, 5X
- Figure 66 Crack Propagation Pattern in an Untreated Marble Specimen, 5X
- Figure 67 Crack Propagation Pattern in a Heat-Treated Marble Specimen, 5X

APPENDIX II

List of Tables

- | | |
|---------|--|
| Table 1 | Properties of Rocks Used in this Study |
| Table 2 | Crack Propagation Pattern for an Unheated Granite Specimen |
| Table 3 | Crack Propagation Pattern for a Heated Granite Specimen |
| Table 4 | Crack Propagation Pattern for a Heated Marble Specimen |
| Table 5 | Crack Propagation Pattern for an Unheated Marble Specimen |

APPENDIX III

ADDITIONAL REFERENCES ON FRACTURE

108. Austin, C.F., et. al., "Shock Wave Attenuation in Elastic and Anelastic Rock Media," Proc. Seventh Symposium on Rock Mechanics, Pennsylvania State University, p. 346, 1965.
109. Bair, K.M., "Shock Waves in Glass," Nature, Vol. 160, p. 24, 1947.
110. Barioli, E., "Physical Properties of Rock Mass," Proc. First Congress of the International Society of Rock Mechanics, Vol. 1, p. 237, 1966.
111. Berger, H., "Influences of the Methods of Measurement on the Validity of Fissure Analysis," Proc. First Congress of the International Society of Rock Mechanics, Vol. 1, p. 145, 1966.
112. Broutman, L.J., and McGarry, F.J., "Fracture Surface Work Measurements on Glassy Polymers by a Cleavage Technique, I. Effects of Temperature," Journal of Applied Polymer Science, Vol. 9, p. 589, 1965.
113. Byerlee, J.D., "The Frictional Characteristics of Westerly Granite," M.I.T. Ph.D. Thesis, Geology, 1966.
114. Coates, D.F., "Rock Mechanics Principles," Department of Mines and Technical Surveys, Mines Branch Monograph 874, Ottawa, Canada, 1965.
115. Cogan, J.P., "The Mechanics of Rock Failure," M.Sc. Thesis, Colorado School of Mines, February 1950.
116. Cook, N.G.W., "The Failure of the Rock," International Journal of Rock Mechanics, and Mining Science, Vol. 2, p. 389, 1965.
117. Gibbs, P., and Cutler, I.B., "On the Fracture of Glass Which is Subjected to Slowly Increasing Stress," Journal of the American Ceramic Society, Vol. 34, No. 7, p. 200, 1951.

118. Gordon, J.E., et. al., "On the Strength and Structure of Glass," Proc. Royal Society, London, A. Vol. 249, p. 65, 1959.
119. Habib, P., "Fissuration of Rocks," Proc. First Congress of the International Society of Rock Mechanics, Vol. 1, p. 185, 1966.
120. Hayashi, M., "A Mechanism of Stress Distribution on the Fissured Foundation," Proc. First Congress of the International Society of Rock Mechanics, Vol. 2, p. 509, 1966.
121. Hayashi, M., "Strength and Dilatancy of Brittle Jointed Mass," Proc. First Congress of the International Society of Rock Mechanics, Vol. 1, p. 295, 1966.
122. Haynes, D.D., "Constant Energy - Variable Velocity Effects in Percussive Drilling," Ph.D. Thesis, Pennsylvania State University, September 1964.
123. Hilliard, J.E., "Volume-Fraction Analysis by Quantitative Metallography," General Electric Research Laboratories, Report No. 01-RL-2652M, March 1961.
124. Hoek, E., "Fracture Propagation Mechanism in Hard Rock," Proc. First Congress of the International Society of Rock Mechanics, Lisbon, 1966.
125. Hoek, E., "A Photoelastic Technique for the Determination of Potential Fracture Zones in Rock Structures," Failure and Breakage of Rock, Eighth Symposium on Rock Mechanics, Society of Mining Engineers, p. 94, 1967.
126. Hyzer, W.G., "Introduction to High Speed Photographic Instrumentation," I.S.A. Transactions, Vol. 5, No. 1, January 1966.
127. Irwin, G.R., "Fracture Dynamics," Fracturing of Metals, American Society of Metals, Cleveland, Ohio, 1948.
128. Irwin, G.R., and Wells, A.A., "A Continuum-Mechanics View of Crack Propagation," Metallurgical Reviews, Vol. 10, No. 38, p. 223, 1965.

129. Jacobi, O., "Research with a View to the Development of Powered Face Support," Proc. Fourth International Conference on Rock Mechanics, Columbia University, New York, p. 166, 1964.
130. Judd, R.W., "Rock Stresses, Rock Mechanics, and Research," State of Stress in the Earth's Crust, Elsevier Press, p. 5, 1964.
131. Kolsky, H., "Fractures Produced by Stress Waves," Fracture Proc. International Conference, M.I.T. Press, p. 281, April 1959.
132. Kondoer, R.L., "Energy Storage and Dissipation Properties of Rocks," Proc. First Congress of the International Society of Rock Mechanics, Vol. 1, p. 273, 1966.
133. Krsmanovic, et. al., "Some Aspects of Rupture of a Rock Mass," Rock Mechanics and Engineering Geology, Supplement #2, 1965, 1965.
134. Le Comte, P., "Methods for Measuring the Dynamic Properties of Rocks," Proc. Rock Mechanics Symposium, Ottawa, p. 15, 1963.
135. Lewis, W.E., "Research Program Summaries," Bureau of Mines, U.S. Department of the Interior, April 13, 1966.
136. Loeb, S., "Propagation of Sound in Compact Masses," Proc. First Congress of the International Society of Rock Mechanics, Vol. 1, p. 91, 1966.
137. Murgatroyd, B.A., "The Significance of Surface Marks on Fractured Glass," Journal of the Society of Glass Technology, Vol. 26, p. 155, 1942.
138. Murphy, V.J., et. al., "Seismic Velocities and Elastic Moduli Measurements," Proc. First Congress of the International Society of Rock Mechanics, Vol. 1, p. 711, 1966.
139. Ortlepp, W.D., "An Experimental Investigation into Certain Aspects of Rock Failure," M.E. Thesis, McGill University, April 1957.

140. Paul, B., et. al., "Initial and Subsequent Fracture Curves for Biaxial Compression of Brittle Materials," Failure and Breakage of Rock, Proc. Eighth Symposium on Rock Mechanics, Society of Mining Engineers, p. 133, 1967.
141. Paulding, B.W., Jr., "Crack Growth During Brittle Fracture in Compression," M.I.T. Ph.D. Thesis, Geology, 1965.
142. Pegler, A.V., "A Study of the Mechanics of Rock Fracturing by Hydraulic Pressure," Proc. Rock Mechanics Symposium, Ottawa, p. 88, 1963.
143. Perami, R., "Micrograph Development in Crystalline Rocks," Proc. First Congress of the International Society of Rock Mechanics, Vol. 1, p. 621, 1956.
144. Rinehart, J.S., "Dynamic Fracture Strengths of Rocks," Proc. Seventh Symposium on Rock Mechanics, Pennsylvania State University, p. 205, 1965.
145. Rinehart, J.S., "Reaction of Rock to Impulsive Loads," Proc. of the First Congress of the International Society of Rock Mechanics, Lisbon, 1966.
146. Robertson, T.S., "Propagation of Brittle Fracture in Steel," Journal of the Iron and Steel Inst., Vol. 175, p. 361, 1953.
147. Rodriguez, F.P., "Anisotropy of Granites," Proc. First Congress of the International Society of Rock Mechanics, Vol. 1, p. 721, 1966.
148. Roesler, F.C., "Brittle Fractures Near Equilibrium," Proc. Physical Society of London, Vol. 8, No. 69, p. 981, 1956.
149. Schon, J., "Velocity of Longitudinal Waves," Proc. of the First Congress of the International Society of Rock Mechanics, Vol. 1, p. 21, 1966.
150. Schwartz, A.E., "An Investigation of the Strength of Rock," Ph.D. Thesis, Georgia Institute of Technology, May 1963.

151. Shand, E.B., "Experimental Study of Fracture of Glass," Journal of the American Ceramic Society, Vol. 37, No. 12, p. 559, 1954.
152. Shand, E.B., "The Fracture Process for Glass," Journal of the American Ceramic Society, Vol. 37, No. 2, p. 52, 1954.
153. Singh, M.M., "Mechanism of Rock Failure under Impact of a Chisel-Shaped Bit," Ph.D. Thesis, Pennsylvania State University, January 1961.
154. Sinitsyn, A.P., "Relation Between the Seismic Elasticity Modulus of Rock Foundation and Wave Resistance," Proc. of the First Congress of the International Society of Rock Mechanics, Vol. 1, p. 87, 1966.
155. Sirieys, B.M., "On the Laws of Rock-Fragmentation," Proc. of the First Congress of the International Society of Rock Mechanics, Lisbon, 1966.
156. Smekal, "Fracture of Glass," Ceramic Abstracts, p. 1285, July 1951.
157. Smith, C.S., and Guttman, L., "Measurement of Internal Boundaries in Three-Dimensional Structures by Random Sectioning," Transactions A.I.M.E., Journal of Metals, p. 81, January 1953.
158. Stroh, A.N., "A Simple Model of a Propagating Crack," Journal Mechanical Physical Solids, Vol. 8, p. 119, 1960.
159. Tetelman, A.S., et. al., Fracture of Structural Materials, Wiley, 1967.
160. Scientific and Technical Applications Forecast, U.S. Department of the Army, Washington, D.C., 1964.
161. Walsh, J.B., et. al. "Elasticity of Rock," Rock Mechanics and Engineering Geology, Vol. 4, No. 4, p. 201, 1966.
162. Williams, M.L., "On the Stress Distribution at the Base of a Stationary Crack," Journal of Applied Mechanics, Vol. 24, No. 1, p. 109, 1957.